Phase Change Material Based Ohmic Switches for Reconfigurable RF Applications

by

Muzhi Wang

A dissertation submitted in partial fulfillment
of the requirements for the degree of
Doctor of Philosophy
(Electrical Engineering)
in the University of Michigan
2017

Doctoral Committee:

Professor Mina Rais-Zadeh, Chair
Professor Katsuo Kurabayashi
Professor Becky Peterson
Professor Kamal Sarabandi

Muzhi Wang

wangmz@umich.edu

ORCID iD: 0000-0001-7021-351X

2017

To my family and friends

ACKNOWLEDGEMENTS

First and foremost, I would like to express my most sincere gratitude to my advisor, Professor Mina Rais-Zadeh, for the precious opportunity to pursue my Ph.D. degree in her research group at the University of Michigan, and for her constant guidance and inspiration throughout the years in my research project. Professor Rais-Zadeh gave me the chance to work on one of her research projects on my third year as an undergraduate student. That was the first time that I was introduced to RF MEMS as well as the hands-on fabrication experience in the cleanroom. This valuable research experience with her made me decide to continue working on the related field as a graduate Ph.D. student in her group. In my Ph.D. study, she has inspired a lot of motivation and enthusiasm in our group, and her guidance and advice has been the key to our research work. My research project would not have been made possible without her knowledge in RF circuits and modules, MEMS and integrated Microsystems and phase change materials. I will always be thankful to her for supporting me and believing in me, and this great Ph.D. study experience with her will have long-lasting influence in my future career.

I would also like to thank my dissertation committee members for their support on my research work. Professor Becky Peterson has been both a great professor and a wonderful friend. She has provided me with great ideas and inspiration that helped me with the issues and difficulties in my research. Professor Kamal Sarabandi has provided me with valuable knowledge in RF circuits and systems, and great advice in the direction and big

picture of my research work. Professor Katsuo Kurabayashi's knowledge mechanical and thermal related topics and aspects has been a great inspiration to an important part of my research work.

The Resonant MEMS Group has been a brilliant team of great colleagues and friends led by Professor Rais-Zadeh. When I first joined the group, it was Dr. Vikram Thakar and Dr. Yonghyun Shim that mentored me on the research work and the fabrication processes in the cleanroom. They have provided me with useful knowledge, great techniques and valuable experience with my research work. Dr. Vikrant Gokhale, Dr. Zhengzheng Wu, Dr. Azadeh Ansari, Dr. Adam Peczalski, Dr. Roozbeh Tabrizian and Dr. Haoshen Zhu have also helped me a lot with the theoretical knowledge and in-lab equipment operations. I am honored to have worked closely with Dr. Feng Lin together on my research related projects, and grateful for his help with the difficulties I experienced. Mohsen, Cesar and Milad have also been my great lab mates. I would like to thank all of them for being such great colleagues and friends.

I would certainly also like to thank all the staff members at the Lurie Nanofabrication Facility (LNF) at the University of Michigan. None of the research work would have been possible without their support on the equipment operations and process development. Their expertise in the fabrication processes and efforts in the tool maintenance have been the key to my fabrication process. The staff members at the Michigan Center for Materials Characterization (MC^2) have also been very helpful with the material characterization and electron microscopic imaging processes that I needed to perform. I am most grateful for their help in the years of my Ph.D. study.

I am very grateful to have had the great friends at the University of Michigan and in Ann Arbor. We share great appreciation for the great college and the wonderful city, and we value the friendship among one another. Being a graduate student in the College of Engineering could sometimes be stressful, and the support from my friends has powered me through times of doubt and depression. I will always cherish the great friendship.

Last but certainly not least, I would like to express my deepest appreciation to my family, especially my parents, for supporting and encouraging me to pursue my dream, and for their unconditional love. Finally, I would like to thank my girlfriend Yue for her love and care. I could not have imagined how wonderful my life would get from the moment I met her.

TABLE OF CONTENTS

LIST OF FIGURES

LIST OF TABLES

LIST OF ABBREVIATIONS

AC	Alternating current
ACP	Air coplanar
AlN	Aluminum nitride
BW	Bandwidth
CABW	Constant absolute bandwidth
CMOS	Complementary metal-oxide-semiconductor
CMP	Chemical mechanical planarization
DC	Direct current
DRAM	Dynamic random access memory
EDXS	Energy-dispersive X-ray spectrometry
fcc	Face-centered cubic
FEA	Finite element analysis
FET	Field-effect transistor
FIB	Focused ion beam
GaAs	Gallium arsenide
GeSb	Germanium antimonide
GeTe	Germanium Telluride
GGG	Gadolinium gallium garnet
GSG	Ground-signal-ground

GST/GeSbTe	Germanium antimony telluride
IIP_3	Input third-order intercept point
IoT	Internet of Thing
ITRS	International Technology Roadmap for Semiconductors
LNF	Lurie Nanofabrication Facility
MEMS	Micro-electromechanical system
MOSFET	Metal-oxide-semiconductor field-effect transistor
NaCl	Sodium chloride
OIP_3	Output third-order intercept point
P_{1dB}	1-dB compression point
PECVD	Plasma-enhanced chemical vapor deposition
HEMT	High electron mobility transistor
RAM	Random access memory
RF	Radio frequency
SEM	Scanning electron microscopy
Si_3N_4	Silicon nitride
SiO_2	Silicon dioxide
SOI	Silicon-on-insulator
SOS	Silicon-on-Sapphire
SP6T	Single-pole-6-throw
SPDT	Single-pole-dual-throw
SPMT	Single-pole-multiple-throw

SPST	Single-pole-single-throw
TCR	Temperature coefficient of resistance
TEM	Transmission electron microscopy
TiN	Titanium nitride
TiW	Titanium-tungsten
Tx/Rx	Transmitter/receiver
XRD	X-ray diffraction
YIG	Yttrium iron garnet

ABSTRACT

This research work is focused on the study and development of chalcogenide phase change materials and their applications in reconfigurable RF modules and systems. Germanium telluride (GeTe), one of the chalcogenide phase change materials, is studied and used in the development process of RF ohmic switches. This thesis presents the study of GeTe and other phase change materials, the design, fabrication and measurements of GeTe phase change material based RF switches, and the performance evaluation as well as the operation and breakdown analysis of the GeTe phase change RF switches. It also discusses the potential applications of GeTe RF switches in reconfigurable RF modules by demonstrating a bandpass filter design.

RF switches based on solid-state transistors and diodes, and micro-electromechanical system (MEMS) as well as other technologies have been reported and used in integrated circuits and systems for RF and microwave applications. Each of these technologies for RF switches shows some limitations regarding RF performance, integration compatibility, cost, fabrication yield, or reliability. This thesis presents a novel alternative for RF switch development using GeTe phase change material. The special phase transition properties of phase change materials have drawn attention for decades. Material study and characterization of phase change materials have been performed for a better understanding of their properties. Phase change materials have since been developed for different applications, with non-volatile memory modules being the most successful

application. With the success in phase change memory design, we have directed our attention to RF switching applications based on phase change materials. Two main types of GeTe phase change material based RF ohmic switches are developed and the design and fabrication of each is discussed in detail. The RF switches designed using GeTe have shown very competitive performance results compared to other existing RF switch designs. Analysis and modeling of the switches have also been performed for a better understanding of the devices and phase change materials as well as their phase transition process. A reconfigurable bandpass filter using GeTe switches have verified the good functionality of phase change RF switches and their promising potential in reconfigurable RF applications.

CHAPTER 1 Introduction

1.1. Motivation and Background

Radio Frequency (RF) modules are widely used in wireless communication systems such as radars and wireless transceivers. In modern designs, RF systems are commonly realized with on-chip integrated circuits. In mobile wireless communication systems, for example, they usually serve as the signal transmitting and receiving front-ends for the baseband analog and digital processing systems. Due to the coexistence of different wireless communication standards in the radios, band switching among different frequencies is often required, which is realized through module or system level reconfigurability. In reconfigurable systems, the key element is the RF switch. Some of the requirements for RF switches include low transmission or insertion loss, high isolation between the input and output RF terminals in the OFF mode, fast switching speed, high RF power handling capability, and high operation linearity across a certain RF power level.

In modern wireless communication systems, RF switches are commonly used for purposes such as Tx/Rx selection, frequency band selection, signal relay and other network reconfiguration activities. Along other tuning/reconfiguring techniques, RF switches are critical in achieving system level reconfigurability in emerging technologies such as the internet of things (IoT). A vast number of solid-state based RF switches have been designed and used in RF systems since several decades ago using various

semiconductor techniques such as silicon on insulator (SOI) or gallium arsenide (GaAs) based integrated circuitry [1, 2, 3]. As predicted by Moore's Law, the number of transistors on a densely integrated circuit doubles in approximately every two years, and the semiconductor industry has been able to follow Moore's Law over the past several decades. In the progression of transistor integration density, miniaturization has played a critical role, with the size of transistors reduced as fabrication technology improved. In recent years, however, as transistor sizes get closer to their physical limits, Moore's Law regarding transistor density is becoming harder to follow. In order to sustain the performance improvement of integrated circuits, utilization of new materials and novel device structures is becoming more critical. This trend in semiconductor technology development is known as the "More-than-Moore" era according to the International Technology Roadmap for Semiconductors (ITRS) (Figure 1.1) [4].

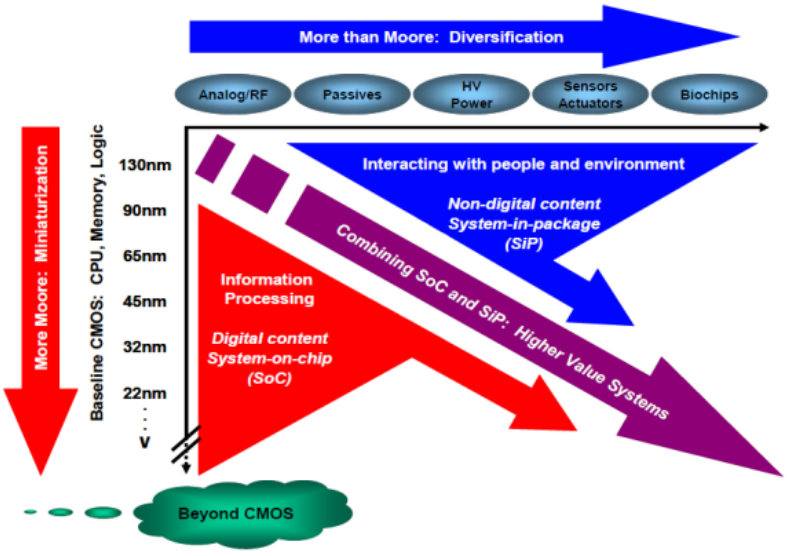

Figure 1.1. The technology trend in semiconductor industry indicating the need for performance improvement by functional diversification in the "More-than-Moore" era [4].

1.2. Overview of RF Switch Technologies

RF and microwave switches have been designed and used in semiconductor integrated circuits and microsystems for control and signal relay purposes. They are among the most effective ways to achieve system configurability. One example of RF switch applications is the RF front-end for wireless communications. In a typical front-end module, single-pole double-throw (SPDT) antenna switches are usually used for selection between the transmitter and receiver modules. For a multi-band front-end module, single-pole multiple-throw (SPMT) RF switches are used for band selection. As wireless products, such as radio transceivers, hand-held devices and other portable devices, become popular in industry and consumer market, the need for improving performance and reducing costs of RF transceivers becomes more noticeable [5]. As RF switches are an important part of wireless RF modules, their performance and cost requirements are also becoming stringent. One of the most important performance requirements for RF switches is the signal transmission and isolation values. High-performance RF switches need to have low signal insertion loss when turned ON, and high signal isolation when turned OFF. Other performance requirements that are common among RF modules include switching speed, indicating how fast the switch can be turned ON or OFF, linearity, indicating whether the switch can operate with minimal harmonics and intermodulation products at frequencies, power consumption, and power handling capability, showing what RF power level the switch can handle without showing degraded functionality. Other than the common performance requirements for RF switches, there are also requirements for good integration compatibility, reasonable

device size, and ease of fabrication technology. RF switches are also preferred to have a low-cost fabrication process with a high yield, in order to reduce the overall cost. Taking all the requirements and specifications into account, a number of RF switch designs have been proposed, built, and used in RF systems.

In semiconductor integrated systems, field effect transistor (FET) based switches are among the earliest switch designs that were developed. Considering the physical properties of FETs, they can be readily implemented as gate-controlled switching devices. Their fabrication process also makes them compatible for co-integration with other semiconductor based modules and systems [6]. Different types of FETs and their microwave operation have been comprehensively summarized in [6], and a dual-gate metal-oxide-semiconductor FET (MOSFET) based amplifier design has been reported, demonstrating a 60-dB dynamic switching range and high switching speed at 4 8 GHz [7]. Significant progress has been made in the development of FETs for microwave applications since 1970's, and various FET based switch designs have been proposed. One of the proposed designs is an FET microwave switch based on gallium arsenide (GaAs) [8].

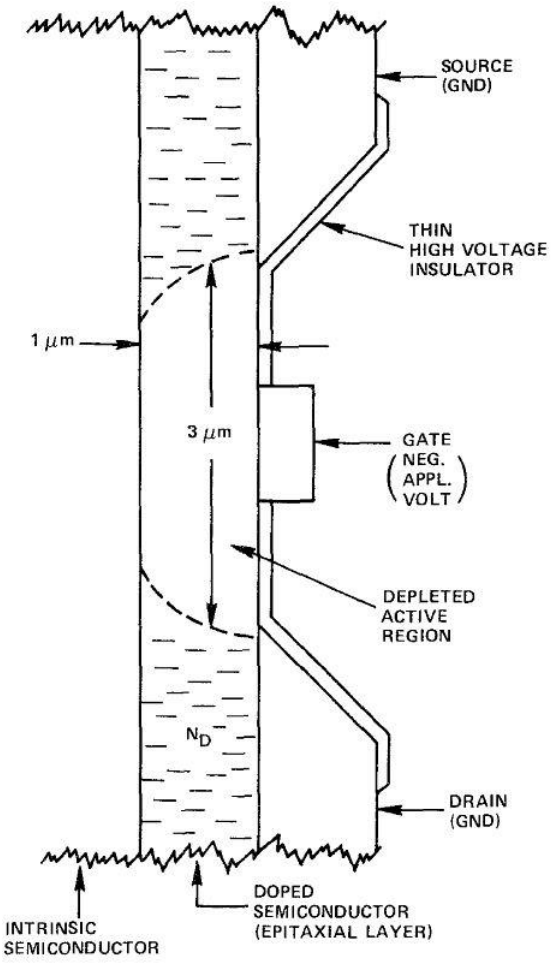

Figure 1.2. A FET structure of a microwave switching element proposed in [8].

The structure of the FET based microwave switch proposed in [8] is shown in Figure 1.2. The device is similar to other FETs, where the source and drain are connected to two terminals of a control diode. A voltage-controlled gate is used to deplete the channel, which is formed with a doped epitaxial layer within an intrinsic semiconductor volume. The results of switch operation and device analysis have also been included. Other GaAs FET based RF switches have also been reported. Compared to other semiconductor technologies, GaAs FET based RF switches offer the advantages such as low bias power

in both states and low loss [2]. The GaAs FET based RF switches reported in [1] also show good power handling capability. An integrated SPDT switch based on GaAs FET has also been reported for mobile communication systems, showing a high-power handling capability of over 5 W (37 dBm) [9]. GaAs FET-based switches have been popular in RF and microwave applications, but they also show certain limitations, such as high level of distortion, especially in the OFF state, caused by the junction capacitance non-linearity [2].

Other than FET-based RF switches, GaAs p-i-n diode based switches have also been designed. RF and microwave switches built with p-i-n diodes are also very popular due to their high breakdown voltages, fast switching characteristics, variable resistance with bias and broadband application capability [3].

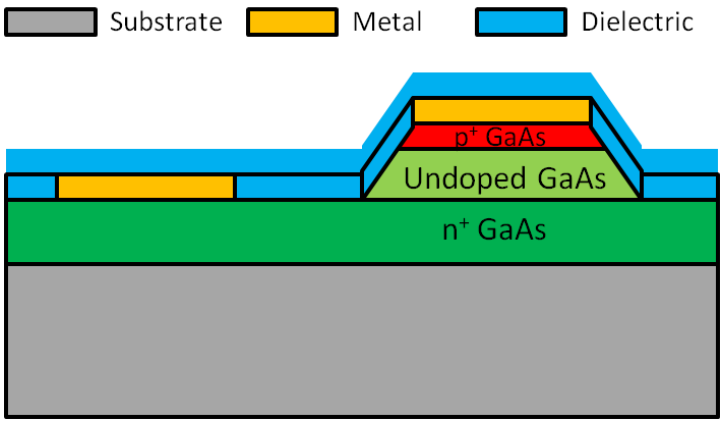

Figure 1.3. Simplified cross-sectional view of a GaAs p-i-n diode based on design in [10].

A GaAs p-i-n diode based SPDT switch design is reported in [10]. A simplified cross-sectional diagram of a p-i-n diode is shown in Figure 1.3. The core component in the

device is the p-type and n-type doped GaAs regions, separated by an undoped GaAs region. Based on p-i-n junction physics, the conductivity between the p and n terminals of the switch is controlled by the DC bias voltage, and this is how the switching activities are controlled. The design in [10] has shown an insertion loss of approximately 1 dB and an isolation above 35 dB up to 30 GHz, which indicates high performance and broadband capability.

The silicon-on-sapphire (SOS) technology, which utilizes a structure of a thin silicon layer on top of a sapphire layer on a silicon substrate, has provided higher performance in RF and microwave applications. Compared to traditional silicon processes, the SOS process is able to eliminate the parasitic capacitances generated from the bulk substrate, and therefore is preferred for high frequency operations. An example of a SOS CMOS RF switch design is proposed in [11]. The reported switch with an SP6T structure was able to provide an insertion loss of less than 1 dB, and an isolation above 40 dB up to 2.5 GHz, and a high power handling with a 1-dB compression (P_{1dB}) of 20 W (43 dBm), and an output third-order intercept point (OIP_3) above 70 dBm, which indicates good RF performance, linearity, and power handling capability.

Silicon-on-insulator (SOI) is another commonly used technology for RF integrated circuits. SOI based RF switches are designed and used in RF transceivers and other applications. SOI structure uses a stack with a thin silicon layer on top of a buried oxide layer on the handling wafer. Like SOS, this insulating structure is also used to reduce the issue with substrate parasitic coupling [12]. While GaAs and SOS technologies tend to

suffer from cost and integration disadvantages, SOI offers a lower cost and easier integration process into silicon based systems, while maintaining good performance.

One issue that is common to Si, SOI, and SOS FET-based devices is the relatively low breakdown voltage. In order for the switches to handle higher voltages without breaking down, the method of switch stacking is very commonly used. This method involves stacking multiple FET switches in series, and through the voltage distribution across the switches, a higher voltage or power can be handled [11, 13].

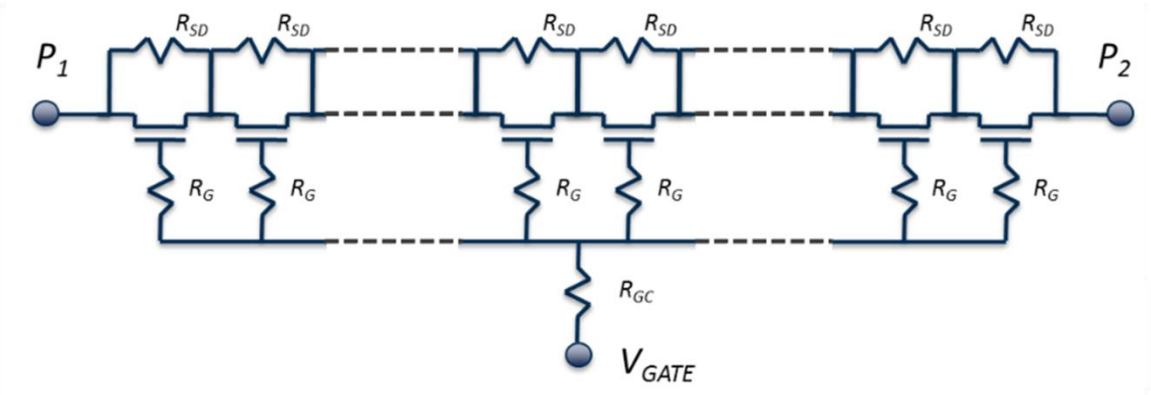

Figure 1.4. Schematic of a switch using stacking structure to handle higher power [13].

A simplified structure of switch stacking is shown in Figure 1.4. With multiple FET switches stacked in series, the voltage distribution allows high power handling capability. The number of stack switches also provides a degree of freedom in the design, which should be enough to handle the specified power, but also ensures a good balance between the insertion loss and isolation based on the specifications. While this method effectively mitigates the issue with device breakdown under high voltages, it introduces a level of

non-linearity. Although the FET switches are ideally modeled with minimal gate and substrate current leakage, the stacking structure of multiple FETs would make the leakage issue more problematic, as the current flowing through each device is not equal due to the leakage. This eventually results in an unevenly distributed voltage across the devices, which causes non-linearity in the switch, especially at high power levels [14].

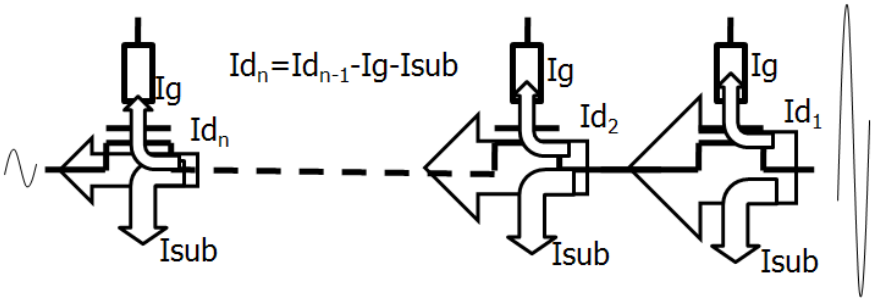

Figure 1.5. Voltage imbalance caused in switch stacking due to different current flowing through each transistor [14].

While solid-state device based switches share the common issue of power handling and linearity limits, micro-electromechanical system (MEMS) based RF switches provide an alternative approach. MEMS switches are typically based on micromechanical membranes, which are actuated through electrostatic control [15]. The mechanical membrane, typically a cantilever beam or a bridge, is used as the control element in the MEMS switch. Electrostatic force generated by the DC bias voltage is used to actuate, or pull in the membrane to achieve contact between two metal electrodes and therefore turn on the switch. When the DC bias voltage is removed, the membrane separates from the contact and the switch is turned off. RF MEMS switches based on a cantilever beam

structure have been reported with successful switching activities and good RF performance [16, 17]. In order to reduce the DC bias voltage required for switch actuation, alternative structures have been proposed. A bridge structure design with meandering supports of the membrane has shown a DC bias voltage as low as 9 V to successfully actuate the MEMS switch [18]. Other than ohmic RF MEMS switches, where the metal electrodes come in direct contact when the switch is turned on, a capacitive RF MEMS switch has a structure where the membrane forms a capacitor with the bottom metal, and is functional at high frequencies [19].

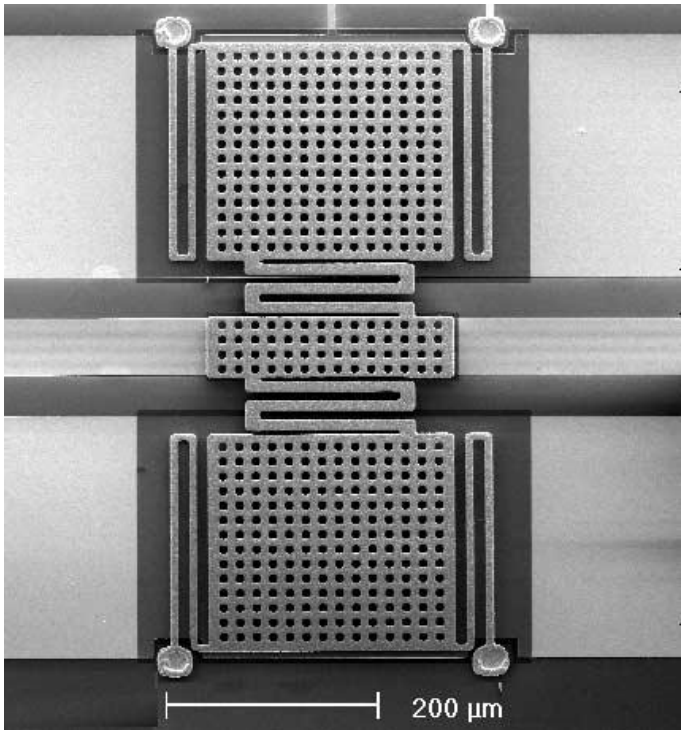

Figure 1.6. An RF MEMS switch with a low spring-constant bridge structure [20].

A top view of an RF MEMS switch is shown in Figure 1.6 [20]. The top membrane in the switch is built into a bridge structure that is anchored at the four corners. The membrane is connected to the anchors through four folded beam in order to reduce the spring constant, which reduces the pull-in voltage required. The membrane has a top and bottom pull-in electrodes, and a center capacitive area that comes in contact with the bottom structure when an actuation voltage is applied. Since RF MEMS ohmic switches use mechanical structures where metal electrodes come in contact to achieve switching, they tend to provide very low insertion loss and high isolation compared to solid-state transistor or diode based switches. However, due to the mechanical structures and mobile components, the fabrication process is usually complicated and has relatively low yield, and the size of MEMS devices are usually much larger compared to transistors or diodes. Therefore MEMS-based RF switches have the limitations of high cost and non-ideal integration compatibility.

1.3. Phase Change Materials in Switching Applications

A new approach of RF ohmic switch implementation has been introduced with the study of phase change materials. Phase change, or resistance change materials, refer to a class of chalcogenide compounds that possess two phases at room temperature: a crystalline phase and an amorphous phase, which can be thermally driven from one state to the other [21]. One of the most significant differences between the crystalline and amorphous states is the drastically different electrical resistivity, which can be several orders of magnitude [22]. The phase transition property and the difference in electrical

resistivity makes phase change material an excellent switching element that can potentially be used in RF and microwave applications.

Phase change materials were first discovered and identified as a type of disordered semiconductors that can experience rapid and reversible transitions between a highly resistive state and highly conductive state [23]. Phase change materials that have been discovered include chalcogenide compounds consisting of a combination of tellurium (Te), germanium (Ge) and/or antimony (Sb) with doping elements such as indium (In), oxygen (O), selenium (Se), tin (Sn), *etc*. Although they do not behave the same under certain thermal and electrical conditions, they share the same property of phase transitions. Because of this property, phase change materials have been used to develop non-volatile memory modules for the past few decades in response to the scalability challenges of non-volatile memory based on floating gate and other technologies [24, 25]. Phase change materials can be scaled down to very small resistive vias, which satisfies the size requirements for memory cells. Their resistivity ratio between the amorphous and crystalline states makes it easy to store information, which ensures good functionality of the memory designs. More details about phase change materials and their applications in non-volatile memory are discussed in the following chapter.

With the same properties that are being used in memory applications, phase change materials are also showing great potential in switching modules for RF and microwave applications. Their low electrical resistivity in the crystalline state ensures low resistance when connecting RF terminals, which is the key to low insertion loss for switch designs. The high electrical resistivity in the amorphous state, on the other hand, ensures high

isolation between RF signal transmission terminals. Compared to solid-state based switches, phase change material based switches offer higher performance, and with the simple resistive via structure, they offer higher integration density than transistor based switches. Compared to MEMS based RF switches, they have the advantages of small size and simple structure, which essentially means easier fabrication process, lower cost, and better integration compatibility. Because of the great potential of phase change materials and their successful insertion non-volatile memory applications, phase change material based RF switches offer a novel and promising solution to switching applications for integrated circuits and systems for the "More-than-Moore" era.

1.4. Research Objectives and Contributions

The main objective of this work is to develop GeTe-based ohmic switches for RF applications with RF performance that is comparable to or better than existing solid-state and MEMS-based RF switches. The performance requirements include good insertion loss and isolation value in the target frequency range, good power handling capability and high linearity performance, as well as reliable switching performance.

This research work to develop a GeTe phase change material based ohmic switch for RF applications has achieved the following milestones:

- Design and fabrication of four-terminal GeTe-based phase change RF switches using direct heating or indirect heating methods: Both types of switches have been measured to have an insertion loss below 0.5 dB and isolation above 13 dB through the frequency range from DC to 20 GHz. The figure-of-merit cut-off

frequency (f_{co}, defined as $1/(2 \cdot \pi \cdot R_{on} \cdot C_{off})$) is above 4 THz. The switches have shown reliable switching activities of up to hundreds of cycles. The four-terminal switch design using direct heating method was the first to be demonstrated in the literature and has been patented.

- Development of a thermoelectric model to analyze the electrical and thermal response of the switches at varying RF power levels and with different heating power levels: This modeling method is used to explore the linearity performance and power handling capability of the switch. Corresponding 1-dB compression point (P_{1dB}) and input third-order intercept point (IIP_3) measurements are taken to verify this model.
- Design and fabrication of a reconfigurable bandpass filter for X-band applications using the GeTe phase change material based RF switches: This design uses the GeTe switches as a proof of concept to show their application in reconfigurable RF modules. The bandpass filter has two operating bands, both of which show an insertion loss of less than 3.2 dB, a bandwidth around 500 MHz and an estimated quality factor of 59.
- Material study of GeTe with the assistance of scanning electron microscopy (SEM), transmission electron microscopy (TEM) and other optical measurements and imaging methods to better understand the phase transition process of GeTe on the atomic level as well as the cause of phase transition failures.

1.5. Organization of Dissertation

This dissertation is divided into five chapters to discuss the related research work in different perspectives. Chapter 1 of the dissertation provided an introduction of Ohmic switch applications in RF modules, and the motivation behind the development of novel RF switches using phase change materials. Chapter 2 discusses the properties of phase change materials. It summarizes the discovery and development process of chalcogenide phase change materials of different types, and their applications in non-volatile memory modules. It then specifically discusses GeTe properties reported in literature as well as those characterized during the course of this Ph.D. research. It also provides detailed observation of GeTe phase transition behavior and its corresponding electrical and optical property change. Chapter 3 discusses detail design and development procedure of RF ohmic switches based on GeTe. In Chapter 3, different types of GeTe-based RF ohmic switches are shown and their structure, principle of operation, design procedure, fabrication process and performance evaluation are detailed. Chapter 3 also provides the thermoelectric modeling method for the GeTe RF switches that relates the thermal properties of the switches to their electrical properties. Testing and characterization results of the switch reliability study are also shown in Chapter 3. Chapter 4 of this dissertation presents a reconfigurable bandpass filter using GeTe RF switches for X-band wireless applications. In Chapter 4, the design process, device structure, fabrication process, and the measurement results of the phase change filter are provided to prove the applicability of phase change switches in reconfigurable RF modules. Finally, Chapter 5

of this dissertation summarizes the achievements and contributions of this research work, and it also provides possible future research directions for continuation of this research.

CHAPTER 2 Chalcogenide Phase Change Material

Over the past few decades, chalcogenide compounds, or chalcogenide materials have received increased attention for consumer electronics applications. A series of shared special properties among various chalcogenide compounds have been observed. Chalcogenide compounds are most recognized by their interchangeable states at room temperature. Typically, a chalcogenide material possesses two or more states at which it exhibits different material properties. Some of the most studied properties of chalcogenide compounds include material crystallinity, electrical resistivity, dielectric relative permittivity, and optical index of refraction. One of the earliest reports on such material behaviors is by Ovshinsky [23], in which various materials called disordered semiconducting materials were observed to experience rapid and reversible transitions between a highly resistive and a highly conductive state effected by an electrical field. One reported experiment in [23] used a sputtered film of an amorphous semiconductor containing 48 at.% tellurium (Te), 30 at.% arsenic (As), 12 at.% silicon (Si) and 10 at.% germanium (Ge). The specimen was structured with two carbon electrodes where voltage signals of different frequencies were applied. The measurements showed repeatable switching activities between a highly resistive state and a highly conductive state, achieved by crossing above or below a holding voltage, V_h, across the electrodes.

Since [23], more efforts have been made to achieve phase transitions of chalcogenide materials through different measures and to systematically categorize and analyze the

phase transition activities of these materials. Reported methods to achieve repeatable phase transitions within chalcogenide materials, other than application of electrical field mentioned in [23], include laser (light) excitation [26], surface-nucleation through melting and quenching [27], *etc*. In the early reported works, the materials used in the experiments consisted of an element combination of arsenic (As), germanium (Ge), tellurium (Te), antimony (Sb) and/or sulfur (S).

More phase transition experiments and analysis on chalcogenide materials have since been reported [28] [29] [30] [31]. The most commonly recognized chalcogenide materials with the phase transition property include semiconductor compounds with Ge, Sb and Te, with various combinations and stoichiometric percentages. Due to the state transitions between a highly conductive state and a highly resistive state, this type of chalcogenide materials is also known as phase change, or resistance change materials.

2.1. GST Based Phase Change Materials

GST, or GeSbTe, refers to the type of phase change materials with the combination of Ge, Sb and Te. Common examples of this family of phase change materials include germanium telluride (Ge_xTe_y, or GeTe), germanium antimony telluride ($Ge_xSb_yTe_z$, or GeSbTe) and germanium antimonide (Ge_xSb_y, or GeSb). Most GST-based materials possess two states at room temperature, known as the crystalline state and the amorphous state, distinguished by their very different material crystallinity [22]. In the crystalline state, they tend to exhibit very low, metal-like electrical resistivity, while in the amorphous state, they usually behave like dielectric materials with very high electrical

resistivity and varying dielectric constants [32]. Other differences such as optical properties can also be observed. These differences between the two states are due to the different atomic structures [33]. Phase transitions between the two states within these materials are essentially achieved by thermal actuation, with the material heated up to a certain temperature, followed by a cooling process with a certain cooling speed [21]. Typically, the phase transition process from the crystalline state to the amorphous state (also known as amorphization process) involves a heating process with a high peak temperature, in some cases above the material's melting point, and a cooling process that is relatively fast. The phase transition process from the amorphous state to the crystalline state (also known as crystallization process) has a relatively lower peak temperature, normally within what is known as the crystallization temperature zone, and a lower cooling speed in comparison, to allow the process of crystallization [34]. A graphic illustration and comparison of the temperature profiles for phase transitions in both directions is shown in Figure 2.1.

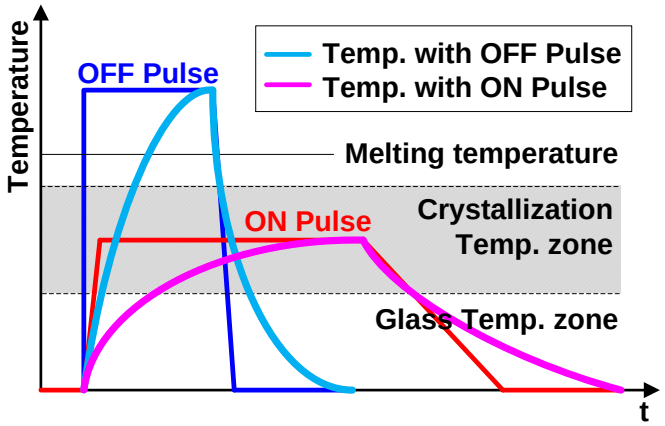

Figure 2.1. Timing diagram of typical temperature profiles for chalcogenide phase change materials to achieve phase transitions between the crystalline and amorphous states.

Due to the large electrical resistance ratio [22] [32] and fast phase transition time [34], phase change materials have been used for various applications where fast changes of electrical resistances can be conveniently utilized. The earliest and most common applications of phase change materials include non-volatile memory [35] and switching devices [36], which are detailed below.

2.2. Phase Change Material Applications in Non-Volatile Memory

Optical storage applications based on the reversible phase transformation between the crystalline and amorphous states of chalcogenide materials were first studied in the early 1970s [26]. Earliest efforts on realizing phase change reversible storage have been made using materials such as $TeGeSnO_x$ [37], TeGeSnAu [38], InSe [39], GeTe [35] and GeSeTe [40]. In order to achieve reversible phase transitions from/to the crystalline state to/from the amorphous state, most commonly reported methods include laser induction, with a more rapid crystallization/amorphization process, and heating state induction, which can be realized by either the application of electrical pulses or in some cases programmed ovenization.

At the early development stages of phase change memories, laser induction was very commonly used as the phase transition method [38] [39] [41] due to the ease of the power delivery process and effectiveness in phase transitions. The typical power level of the applied laser pulses has been within 100 mW, with a pulse duration of less than 500 ns [39] [41], depending on the structure of the memory cell, the phase change material used as the recording film, and whether the phase transition is crystallization or amorphization.

Normally a dual beam configuration is required in the structure, since the crystallization time of the phase change material is usually less than 100 ns, typically around 50 ns, and the amorphization time is between 200 ns and 500 ns; the time difference is too large for the same pulse duration of laser to be used for both phase transition processes. In the example reported in [41], though, where a stoichiometric compound of $GeSb_2Te_4$ was used as the phase change material, a laser pulse duration of 50 ns was used for both directions of phase transitions, with the crystallization process at a power level of 8 mW, and the amorphization process at 20 mW. This reported prototype was used to perform direct overwriting cycle tests on a revolving disk system for 10^5 times using a single laser beam configuration, proving the material applicable to high data rate direct over-writable disk media. This revolving disk based structure has individual phase change memory cells laid out on the disk tracks, with the phase change recording film sandwiched by protective layers on both the top and bottom sides. Then specific adjacent layers are designed to suit the laser light pulse induction setup, typically with a light curing resin on the top or bottom of the recording film, and the laser light pulses applied on the opposite side [39] [41]. A typical layer configuration for phase change optical storage systems is shown in Figure 2.2.

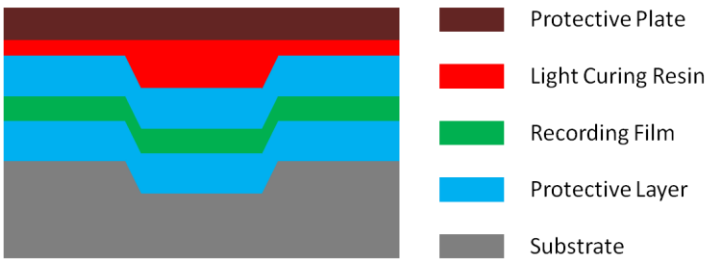

Figure 2.2. Cross-sectional schematic of a typical phase change optical disk with laser induction as the phase transition method [39] [41] [42].

Phase change optical storage designs based on different materials have since been reported, with modifications in the exact structure and procedure for phase transitions, such as the laser pulse durations, power levels, *etc*. [24] [43]. The progress in realizing optical storage media with phase change materials and its issues have also been analyzed and summarized [44]. Most phase change materials used in optical memories are tellurium based chalcogenide compounds, among which GeSbTe, or GST being the most popular choice in terms of performance parameters such as the optical and electrical property difference in the crystalline and amorphous states, phase transition speed, and laser induction power consumption [42] [24].

Optically programmable storage devices using chalcogenide phase change materials and their applications in digital computers as non-volatile memory attracted significant interest in the 1980s and early 1990s. Rewritable optical memory disks using a laser induced structural phase change in a chalcogenide material was commercialized and produced. But in order to further improve the density and performance, phase change memory using electrical heating methods was also designed and proposed. The example reported in [45] presented a non-volatile phase change memory with high integration density and high performance. The chalcogenide compound GeSbTe was used in the design, as it had a crystallization speed of under 50 ns, which was practical in building high-speed memory cells. The alloy had a glass transition temperature above 300 °C, and a melting point above 600 °C. Unlike optical memory disks using these chalcogenide alloys which rely on the differences in the optical characteristics between the crystalline and amorphous states of the materials, this electronic memory relied on the changes in

electrical properties of the material upon phase transitions. The measured change in electrical conductivity was up to 6 orders of magnitude between the crystalline and amorphous states.

In [45], the electronic memory cells were constructed with a matrix of isolation transistors, which could provide power to a memory cell in order to melt a portion of the chalcogenide alloy. The transistors were connected to the array to form the memory matrix, with a heat sinking substrate and metallization to provide good thermal insulation and heat dissipation in order to avoid cell cross-talk. A simplified schematic of the memory cell layout is shown in Figure 2.3.

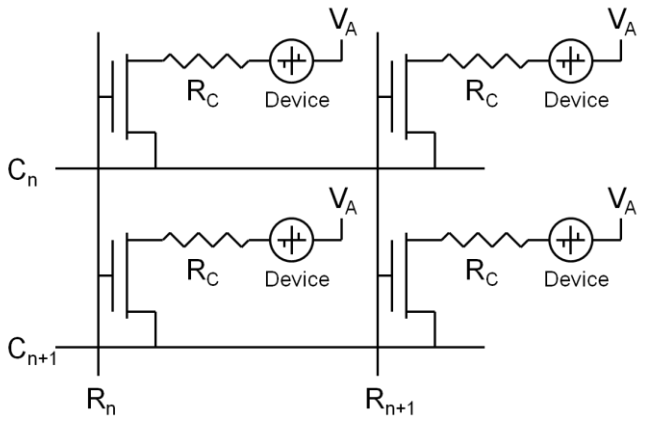

Figure 2.3. Simplified schematic illustration of a memory array circuitry built using chalcogenide alloy, showing four adjacent memory cells [45].

The read and write activities of the memory cells is achieved by the applied voltage to the memory array V_A, together with the row and column lines R and C. In the read mode, a low voltage V_A is applied to the device, while the access transistor is activated through the R line. If the chalcogenide alloy is reset to the amorphous state, only a small current will pass through the transistor and read by the C line. And if the material is set to the

crystalline state, a larger current, which is limited by the resistance R_C, will be read through the C line. In the reset mode, where the chalcogenide alloy needs to be reset to the amorphous state, a high voltage V_A is applied to the cell while the transistor is biased to conduct sufficient current to heat up the material above its melting temperature. When the current is removed, the material will rapidly quench into the amorphous state, given that the thermal time constant of the device has been properly designed to allow a fast cooling speed. In the set mode, a high voltage V_A is also applied but the transistor is biased to allow a smaller current so that the material is heated up, but not melted. The duration of the voltage pulse must be sufficiently long to allow the nucleation and formation of the crystal.

Figure 2.4. Cross-sectional diagram of the phase change via in the memory cell [45].

The design from [45] shows successful integration of a chalcogenide phase change material into electronic memory cells. The structure of the phase change device is also simple, with the chalcogenide alloy sandwiched by top and bottom contacts. The via is defined by etching through the insulating layer, obtaining a circular pillar shaped via. A cross-sectional diagram of the device is shown in Figure 2.4. This design ensured a simple device structure that is integration compatible to the memory matrix and it showed

performance comparable to existing memories such as dynamic RAM, flash memory, *etc*., with great potential in terms of density, speed, and ease of fabrication.

With these promising results being reported, more phase change electronic memory designs featuring mainly GST and GeTe have been reported with both structural and performance enhancements. Efforts have also been made to study the memory device at the atomistic level using both electronic measurements and electron microscopy to physically model the GST [25] and GeTe [46] material structures in different phases and during their phase transitions. Atomistic models of phase change materials have been proposed to account for their electronic behaviors and temperature response [47]. By the time of early 2000s, chalcogenide material-based phase change electronic memories were commercialized and showed very competitive performance, with a typical cell set/reset time within 50 ns, and number of phase transition cycles over 10^{12} [48]. Special heating structures have also developed to further enhance the reliability of the memory cells. From a cell structure similar to the one shown in Figure 2.4 [45], for example, a modification with a titanium nitride (TiN) heater layer was introduced in contact with the phase change material layer, with certain levels of oxidization in the TiN film, and the performance was compared and evaluated among the variations, proving that an oxidized layer of TiN in contact with the phase change material layer helped with the stabilization of the memory cells. There have been other reported designs of phase change memories with new structures such as phase change material nanowires [49] and hybrid memory structure combining a phase change memory and a DRAM buffer to improve the performance [50]. With the great success that the chalcogenide phase change memory has

achieved [51], phase change materials have drawn attention for other applications, such as switching applications [36] [52]. Among different types of phase change materials used for memories, phase change material based ohmic switches have most commonly used GeTe as the phase change material [53].

2.3. GeTe Phase Change Material and Switching Activities

Germanium telluride (Ge_xTe_y, or GeTe) with some similar properties to other GST based chalcogenide compounds, consists of only Ge and Te, with different possible stoichiometric combinations. Early material studies identified GeTe as a type of semiconductor based on its electronic behaviors, and it was recognized to possess two stable and interchangeable states, amorphous and crystalline, at room temperature. Further studies have been performed on GeTe regarding its atomistic structures, phase transition mechanism, electrical and optical properties as well as the material growth. The phase transition property of GeTe has been put into use in multiple application areas including non-volatile memory and ohmic switch applications.

2.3.1. Amorphous versus Crystalline GeTe

Like other chalcogenide compounds, GeTe has been known to exhibit amorphous and crystalline states, stable at room temperature. The crystalline form of GeTe can vary in structure, depending on the growth method and conditions [54]. According to the study reported in [54], GeTe films can be prepared with different states by controlling the deposition conditions such as the temperature, applied electric field on the substrate, seed

layer structure and deposition method (*i.e.*, evaporation, sputtering, epitaxial growth). Deposited GeTe films are in polycrystalline state when they are deposited at a temperature above 130°C and below 250°C. When deposited at temperatures above 250°C, a crystalline state GeTe film with a NaCl structure (or fcc structure) can be grown. If the GeTe film is grown on a substrate of NaCl or mica as the seed layer, and the deposition temperature is near 250°C, a crystalline state GeTe film with the rhombohedral structure is formed. GeTe films deposited at a temperature below 130°C are found to be amorphous. A graphic illustration of different GeTe states is shown in Figure 2.5. Similar results have also been reported in [31] and [33]. Discrepancies across different reported works could be due to in-lab film preparation process variations.

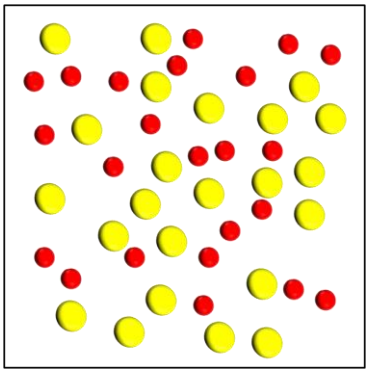

(a)

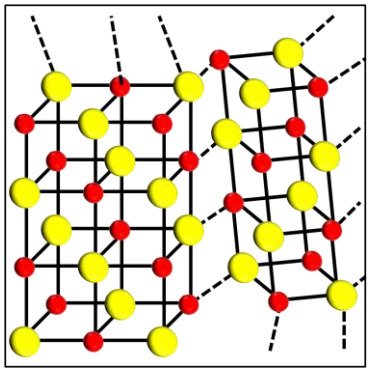

(b)

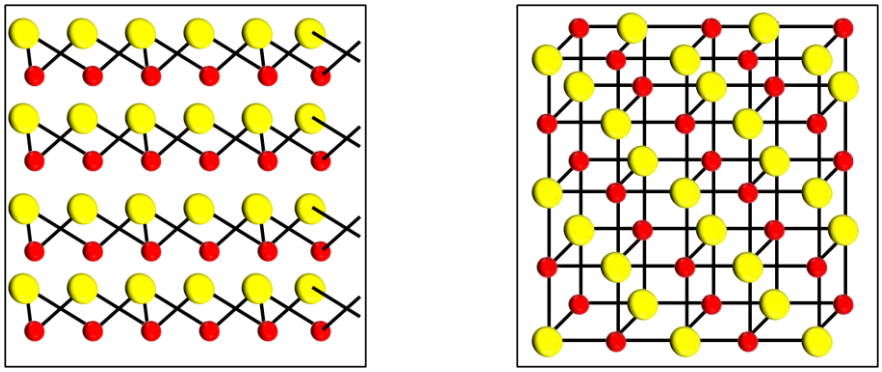

(c) (d)

Figure 2.5. Atomistic structure diagrams of GeTe at different states according to the results from [54]. The smaller red dots represent Ge atoms and the larger yellow dots represent Te atoms. (a) Amorphous GeTe when deposited at a temperature below 130°C; (b) polycrystalline GeTe, with multiple crystalline orientations, when deposited at a temperature between 130°C and 250°C; (c) single-crystalline GeTe with a rhombohedral structure, when deposited at a temperature around 250°C, typically grown on a NaCl or mica substrate as the seed layer; (d), single-crystalline GeTe with a NaCl (or fcc) structure, when epitaxially grown at the temperature above 250°C.

Based on the most distinct electrical and optical properties that GeTe films exhibit at different atomistic states, they can be generally categorized into the crystalline (single-crystalline or polycrystalline) state and the amorphous state. In terms of electrical resistivity, crystalline state GeTe films exhibit a low, metal-like resistivity at room temperature, which generally changes with temperature very slowly and linearly at low temperature (near or below room temperature), and more rapidly at higher temperatures (close to the crystallization temperature); amorphous state GeTe films have a much higher electrical resistivity at room temperature in comparison, usually several orders of magnitude higher than that of the crystalline GeTe, and the resistivity in the amorphous phase changes much more rapidly with a changing temperature [55]. Another very

important factor that affects the electrical resistivity of the GeTe films in either state is the stoichiometric ratio between Ge and Te in the GeTe alloy-like compound. As reported in both [22] and [32], GeTe films with variable composition ratios exhibit very different crystalline and amorphous state electrical resistivity values. In each of the GeTe film with a certain composition ratio, the amorphous versus crystalline state typically shows an electrical resistivity ratio of 3 – 6 orders of magnitude. For readers' convenience, a temperature response chart of electrical resistivity of GeTe films with different composition ratios from [22] is used and shown in Figure 2.6.

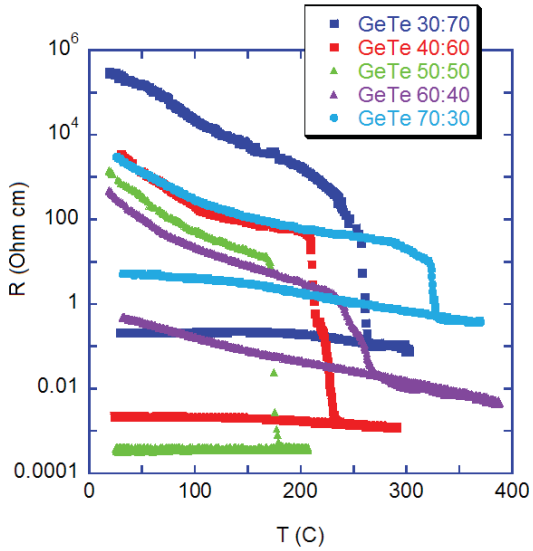

Figure 2.6. Temperature response of electrical resistivity of GeTe films with different composition ratios [22].

The GeTe films shown in Figure 2.6 have a Ge atomic percentage from 30 at.% to 70 at.%. It can be seen that $Ge_{30}Te_{70}$, $Ge_{40}Te_{60}$ and $Ge_{50}Te_{50}$ films have a relatively larger amorphous to crystalline electrical resistivity ratio than $Ge_{60}Te_{40}$ and $Ge_{70}Te_{30}$ films, and $Ge_{40}Te_{60}$ and $Ge_{50}Te_{50}$ films have a much lower crystalline-state electrical resistivity than

$Ge_{30}Te_{70}$, $Ge_{60}Te_{40}$ and $Ge_{70}Te_{30}$ films. Figure 2.6 also reflects the phase transition behavior between the crystalline and amorphous states, which will be discussed in the next section.

Other than the electrical resistivity, optical properties of GeTe films at the crystalline and amorphous states are also significantly different. Due to process variations during in-lab film preparation and differences in crystallinity of GeTe films, reported works on GeTe film optical properties show slight discrepancies, while following a general trend in terms of optical behaviors in the crystalline and amorphous states. The observations in [56] state that at the wavelength of 1.5 μm, the crystalline state GeTe film shows a relatively higher refractive index (n = 5.5) than the amorphous state GeTe film (n = 4.2). Across the wavelength range from 0.83 μm to 2.5 μm, the amorphous GeTe film (thickness of 9300 Å) shows a much higher transmittance than the crystalline GeTe film (thickness of 5800 Å). The observed trend is in good agreement with the results in [57] and [58], which states that the amorphous GeTe film shows a lower refractive index and extinction coefficient, as well as a higher transmittance than the crystalline state in the mid-IR and near-IR wavelength range. This optical property is used in [57] to build an optical modulator with an integrated heater as the phase transition vehicle. Figure 2.7 shows the refractive index measurements through ellipsometry for $Ge_{50}Te_{50}$ films in crystalline and amorphous states for visible light and near-IR ranges. The real and imaginary components of the refractive index of GeTe are quite different between the crystalline and amorphous states.

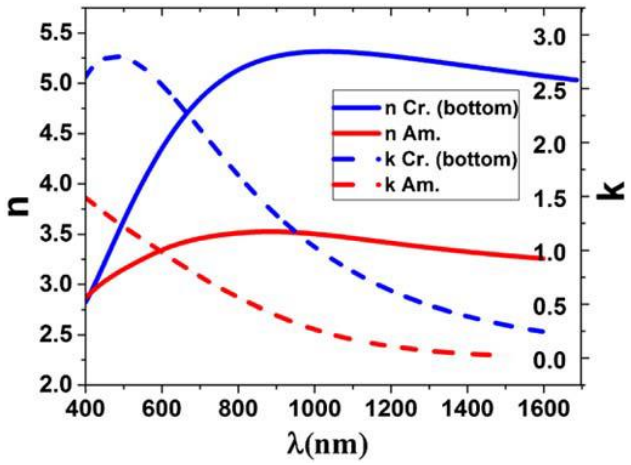

Figure 2.7. Optical refractive index of GeTe in amorphous and crystalline state for visible and near-IR frequency ranges derived from ellipsometry measurements [57].

Exploring the reflective index is useful in estimating the permittivity of GeTe film in the amorphous state. Since GeTe behaves like a dielectric insulating material in the amorphous state, the optical refractive index and the relative permittivity can be related through Maxwell's Equations:

$$[n(\omega) + i \cdot k(\omega)] = \sqrt{\varepsilon_r(\omega)/\varepsilon_0},$$

where n and k are the real and imaginary parts of the reflective index, ε is the electric permittivity of the medium, ε_0 is the electric permittivity of vacuum, and ω is the angular frequency. This is very important in estimating the capacitive component contributed by the GeTe in the amorphous state in the RF switches, as discussed in the next chapter.

2.3.2. Phase Transitions between Amorphous and Crystalline States of GeTe

While both the amorphous and crystalline states of GeTe films can be found at room temperature, phase transitions between the two states can be achieved at elevated temperatures. As mentioned before, the temperature change during a phase transition process of phase change materials can be divided into a heating process and a cooling process. The transition from the amorphous to the crystalline state is known as crystallization, and the phase transition from the crystalline to the amorphous state is known as amorphization.

In order for an amorphous GeTe film to experience the crystallization process, the temperature needs to be elevated for the nucleation process to happen within the film. As discussed in [54], at an elevated temperature (above the crystallization temperature), the nucleation process will start to take place within the GeTe film rapidly via multiple nucleation centers, and eventually expands across the entire volume of the GeTe film. When the film is cooled down to room temperature, the crystallization process is complete and the crystalline GeTe film is formed. The crystallization temperature, at which nucleation happens within the GeTe films, can vary according to factors including film preparation conditions, substrate properties [54], and GeTe stoichiometric ratio [59]. Most reported crystallization temperatures are above 145°C.

In order to monitor the formation of crystalline structure within the GeTe films during the crystallization process, an X-ray diffraction (XRD) *insitu* measurement is commonly used. Intensity peaks shown in the XRD measurements can indicate the formation of crystallized structures, and multiple peaks at the same time means multiple crystalline

orientations within the GeTe film. A series of XRD measurements is reported in [22] on GeTe films with five different composition ratios. For readers' convenience, the XRD measurement results are shown in Figure 2.8.

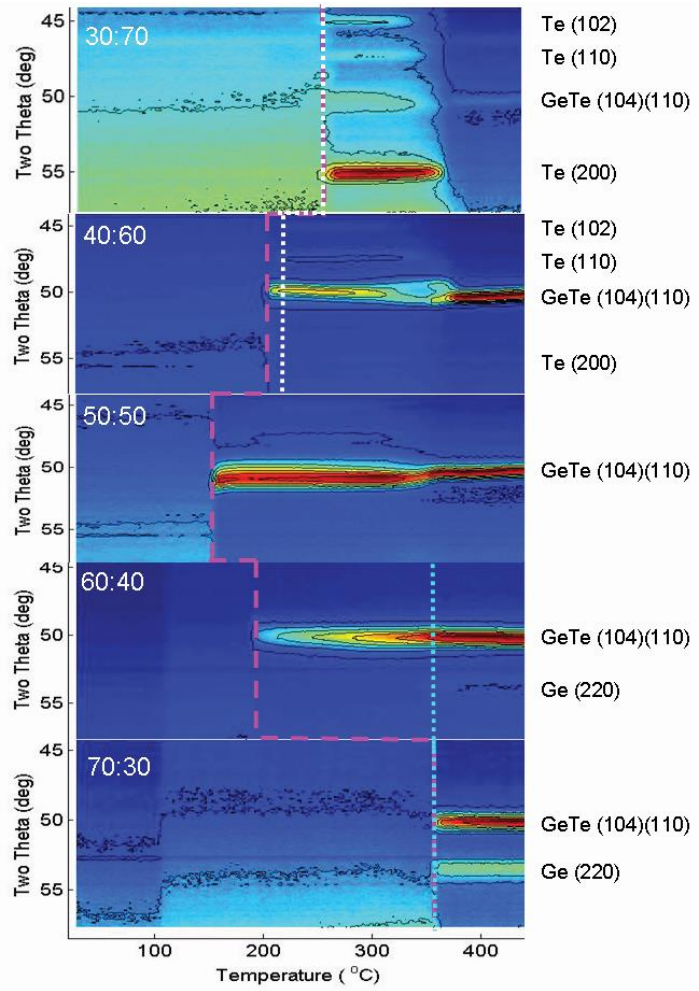

Figure 2.8. XRD measurements as a function of increasing temperature for GeTe films with different composition ratios [22].

From the XRD measurement results in Figure 2.8, two-theta (2θ) peaks in all five type of GeTe films appear after the corresponding crystallization temperatures are

reached, which indicate that a certain level of crystalline structure is formed in all GeTe films. Among these five samples, $Ge_{50}Te_{50}$ has the lowest crystallization temperature of approximately 180°C, and $Ge_{70}Te_{30}$ has the highest crystallization temperature of approximately 360°C. The crystalline orientations corresponding to each peak are also listed in the figure, indicating that most GeTe films crystallized through this annealing process are showing a polycrystalline structure. In the case of $Ge_{50}Te_{50}$, an initial 2θ peak at about 50° appears above 180°C, and another sharper peak at the similar angle appears above 360°C, which could potentially indicate different orientations that have different crystallization temperatures and coinciding 2θ peaks.

Unlike the crystallization process, the amorphization process of GeTe films take place under a different annealing temperature profile and has a different mechanism. While it also requires a heating and a cooling process, the amorphization process of GeTe films typically needs a higher peak temperature that is well above the crystallization temperature, and is often preferred to be above the melting temperature of the GeTe film. The cooling process during amorphization needs to be even faster than that for crystallization, so that the nucleation process does not have enough time to take place and after the temperature is quickly dropped back to room temperature, the atoms in the film are locked in their disordered state, without being able to nucleate unless temperature is raised again. Thus, the amorphous GeTe film is formed and the amorphization process is complete. The crystallization time is typically several times slower than the amorphization time (Figure 2.1).

2.3.3. GeTe Fabrication Process for RF Switch Applications

This section will be focused on the results and findings from the GeTe film preparation process, sample annealing process, as well as other material study experiments that have been performed here at the University of Michigan. Process variations play a significant role in the final physical properties of the film. Therefore, while the results reported in this section is generally in agreement with the results from reported works summarized in the previous sections, differences in details can be seen.

2.3.3.1. GeTe Film Deposition Process and Basic Electrical Properties

In this work, GeTe films are prepared at the Lurie Nanofabrication Facility (LNF) at the University of Michigan. The thin-film deposition process of GeTe, both for film property characterizations and for RF Ohmic switch fabrication, is performed on passivated silicon substrates. The deposition of GeTe films are done by sputtering using a Lab 18 Modular Thin Film Deposition System manufactured by Kurt J. Lesker Company. The sputtering process uses an RF power enabled plasma sputtering source on a single target of $Ge_{50}Te_{50}$ alloy, and is performed under a high vacuum chamber condition, with a base chamber pressure of 3×10^{-6} Torr or lower. The RF power used for sputtering varies from 40 W to 70 W, without the presence of DC voltage bias. The partial pressure during the sputtering process varies from 3.5 mTorr to 5 mTorr. The sputtering process is done at room temperature. In order to optimize the sputtering process to obtain GeTe films with best quality, the base chamber pressure, the RF power and the partial pressure have

been varied in the sputtering experiment in order to find a combination that yields the best result.

The as-sputtered GeTe film is in the amorphous state, with an electrical resistivity higher than 0.1 Ω·m. Phase transition from the amorphous to the crystalline state is achieved by a standard ovenization at 200°C for approximately 30 min. The temperature ramping rate from room temperature to 200°C is about 6°C/min. After successful crystallization, the GeTe film exhibits the crystalline state, with an electrical resistivity lower than 5×10^{-5} Ω·m, which shows an amorphous/crystalline resistivity ratio higher than 2×10^{3}. Other than the standard ovenization used for crystallization, different methods have also been characterized to achieve higher effectiveness of phase transition. Both the GeTe film sputtering process and the crystallization process have been proven to directly affect the crystalline quality of the GeTe film after the as-deposited amorphous GeTe is transitioned into crystalline GeTe.

During the GeTe sputtering process, the sputtering speed, or film deposition rate, can affect the film quality. Generally, a higher deposition rate tends to result in a better film quality with lower electrical resistivity after crystallization and less introduced impurity in the film [60]. The measured film deposition rate of GeTe films varies from 0.5 Å/s to 1.8 Å/s, depending on the combinations of sputtering conditions. With the RF sputtering power varying from 40 W to 70 W, and the partial sputtering pressure between 3.5 mTorr and 5 mTorr, a series of measured deposition rates are plotted in Figure 2.9. The trend shows that the combination of a higher power and a lower partial pressure tends to yield a higher deposition rate. The electrical conductivity of GeTe film samples of the same

thickness after crystallization are plotted in Figure 2.10, which shows a very similar trend, indicating that higher film deposition rates result in higher crystalline state conductivity of GeTe films. The reason that the GeTe film sputtered at 3.5 mTorr with a power of 70 W shows a lower conductivity than the sample with 60 W could be due to impurity in the process chamber that has been excited at a higher RF power and sputtered into the film.

Since the crystalline GeTe film also exhibits semiconductor like properties, Hall Effect measurements were taken to identify the semiconductor type. The deposited and crystallized GeTe films are measured to be p-type semiconductors, with a hole concentration of $1.2 – 1.5 \times 10^{21}$ cm^{-3}, and a mobility of $2 – 5$ $cm^2/V{\cdot}s$.

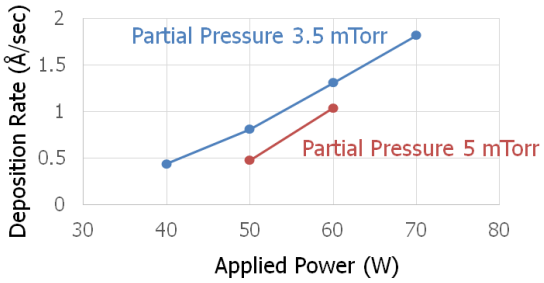

Figure 2.9. Measured deposition rate of GeTe films at different RF power levels and different sputtering partial pressures in the chamber.

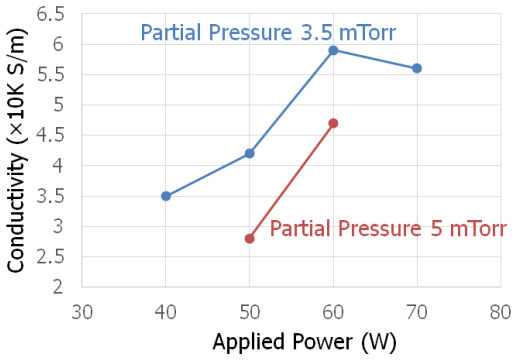

Figure 2.10. Measured electrical conductivity of GeTe films after a standard crystallization process versus the sputtering RF power at different sputtering partial pressures.

2.3.3.2. GeTe Annealing Process and Crystallization Optimization

The deposited GeTe are annealed using a standard ovenization process. Multiple samples of GeTe films are tested under the ovenization process with various peak temperatures to determine the crystallization temperature of the GeTe film. Based on this study, GeTe starts to crystallize at temperatures above 180°C. While the crystallization temperature is in good agreement with [22], the electrical conductivity of GeTe measured after crystallization is about 5 to 10 time lower in many samples, which indicates poor crystalline film quality. In order to improve the film quality and reduce the electrical resistivity of crystalline GeTe films, further efforts have been made to optimize the annealing process parameters, including the annealing temperature, annealing duration and oven environment (pressure, air/N_2 gas, *etc*.). It has been found out that a low-pressure annealing process (< 250 mTorr) with a N_2 based oven environment tends to result in the best crystalline GeTe film quality. This is possibly because in air, GeTe is prone to oxidization, which results in the formation of nano-crystalline structures consisting of GeO_x and TeO_x. The reduced oven pressure also contributes to reduced chance of oxidization.

After the optimal oven conditions for GeTe crystallization has been characterized, the crystallization temperature is determined by comparing the quality of GeTe film samples crystallized with different crystallization temperatures under the same oven condition described above. From the lowest crystallization temperature of 180°C that has been observed to be able to crystallize the GeTe films, temperature is varied from 180°C to 350°C. All of the GeTe film samples are annealed in a 250 mTorr low-pressure N_2

environment, with a temperature ramping rate of approximately 10°C/min, and a peak temperature dwelling duration of 30 min. The electrical resistivity of the samples after annealing are measured and compared. The measured electrical conductivity of GeTe thin films crystallized under different annealing temperatures is shown in Table 2.1.

Table 2.1. Electrical conductivity measurements of GeTe films crystallized at different peak oven temperatures.

Peak Temperature	Electrical Conductivity
180°C	2.0×10^4 S/m
200°C	2.5×10^4 S/m
220°C	4.5×10^4 S/m
260°C	5.0×10^4 S/m
300°C	7.7×10^4 S/m
350°C	1.0×10^5 S/m

At the optimal ovenization conditions with a peak oven temperature of 350°C, the highest electrical conductivity measured on crystallized GeTe films is approximately 10^5 S/m, although it is measured to be lower in some samples with the same conditions due to process variations and random defects generated on the GeTe films during the sputtering process.

2.3.3.3. Atomistic Study of Crystalline GeTe Films

In order to analyze the crystallization structure and process of GeTe, further measurement and imaging processes are performed including in-situ X-ray diffraction (XRD) measurements and transmission electron microscopy (TEM) imaging. Both methods can be used to determine the crystalline type of GeTe film: whether it is single-crystalline or poly crystalline.

The in-situ XRD measurements are performed by our collaborators at North Carolina State University (Prof. Jacob Jones group). The as-deposited amorphous GeTe film is annealed through ovenization, while the XRD measurements are taken. This allows us to see the real-time response of the crystalline 2θ peaks with the changing temperature.

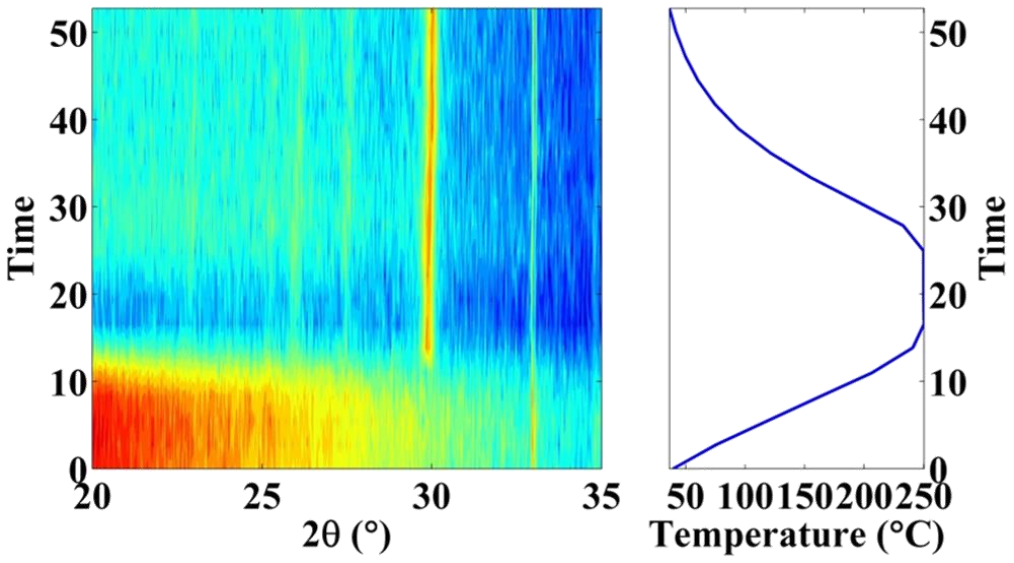

Figure 2.11. XRD in-situ measurement of a sputtered GeTe film during the annealing process with a peak temperature of 250°C.

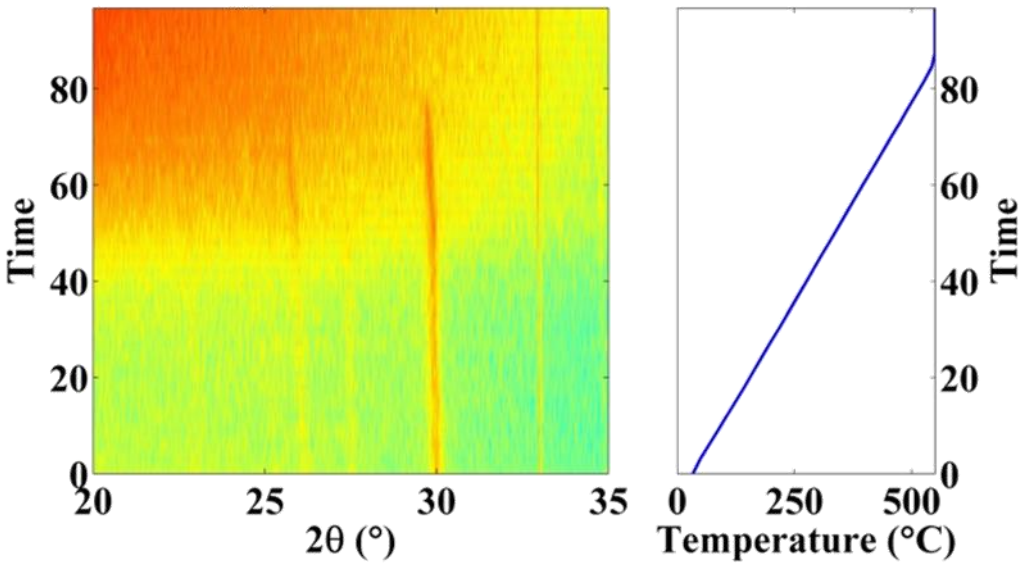

Figure 2.12. XRD in-situ measurement of a sputtered GeTe film during the annealing process with a peak temperature of 550°C.

The XRD in-situ measurements results with a peak ovenization temperature of 250°C and 500°C are shown in Figure 2.11 and Figure 2.12, respectively. Figure 2.11 shows that as the temperature ramps up from room temperature to 250°C, a dominating 2θ peak at approximately 30° appears when the temperature reaches 220°C (at 13 min), but several other peaks at different 2θ angles are also showing as the temperature rises. The second XRD measurement (shown in Figure 2.12) with a higher annealing temperature on a crystalline GeTe indicates that when the temperature reaches about 350°C, the XRD peak at 2θ = 30° is slightly twisted with an increased sharpness. This measurement also indicates that 550°C is not sufficiently high to completely melt GeTe and remove all crystalline sites. The multiple peaks in XRD measurement results indicate that the GeTe film samples deposited and annealed under the conditions discussed above are showing a poly-crystalline structure, with multiple crystalline orientations within the same sample.

In order to observe the crystalline volume and grain sizes of crystalline GeTe, further imaging processes using TEM are performed. With the high-resolution imaging using TEM, the GeTe film can be viewed on the atomic level, with sub-million and million times magnification, so the crystalline structure can be clearly seen. For our TEM imaging, the sample thickness needs to be less than 100 nm. To take cross-sectional image of the GeTe thin-film, focused ion beam (FIB) process was used. The TEM imaging was then performed using a JEOL 3011 High-Resolution Electron Microscope with an accelerating voltage of 300 kV.

TEM images show that the crystalline GeTe film prepared using the characterized sputtering and annealing processes exhibits a polycrystalline structure. In the TEM imaging sample, the GeTe film can be seen with a poly-crystalline structure, where multiple crystalline orientations can be observed within the same sample, which is one of the cases discussed in [54]. However, the crystalline grain size of GeTe varies a lot across different samples and different spots within the same sample. In Figure 2.13, the TEM image of the GeTe film is showing the interfaces among at least three grain orientations, with the grain sizes varying roughly from 5 nm to 30 nm. The diffraction pattern shown in Figure 2.13(e), with bright diffraction dots distributed along concentric circuits, also suggests a poly-crystalline structure. In some areas, larger grain sizes are also observed, as shown in Figure 2.14.

The results shown in this chapter indicate that using our ovenization process, the GeTe thin film cannot be completely crystallized resulting in lower electrical

conductivity at the ON state of the switch. Further studies are needed to better optimize the crystallization process.

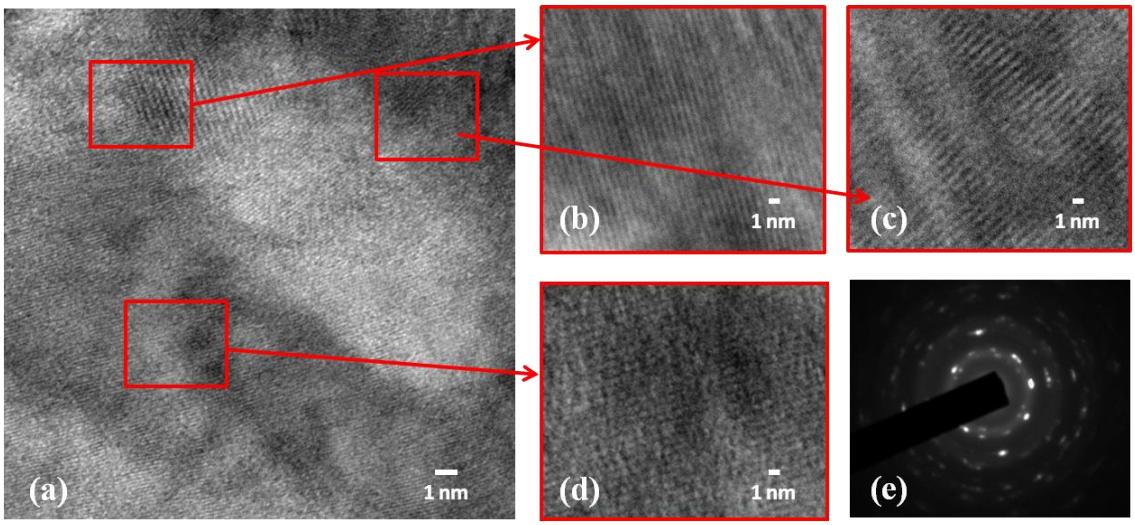

Figure 2.13. TEM images of a crystalline GeTe film showing (a) multiple crystalline orientations within a small imaging area and (b)(c)(d) enlarged view of each area showing a different crystalline orientation. (e) The diffraction imaging pattern also suggests a poly-crystalline structure for the GeTe film.

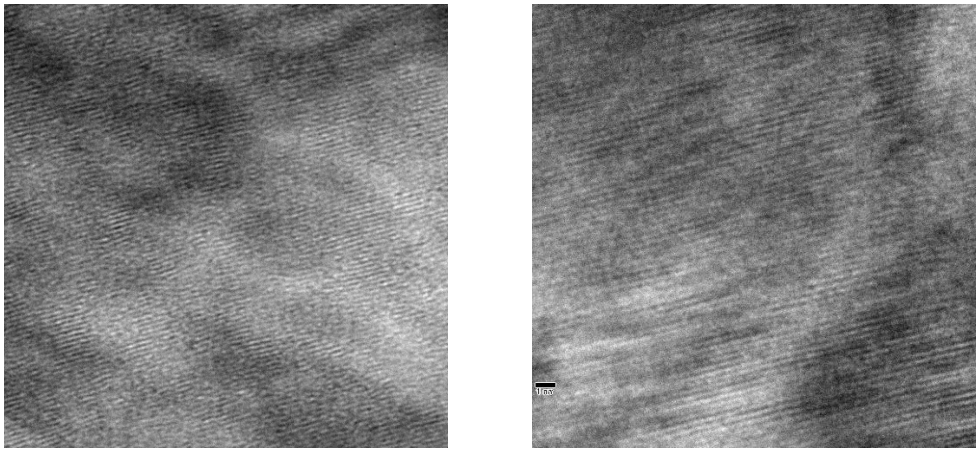

(a) (b)

Figure 2.14. TEM images showing large grain sizes of single crystalline orientations within the poly-crystalline GeTe film.

CHAPTER 3 GeTe Phase Change Material Based RF Ohmic Switches

As discussed in the previous chapter, GeTe films have been proven to possess a low-resistivity crystalline state and a high-resistivity amorphous state at room temperature, and phase transitions between these two states are achievable with thermal actuation at a fast speed. Optical storage applications using GeTe have also demonstrated good reliability of GeTe film. Therefore, GeTe is a strong candidate for RF switching applications. In phase change material-based RF switches using GeTe or GST materials in general, the core structure is the phase change material via connecting two or more RF terminals to form the switch connection. In order to achieve phase transitions for switching activities, thermal actuation structures need to be designed along with the RF switching element. The most commonly used methods for thermal actuation include laser induction [28] [29], and joule heating using a heating current drawn through a resistive heater. The latter is a more popular way for RF switch designs, and will be talked about in detail in this chapter.

3.1. Early Designs of Phase Change Material Based RF Switches

3.1.1. RF Switches Using Different Phase Change Materials

One of the earliest proposed designs of phase change RF switches uses $Ge_2Sb_2Te_5$ via as the switching element, and a lateral heater path through the via as the thermal actuation conduit [36]. In this design, the two switch terminals are vertically connected by the GST via and the prototype device is fabricated in a standard 180-nm CMOS copper back-end technology. As one of the earliest proof-of-concept designs of an Ohmic switch using phase change materials, this work has reported successful phase transitions of the GST material and showed switching activities of the device for up to 100 switching cycles with a stable OFF/ON DC resistance ratio of over 200. In the ON state, the DC resistance of the switch was approximately 5 kΩ, which is very high for most applications. The high ON-state resistance is due to the material properties of $Ge_2Sb_2Te_5$, which has a relatively high crystalline state resistivity. While this is acceptable in memory-related applications as long as the amorphous-crystalline resistivity ratio is high and stable, it creates great limitations in RF switch designs. For this reason, alternative phase change materials such as GeSb and GeTe have been investigated for designing Ohmic switches. A novel three-terminal phase change switch design has been reported using $Ge_{50}Sb_{50}$, or GeSb as the switching element [52]. The GeSb electronic switches are demonstrated in a reconfigurable inductor design where the GeSb switches are used to reconfigure the inductance value. In this reported work, the switches use the structure where lateral metal electrodes are connected by the GeSb vias, and through switching activities, the

integrated spiral shaped inductor is reconfigured into different inductance values. In order to reduce the via size of each individual GeSb via, this design uses a parallel array configuration of multiple GeSb vias, which reduces the required switching current level. The phase transitions of GeSb are measured to be stable with an OFF/ON resistance ratio of approximately 100. This work provided the idea of a novel structure for phase change switch design that requires a switching power level that is more acceptable in many integrated systems.

Among different phase change materials, a low crystalline state resistivity is much preferred in Ohmic switch designs, as it is the key to achieve a low ON-state insertion loss and therefore a better performance. Compared to the two phase change switch designs discussed above using $Ge_2Sb_2Te_5$ and GeSb, another proposed design of phase change switch using GeTe has shown much lower ON-state resistance and a much higher switch isolation [53]. The improved performance of this design is mostly because of the material properties of GeTe. The GeTe film deposited and measured in [53] is reported to have a crystalline state resistivity of 4×10^{-6} Ω·m, and an amorphous state resistivity of 76 Ω·m, showing an amorphous-crystalline state resistivity ratio of 1.9×10^{7}. The switch uses a vertical RF connection structure, with a top and a bottom electrode connected through the GeTe via, and the via area is defined by a SiO_2 layer patterned through etching. The switch after fabrication is measured to have an ON-state resistance of 180 Ω and an OFF-state resistance of approximately 1.3 MΩ, showing an OFF/ON resistance ratio of 7×10^{3} for the switch, which is a significant performance improvement compared to the designs reported in [36] and [52].

Early designs of phase change material switches, especially GeTe-based switches have shown their great potential in RF switching applications. Compared to solid-state based RF switches using different technologies, such as bulk-Si, SOI, SOS, pHEMT, *etc*., phase change material based switches have the advantage of lower ON state resistance and higher linearity, as will be shown in this chapter. Since the reported works discussed above, efforts have been made to build phase change RF switches with improved performance that is comparable to or better than other switch technologies.

3.1.2. Low-Loss Two-Terminal GeTe Based RF Switch

The switch designs discussed above have proven good functionality of phase change materials in switching applications, but the reported performance parameters such as insertion loss are not competitive compared to existing switch designs. Improving the performance is critical for phase change material based switches to show their advantages against other types of switches, especially in reconfigurable RF applications. A two-terminal RF Ohmic switch using GeTe has since been proposed, showing very low loss across a wide frequency range [61]. The cross-sectional schematic of the GeTe RF switch proposed in [61] is shown in Figure 3.1 for easier understanding of the structure.

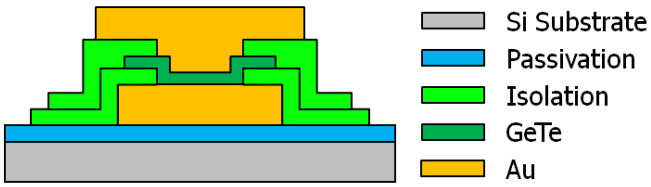

Figure 3.1. Cross-sectional schematic of the two-port GeTe-based RF switch [61].

This two-port switch uses a vertical connection of two metal electrodes as the two terminals. These two terminals are responsible for both RF signal transmission and GeTe thermal actuation for phase transitions. The GeTe connection via area between the top and bottom electrodes is defined by the SiO_2 interlayer patterned through plasma etching. When the GeTe via is in the crystalline state, the insertion loss of the switch is mainly determined by the electrical resistivity of the GeTe film and the dimensions of the connection via. Since the resistivity of crystalline GeTe and the film thickness are fixed by the fabrication process, the sizing of the connection via area is used to balance the ON-state insertion loss and OFF-state isolation.

For a lower insertion loss when the switch is turned on, it is preferred to have a larger GeTe via area connecting the two RF terminals. However, a larger area will result in a slower switching speed due to the increased volume of GeTe that needs to go through the phase transitions. Therefore, an alternative structure of multiple GeTe via connections is also proposed in this work, where the RF terminals are connected by multiple GeTe vias in parallel with each GeTe via having a small area. This structure results in both a low insertion loss and a fast switching speed. The SEM images in Figure 3.2 show the examples of the GeTe based RF switches with a single-via and a multi-via configuration.

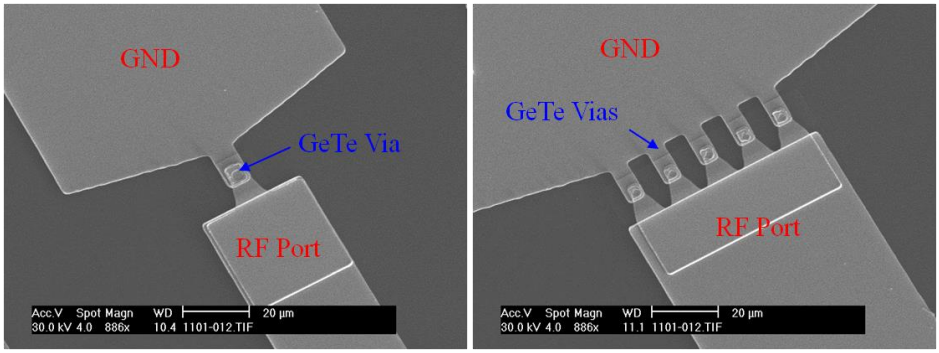

(a) (b)

Figure 3.2. SEM images of the GeTe-based RF switches reported in [61] with (a) a single 3µm×3µm via configuration and (b) a multi-via configuration with five 2µm×2µm vias connected in parallel [61].

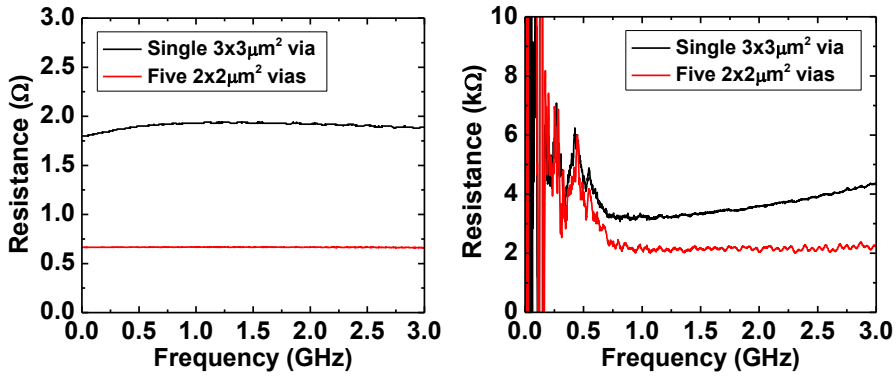

(a) (b)

Figure 3.3. Measured resistance of GeTe RF switches with a single-via and multi-via configurations from DC to 3 GHz when the GeTe via is at the (a) crystalline state and (b) amorphous state [61].

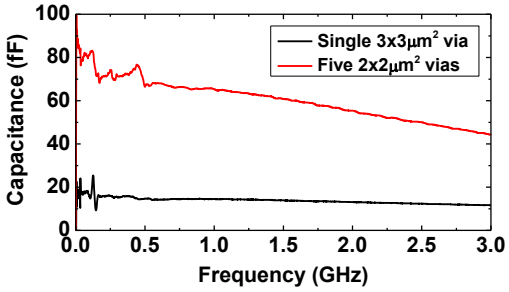

Figure 3.4. Measured intrinsic capacitance of the GeTe RF switches when the GeTe is at the amorphous state.

The measured resistances of the switches with the single-via and multi-via configurations at the GeTe crystalline and amorphous states are shown in Figure 3.3, and the measured capacitances of the switches when the GeTe is at the amorphous state is shown in Figure 3.4. When the switch is turned ON with GeTe at the crystalline state, the low resistance between the two RF terminals determines the insertion loss, and when the switch is turned OFF with GeTe at the amorphous state, although the resistance of the switch is much higher, capacitance across the terminals becomes dominant in the isolation, especially at higher frequencies. The measured scattering (S)-parameters of the switch with the single-via configuration in both the ON and OFF states are shown in Figure 3.5, which show competitive insertion loss and isolation of this type of switch design compared to other existing technologies.

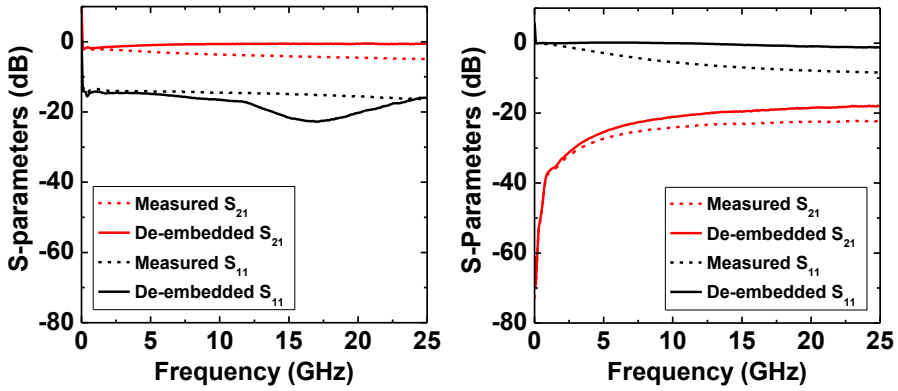

(a) (b)

Figure 3.5. Measured and de-embedded S_{11} and S_{21} of the GeTe RF switch with the single-via configuration (a) at the crystalline and (b) amorphous states of GeTe.

In this two-terminal switch structure, the RF signal path and the heating path share the same two terminals. However, the requirements for the terminals used for RF signal transmissions and thermal actuations are very different. For RF signal transmissions, it is preferred to have low-resistance metal electrodes for good loss performance, but for thermal actuations, the heating path needs to have a high resistance level. Therefore, the two-terminal structure has a limited performance as both heating and RF structures cannot be optimized simultaneously. To deal with this problem, we have proposed four-terminal structures with two RF terminals and two separate heating terminals.

3.2. Four-Terminal GeTe RF Switches

The four-terminal structure of GeTe-based RF switches is intended to separate the thermal actuation signal path from the RF path. With the RF signal path and the heating path separated, it is possible to separately design the two paths to be optimal for each function. An early proposed design of a four-terminal GeTe-based RF switch is reported in [62] and later in [63]. This four-terminal RF switch uses an inline structure with the two RF terminals laterally connected by the GeTe via whose size is defined by directly patterning the GeTe film. The two heating terminals are connected through a resistive heater path that is electrically isolated from the RF signal path. Thermal actuation is achieved by drawing heating current from the heater path to heat up the GeTe via through thermal coupling. In this design, only the RF terminals are in direct contact with the GeTe via, which reduces the parasitics associated with the heater terminals and both the performance and reliability are improved from previous designs.

With the similar idea in mind, we have proposed a novel phase change RF switch design having four terminals. In this section, two different structures of four-terminal GeTe RF switches will be discussed. Their design procedures, structures, fabrication processes, and performance will be discussed in detail. A comparison between the two structures will also be presented.

3.2.1. Four-Terminal GeTe RF Switch with Direct Heating Scheme

The directly heated switch structure, similar to the one in [62], has four terminals, two RF ports and two for Joule heating. The most significant difference between the in-line four terminal structure in [62] and our design is that in the directly heated switch, the heating current is drawn through the GeTe via itself to achieve phase transitions. This design offers a higher heating efficiency compared to the design with a separated heater in [62]. The directly heated phase change switch design was first published in [64], with a brief discussion of the working principle, structure, fabrication process, and the performance evaluation. The structure and fabrication process were then slightly modified for an improved performance and the results were then reported in [65]. This structure is similar to the one reported in [36], where a resistive heater is placed through the GST via, but in this design the GeTe via is not in a simple pillar or via shape, but instead has been designed into a more complicated structure considering the functionality, thermal actuation effectiveness, and RF performance [66]. Details about the GeTe RF switch with direct heating scheme will be discussed in this sub-section.

3.2.1.1. Device Structure

The GeTe RF switch with direct heating consists of two RF terminals laterally connected by the GeTe via with an in-line structure, and the two heater terminals are vertically connected through the GeTe via. The RF signals and heating pulses follow the lateral and vertical electrical paths, respectively.

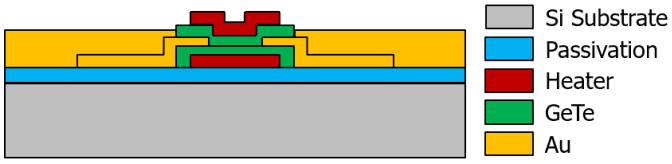

Figure 3.6. Cross-sectional schematic showing the structure of the four-terminal GeTe RF switch using the direct heating method.

The cross-sectional schematic of the four-terminal GeTe RF switch with direct heating is shown in Figure 3.6. The two RF terminals represented by the gold layer is laterally connected through the GeTe via, forming a lateral RF signal path. The two heater terminals are also connected through the GeTe via, but in a vertical direction. The switching activities are realized by applying heating signal pulses from the heater terminals, and the GeTe via is thermally actuated by the current drawn through it. In this structure, it is important to ensure that the RF electrodes and heater electrodes do not come in direct contact with each other. For this reason, the GeTe film is deposited twice in the switch fabrication process. The first GeTe layer completely covers the bottom heater terminal, and the RF electrodes are sandwiched by the two GeTe layers to avoid direct contact with the heater layers. Although all four terminals are electrically

connected to the GeTe via, a high resistive material is used for the heater layers to ensure good isolation between the RF signals and the heating pulses, and also to maximize the heating efficiency. The RF terminals, on the other hand, are designed with very low resistance for good loss performance of the switch.

The design of the heating terminals in this type of GeTe switch is critical to obtain both good heating effectiveness and minimal interference with RF signal transmission. In terms of resistance, the heater path needs to be designed with good impedance matching to get to heat delivery to the GeTe via. In the meantime, since the RF electrodes are in indirect contact with the heater electrodes through the GeTe layer, the heaters also need to have a high enough resistance to ensure good isolation between the two paths in order to minimize the heating pulse interference to RF signals. This essentially limits the choices of material for heater paths. In the initial designs, titanium nitride (TiN) was used as the resistive heater material, which was also proven to be a very effective and reliable choice. The TiN film is a metal-like ceramic material, which has a much higher resistivity than most conductive metals, but can be used as resistors. It has also been tested with good stability at high temperatures.

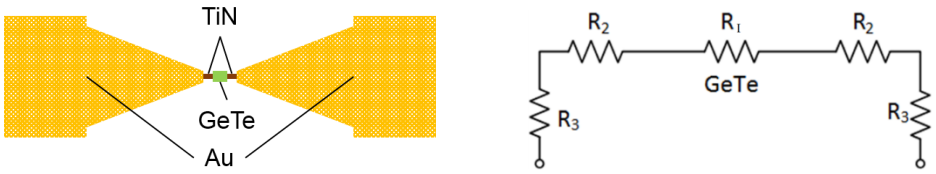

(a) (b)

Figure 3.7. (a) Top-view layout of the heater path in the GeTe switch and its material combinations. (b) Simplified equivalent circuit model of the heater path.

The layout of the heater path in the GeTe RF switch with direct heating scheme and its simplified equivalent circuit model are shown in Figure 3.7. In Figure 3.7(b), resistor R_1 represents the vertical resistance of GeTe, which varies between the crystalline and amorphous states. Resistors R_2 represent the TiN sections of the heater path, which are next to and in direct contact with the GeTe via. Finally, resistors R_3 are the resistance of each DC pad covered with gold. From modeling and simulation, the value of R_1 (GeTe resistance) is smaller than 5 Ω at the crystalline state, and is above 5 kΩ at amorphous state. R_3 is within 5 Ω as gold is a good conductor. R_2 is designed to be greater than 0.5 kΩ. Therefore, when GeTe is at crystalline state, the resistance along the heater path is concentrated at the TiN sections, ensuring that the heat is effectively delivered to the GeTe via. When GeTe is at the amorphous state, R_1 becomes the dominant resistance, and the resistance of TiN (R_2) serves as protection for GeTe, so that once GeTe is back to the crystalline state, most power is dissipated in the TiN sections and GeTe is not accidentally heated back to the amorphous state. The basic heater path structure used in directly heated switches is the one shown in Figure 3.7, but the sizing, material choice and fabrication process have been modified slightly as the switch design was matured.

To verify the required conditions for Joule heating of GeTe, thermal simulations are performed using COMSOL multi-physics FEA simulation tool. As previously discussed, to convert GeTe from crystalline to amorphous state, the Joule heating temperature should rise above the GeTe melting point. Heat dissipation to the substrate needs to be rapid enough, so the atoms in the GeTe layer cannot nucleate and re-crystallize. Thus, GeTe should have good thermal coupling to the substrate. In order to achieve phase

transition from the amorphous state back to the crystalline state, lower power needs to be applied. The temperature must rise above the crystallization temperature of 250°C or higher, while remaining below the melting temperature. The switch should cool down gradually by slow removal of the heating current to convert the via back to the crystalline state. In COMSOL simulations, is the crystallization and amorphization conditions are realized by applying appropriate heating pulses, and the thermal responses are shown in Figure 3.8. It is shown that both crystallization and amorphization requirements are met with the heater design.

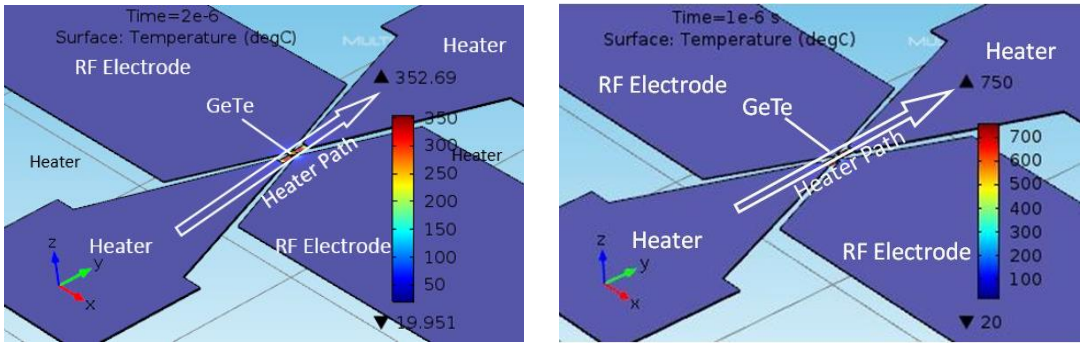

(a) (b)

Figure 3.8. COMSOL simulation for Joule heating conditions of the GeTe switch. (a) For GeTe crystallization, a voltage pulse with an amplitude of 7 V is applied for a duration of 2 μs, and the maximum temperature at the GeTe volume reaches 310 °C. (b) For GeTe amorphization, a voltage pulse with an amplitude of 12.5 V is applied for a duration of 1μs, and the maximum temperature at the GeTe volume is above 710 °C. The simulation results verify that the heating conditions meet the requirements for GeTe phase transitions.

3.2.1.2. Fabrication Process

The fabrication process of the GeTe RF switch with direct heating is performed on a silicon substrate, passivated with a dielectric layer. Throughout the development process, silicon substrates with different quality and properties have been used. Based on the measurement results from devices fabricated on different substrates, it is believed that the doping type of the silicon substrate does not affect the quality of the fabricated devices significantly. However, devices on a high resistivity substrate is found to have improved performance at high frequencies compared to those on a substrate with low resistivity. For example, a device fabricated on a 1000 Ω·cm silicon substrate is measured to perform better than a device fabricated on a 30 Ω·cm silicon substrate having an insertion loss that is lower by a few dB at frequencies over 1 GHz. In the measurement process, however, the performance degradation caused by substrate loss can be de-embedded based on reference devices. Details about the measurement process will be discussed later.

Details of the fabrication process of the GeTe switches have been repeatedly modified in terms of both material choice and process flow in order to improve the overall device quality, but a general fabrication process flow is shown in Figure 3.9.

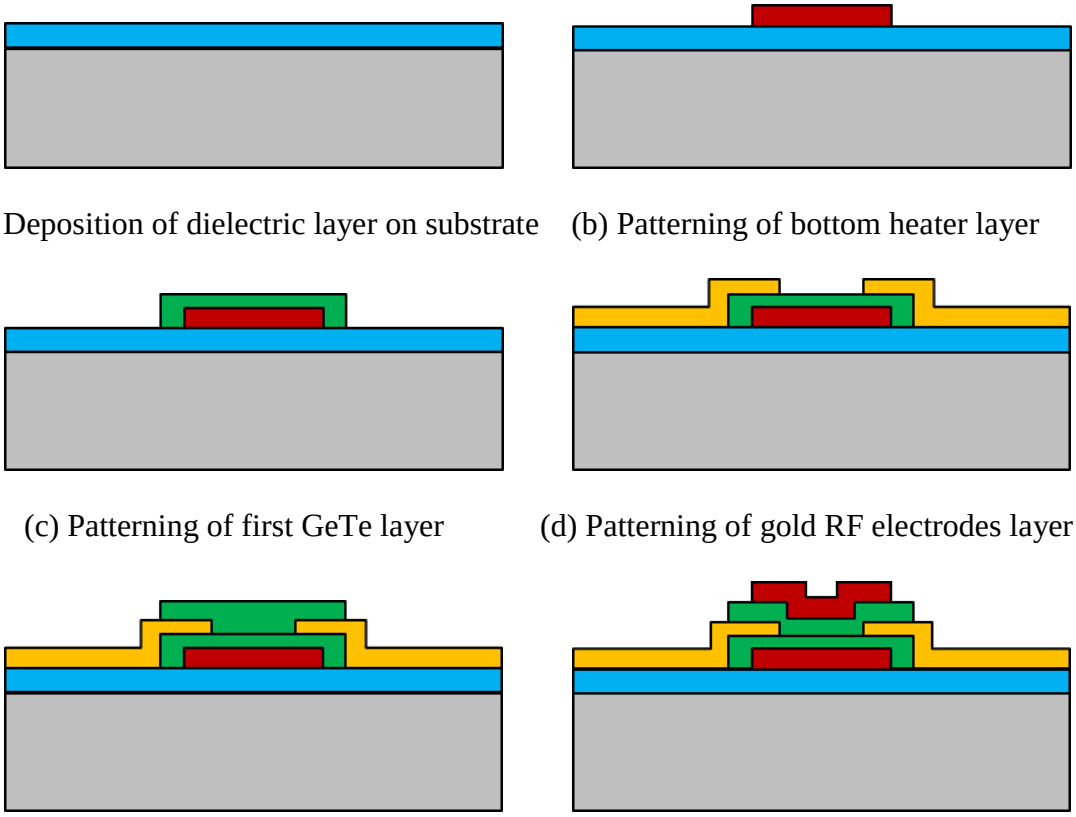

(a) Deposition of dielectric layer on substrate (b) Patterning of bottom heater layer

(c) Patterning of first GeTe layer (d) Patterning of gold RF electrodes layer

(e) Patterning of second GeTe layer (f) Patterning of top heater layer

Figure 3.9.Fabrication process flow of the GeTe RF switch with direct heating

The first step of fabrication is to deposit a dielectric layer on the silicon substrate to passivate the substrate. The choices of dielectrics that have been used include aluminum nitride (AlN) through sputtering and silicon dioxide (SiO_2) through plasma-enhanced chemical vapor deposition (PECVD) or thermal growth. The typical thickness of the passivation layer is between 1 μm and 2 μm. After the passivation dielectric layer is deposited, the bottom heater layer of the device is deposited and patterned. The typical bottom heater layer used is TiN with a thickness of approximately 200 nm. After the bottom heater layer, the first GeTe layer is deposited through sputtering from a single

GeTe target, as discussed in the previous chapter. The thickness of the GeTe layer is about 100 nm. The patterned GeTe layer needs to completely cover the bottom heater layer in order to prevent any direct contact between the heater line and the RF electrodes, which are deposited after the GeTe layer. After the gold RF electrode layer with a thickness of 200 nm is patterned, the second GeTe layer is deposited with the same pattern as the first GeTe layer. The two GeTe layers form a sandwiching structure against the RF electrodes. The second GeTe layer also has a thickness of about 100 nm, giving a total thickness of 200 nm at the via area. Finally, a top heater layer of 200 nm TiN is patterned to form the heating signal path. After the major steps, an additional gold layer patterning is performed on both the RF and heater terminals to reduce the resistance of the heater and RF pads. A top passivation layer is also deposited in some batches of devices as a protection layer, and also for performance comparison.

In this fabrication process, all non-dielectric layers are patterned through lift-off. A photoresist layer is built with patterns created by photo-lithography before the layer deposition. A standard photoresist lift-off process is performed after the deposition with an overnight acetone treatment, followed by an acetone-IPA-deionized (DI) water cleaning cycle while applying an ultrasonic agitation. The sample is finally rinsed with DI water and dried with compressed N_2 gas.

After patterning of each GeTe layer, it is preferred to immediately perform the annealing process for GeTe crystallization, since the as-deposited GeTe film is amorphous, as previously discussed. The annealing process is generally performed in a convection oven at a temperature of at least 220°C for good crystallization results. In

later developments, an annealing temperature of 350°C is often used. In some fabricated device batches, the annealing process has been performed after all layers have been patterned. From our observations, the quality of the crystallized GeTe layers generally does not differ too much from the ones with the first approach, but slight surface oxidization of GeTe layers does happen slowly when GeTe is exposed in air, and a postponed annealing process could slightly affect the quality of GeTe due to the surface oxidization.

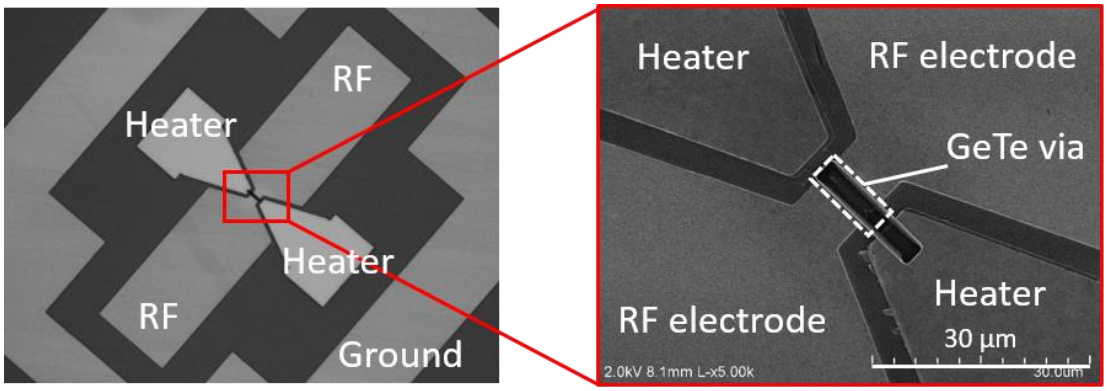

Figure 3.10. SEM images of the GeTe RF switch with direct heating.

Scanning electron microscope (SEM) images of the devices are taken to visually evaluate the fabrication quality. SEM images of a fabricated GeTe RF switch with direct heating are shown in Figure 3.10, with an entire device view (left) and a zoomed-in view of the GeTe via area (right). In the zoomed-out image on the left, the two RF terminals and two heater terminals as well as the ground ring are visible. In the zoomed-in image on the right, the GeTe via area can be seen as the connecting point of the four terminals.

It can be seen that the RF path and heater path are perpendicular to each other in the same plane, but at the GeTe via area, the two heater electrodes are vertically connected by GeTe and the RF electrodes are laterally connected, as discussed before.

3.2.1.3. Measurement Results

The GeTe via in the RF switch can be treated as a resistor pad connecting the RF terminals, so the sizing of the GeTe via connection poses a trade-off between insertion loss and isolation of the switch. The dimensions of the connection are defined by the gap between the two RF electrodes, the width of the RF electrodes and the total thickness of the GeTe film. Naturally, it is preferred to have a small gap between the RF electrodes and big RF electrode widths with a thicker GeTe layer in order to have a lower ON-state resistance and thus a lower insertion loss. But the OFF-state isolation is consequently limited by this aggressive design method. For example, a close metal gap between the electrodes can greatly increase the gap capacitance, and wider RF electrodes can also increase the parasitic capacitance formed between the metal and the substrate, both of which is a significant contribution to the OFF-state capacitance. Besides, the fabrication process also has limitations such as minimum feature size and maximum pattern aspect ratio, which also need to be taken into account when determining the sizing of devices.

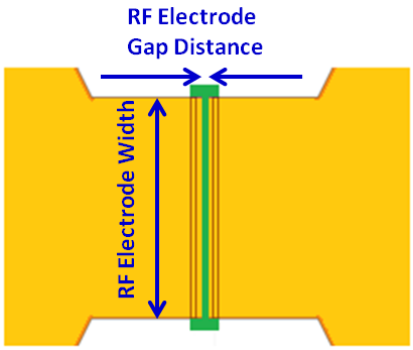

Figure 3.11. Simplified top view of the RF electrode connection through GeTe via showing how the dimensions of the connection are defined.

A simplified top view of the GeTe via area of the switch is shown in Figure 3.11 for easier understanding. If the GeTe via is treated as a block of resistor, the RF electrode gap distance will define the length of the resistor, and the RF electrode width will define the width. The height of the resistor is defined by the total thickness of GeTe. In the actual structure of the device, the GeTe layer has a larger area for overlapping with and sandwiching the RF electrodes, and thus additional fringing effects, contact resistance, and parasitics need to be considered as well. For a more accurate sizing evaluation, electromagnetic simulations are performed using ANSYS HFSS to predict the insertion loss and isolation of the switch with different sizing parameters. In a sample series of simulations, the thickness of the GeTe layer is set to be either 100 nm or 200 nm, and the RF electrode gap is varied among 0.25 μm, 0.5 μm, and 1 μm. The width of RF electrodes is fixed at 20 μm for fewer combinations, but in the case of actual fabrication, the RF electrode width is varied across devices to evaluate the design trade-off.

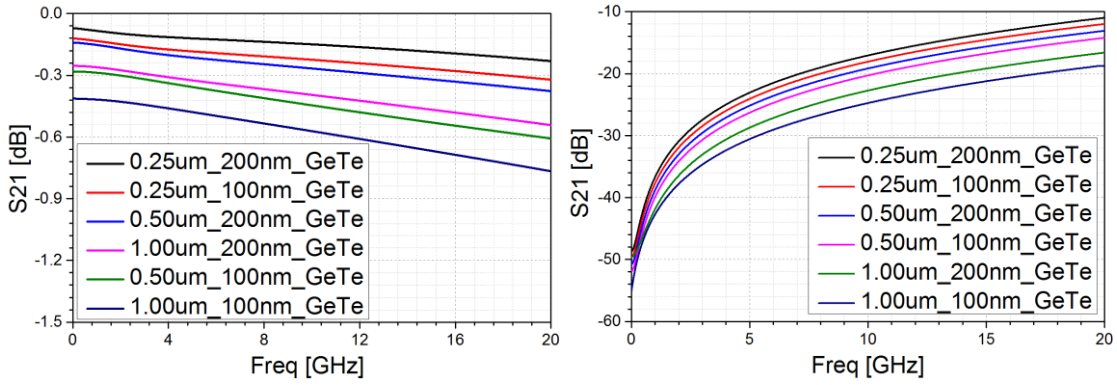

(a) (b)

Figure 3.12. Simulated (a) ON-state insertion loss and (b) OFF-state isolation of the GeTe RF switch with various sizing parameters.

The size variations among the GeTe switches are clearly showing the trade-off between the ON-state and OFF-state performance. As seen in Figure 3.12, across a frequency range from DC to 20 GHz, the device with a GeTe thickness of 200 nm and an RF electrode gap distance of 0.25 μm is showing simulated insertion loss of 0.25 dB or less, but the corresponding isolation is only slightly above 10 dB at 20 GHz. And with the least aggressive design where the GeTe thickness is 100 nm and the RF electrode gap distance is 1 μm, the isolation is close to 20 dB at 20 GHz, but the corresponding insertion loss is over 0.75 dB. It can also be seen that changing the RF electrode gap distance and changing the GeTe thickness are influencing the performance in a fashion that is not completely linear, because the electromagnetic simulation is using the finite element analysis (FEA) method, taking into account more details than simple calculations. Based on the simulation results and the fabrication limitations, the total thickness of GeTe is chosen to be 200 nm for a lower insertion loss, and the RF electrode gap distance is set to be 1 μm, since this is close to the limit of the minimum feature size from the

lithography, and any smaller size may cause pattern quality and yield issues. Throughout the development process, the sizing has been slightly modified to better address the fabrication process characterization results.

In the fabrication process, the metal contact pads are integrated with the GeTe RF switch for RF and DC measurement purposes. As seen in Figure 3.10(a), the terminal pads and the ground ring form coplanar waveguide (CPW) transmission lines are connected to the switch for RF measurements. A pair of air-coplanar (ACP) RF probes with the ground-signal-ground (GSG) configuration is used for the two-port scattering parameters measurements to evaluate the insertion loss and isolation. The thermal actuation for switching activities is achieved by applying a DC voltage pulse generated from a waveform signal generator and delivered by two DC probes connected to the two heater terminal pads.

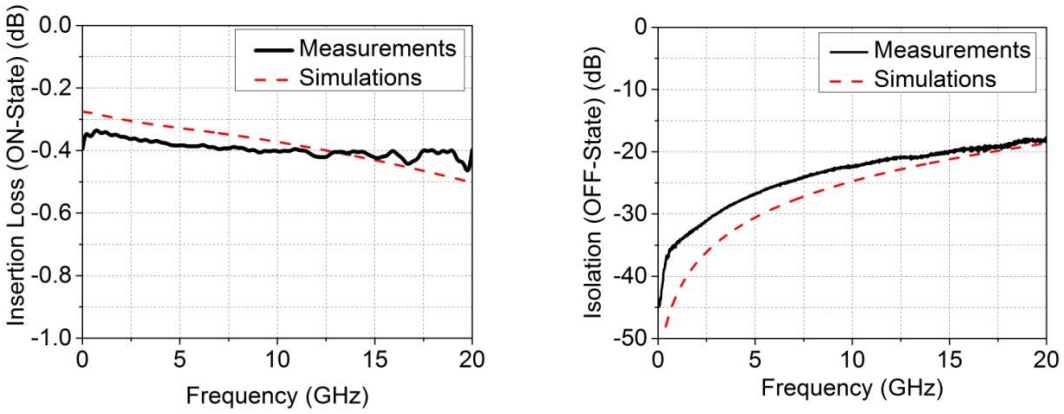

(a) (b)

Figure 3.13. Measured (de-embedded) and simulated RF response of the GeTe RF switch. (a) Insertion loss at the ON-state. (b) Isolation at the OFF-state.

RF measurements are performed using Cascade ACP probes landed on the RF terminal pads of the device, and the RF signal transmission S-parameters are measured with the Agilent N5242 PNA-X network analyzer. The on-wafer measurement results have been de-embedded using a reference device from the same wafer in order to eliminate inaccuracy caused by probe contact and measurement setup. Electromagnetic simulation results acquired using ANSYS HFSS are also included for comparison. The measured S_{21} parameters at the ON-state and OFF-state are shown in Figure 3.13. In simulations, the electrical conductivity of GeTe in crystalline state is set to 5×10^4 S/m, while its amorphous state conductivity is set to 1 S/m. The discrepancy between measurements and simulations are mostly due to a lower OFF/ON resistance ratio achieved in the fabrication as well as other effects that are not taken into account by the simulation. From the measurement results, the GeTe RF switch with direct heating scheme shows an insertion loss of less than 0.5 dB and an isolation over 18 dB from DC to 20 GHz, which indicates very competitive performance compared to other existing types of RF switches such as MEMS and solid-state switches.

In order to better analyze the performance and illustrate how the RF response is affected by the resistive and reactive elements from the switch and the external circuits, an equivalent electrical model is developed. For the GeTe switch with the direct heating method, the equivalent circuit is shown in Figure 3.14.

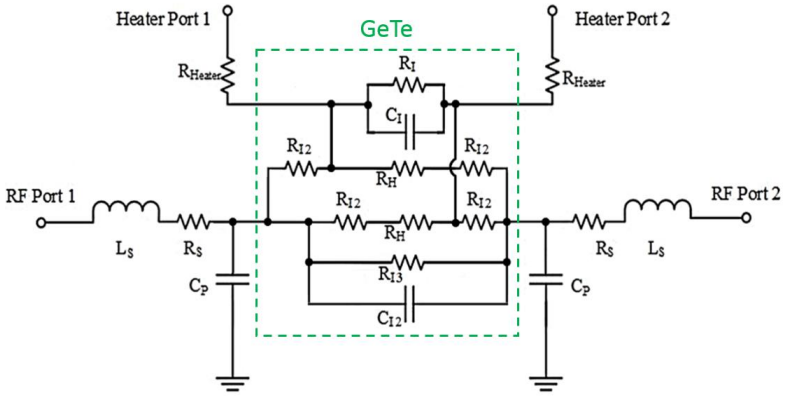

Figure 3.14. Equivalent circuit model of the four-terminal GeTe RF switch with direct heating. The circuit elements shown in the model include resistive and reactive parts from the components of the GeTe switch and the external metal routing as well as the measurement setup.

This model was first proposed by us in [65]. Based on the specific material properties of phase change material, the GeTe via is essentially modeled as a parallel connection of a resistor, a capacitive component, and a series R-C connection to simulate the RF response. Since both the two RF terminals and the two heater terminals are connected to the GeTe via through a lateral and a vertical path, respectively, additional resistive components are used to model the electrical connections among the terminals. The resistors R_I, R_{I2} and R_{I3} represent the resistance from different portions of GeTe, and R_H represents the resistance from the heater, which is in contact with GeTe. The parallel capacitance of the GeTe pad is modeled by C_I. Since the GeTe is in direct contact with both the RF and the heater terminals, it is divided into multiple elements. Along the RF path from Port 1 to Port 2, several parallel paths exist: Path 1 connects the two RF lines through GeTe laterally (R_{I3}); Paths 2 and 3 are due to the overlap of RF signal line with the heater line through vertical GeTe resistance (R_{I2}). Here, R_H models the lateral

resistance of the heater line. Along the RF path, there is also a feed-through capacitance, modeling the lateral capacitance of GeTe (C_{I2}). Along the heating path, the main elements are the resistive components of the heater and the GeTe via that is vertically connecting the two heater terminals. Additional connections between the heater terminals exist because they are also in contact with the RF signal paths, but those connections have much higher impedance so they have a smaller effect in comparison. All the resistive components that represent the portions of the GeTe vias have a variable resistance switching between the crystalline and amorphous states. In addition to the GeTe switch, there are parasitic elements from the metal RF transmission lines as well as the measurement setup. The resistive component R_S and inductive component L_S represent small parasitics from the RF probes and cables that are not calibrated out. The capacitive component C_P models the small parallel-plate capacitor formed by the deposited gold metal lines and the substrate with the passivation layer in between.

When the GeTe switch is turned on, the GeTe is in the crystalline state with low resistivity, and the switch impedance is determined primarily by the resistance through the RF terminals. When the switch is turned off, the GeTe is in the amorphous state with much higher resistivity. The switch impedance, especially at higher frequencies, is greatly dependent on the capacitance that the GeTe via creates. Based on the measurements, the GeTe thin film offers a resistivity of roughly 0.015 – 0.02 Ω·mm in the crystalline state, and 0.5 – 0.7 Ω·m in the amorphous state. As mentioned before, the devices have size variations across each wafer. The sample used for measurements and RF performance evaluation has an RF electrode width of 20 μm and an RF electrode gap

distance of 1 μm (the actual gap distance measured from fabricated devices was close to 0.9 μm due to feature accuracy of the lithography process). The extracted values of elements from Figure 3.14 are used to determine the figure-of-merit cut-off frequency of the device, which is defined by $f_{co} = 1/(2 \cdot \pi \cdot R_{ON} \cdot C_{OFF})$. When the switch is turned ON, the resistance from the RF terminals is $R_{ON} \approx 4.8\ \Omega$, and when it is turned OFF, the capacitance from the RF terminals is $C_{OFF} \approx 8$ fF. Therefore, the switch has a cut-off frequency of over 4 THz. Later designs of the switch have improved performance and a higher cut-off frequency.

The switching activities between the ON and OFF states of the device are achieved by applying heating voltage pulses from the heater terminals. The heating pulses are programmed and generated from a function generator. An AC amplifier is used to get the required voltage amplitude. For the amorphization process, a voltage pulse of approximately 12 V peak-to-peak is applied to the heater terminals, with a pulse with of 0.5 – 1.5 μs. The voltage level needs to be slightly tuned around this level each time for effective amorphization. The average power drawn from the heater path for each amorphization pulse is about 80 mW. For the crystallization process, the voltage level is generally between 5 V and 7 V peak to peak and the voltage pulse duration is 1.5 – 2 μs. The average power for each crystallization cycle is about 5 mW.

Although the direct heating method provides high power efficiency during switching activities, this design has a potential issue with electrical isolation between the RF and heater terminals, since all four terminals are in electrical contact with the GeTe via. In order to ensure that the GeTe switch functions normally during switching activities, it is

important to maintain a high signal isolation between the RF terminals and the heater terminals at all times, especially when the switch is turned ON, since the relatively low impedance between the RF and heater lines (at low-resistance state of GeTe) compromises the isolation between the heater and RF ports. The current path between the RF lines and the RF to heater line is highlighted in Figure 3.15.

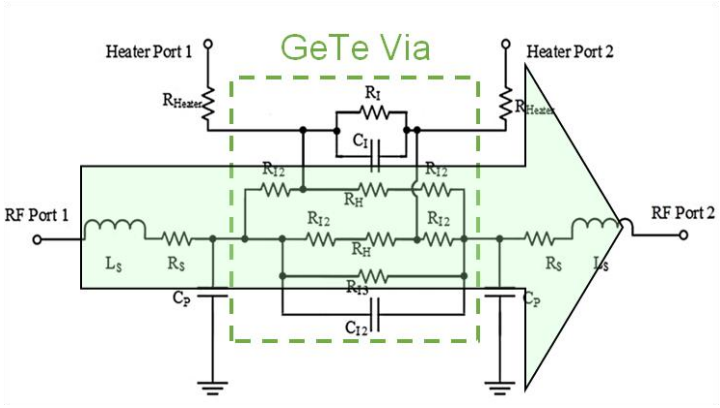

(a)

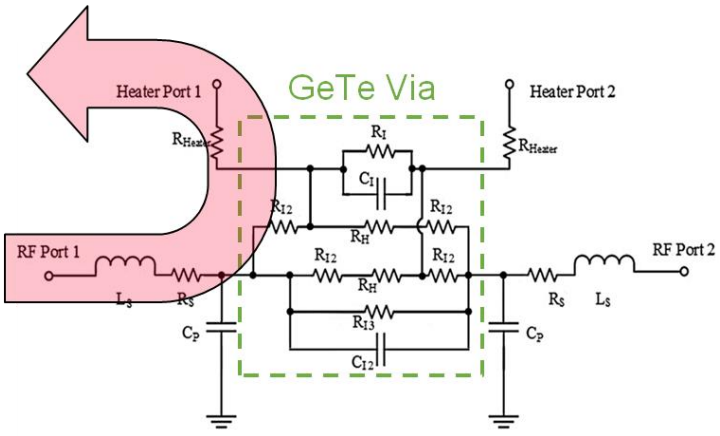

(b)

Figure 3.15. Demonstration RF power flow within the GeTe switch with direct heating when it is in the (a) ON-state and (b) OFF-state. In the OFF-state, the high impedance between the two RF terminals will force a big portion of RF power to flow through the heater terminals, and thus it is important to ensure good isolation between the heater and RF terminals.

The RF/heater signal isolation is ensured mainly through two methods. The first one is through the proper design and material choice of the resistive heater path with good impedance matching in order to provide high impedance between the RF and heater terminals while maintaining high heat delivery efficiency. The layout of the heater path is shown in Figure 3.7, which ensures a high resistance along the heater path, and that the resistance is concentrated near the GeTe via area. As for the material choice, TiN is used as the resistive heater material, deposited through a reactive sputtering process of Ti film with a N_2 environment. This deposition process is proven to be able to form a TiN layer that is metal-like, but more resistive than most metals due to the ceramic properties. TiN is also very thermally stable, which makes it a good choice for this purpose [67, 68]. The thickness of the TiN layer, along with the dimensions in the layout, is designed based on the electrical resistivity of the film so that the heater layer provides good heat delivery to GeTe and good isolation from the RF terminals.

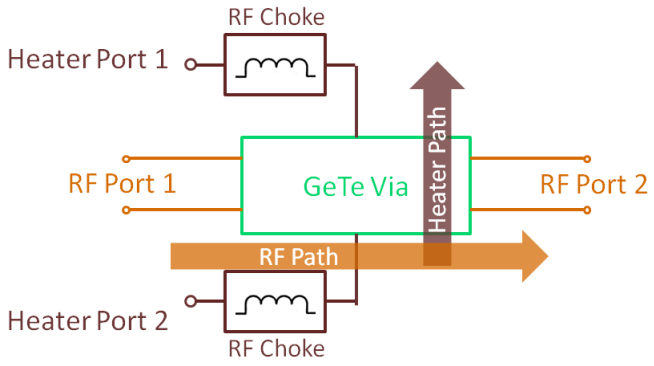

Figure 3.16. Schematic of the GeTe switch with RF choke modules connected to the heater terminals during measurement to ensure high isolation between RF and heater terminals.

The other method to maintain high signal isolation between the RF and heater terminals is through external circuit design. Compared to the operating frequency of the switch for RF signal transmission, the heating current pulses are considered low frequency. A good practice to improve isolation is to connect an RF choke to the heater terminals in order to block the RF signal leakage. A simplified schematic configuration of the device is shown in Figure 3.16.

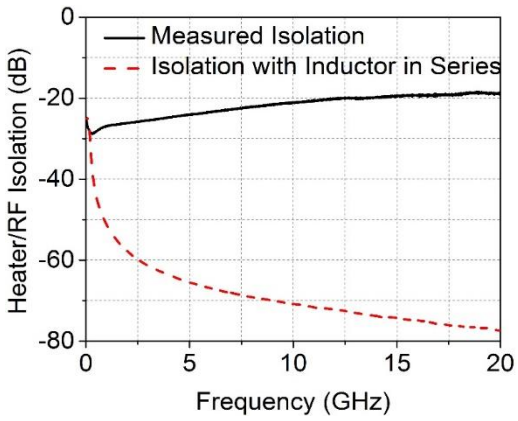

Figure 3.17. The S_{21} response between an RF terminal and a heater terminal from measurement and simulation with a 100 nH RF choke connected to the heater terminal.

To make sure that the RF power leakage through the heater terminals is not high enough to cause operation issues, an RF transmission measurement between an RF terminal and a heater terminal is performed to see the isolation. The results shown in Figure 3.17 suggests that the isolation between the two terminals is above 20 dB, which is considered high enough for low power operations, but with the RF choke modules connected to the heater terminal during switching activities, an even higher isolation between the RF and heater terminals can be achieved.

In order to evaluate the switching speed of the GeTe RF switches, measurement has been taken with an oscilloscope where heating voltage pulses and RF signal are applied to the GeTe switch and observed at the same time. In this measurement, the network analyzer is connected to input RF port of the device as the RF signal source, and the output RF port is connected to the oscilloscope for RF power level observation. The heating path connection is the same as normal switch operation, where the heater terminals are connected to the heating voltage source. Necessary matching networks are connected to the terminals in order to isolate the RF and heating signals from each other. A simplified block diagram for the measurement setup is shown in Figure 3.18.

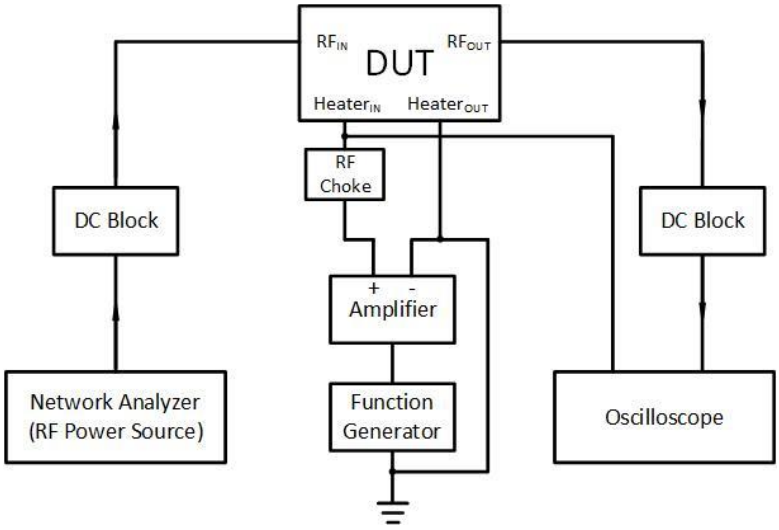

Figure 3.18. Simplified block diagram showing the setup for switching speed measurement for GeTe RF switches.

The heating voltage pulses are programmed and generated by the function generator and amplified through an amplifier to obtain the desired amplitude. For GeTe

amorphization to turn the switch OFF, the heating pulse is set with a width of approximately 0.5 μs, and the rise and fall times are both 0.2 μs. For GeTe crystallization to turn the switch ON, the pulse rise time is still set at 0.2 μs, but both the pulse width and the fall time are extended to at least 1.5 μs. The measurement results for switching speed in both directions are shown in Figure 3.19. The switching speed is approximately 0.75 μs for switching from ON to OFF, and 2.8 μs from OFF to ON.

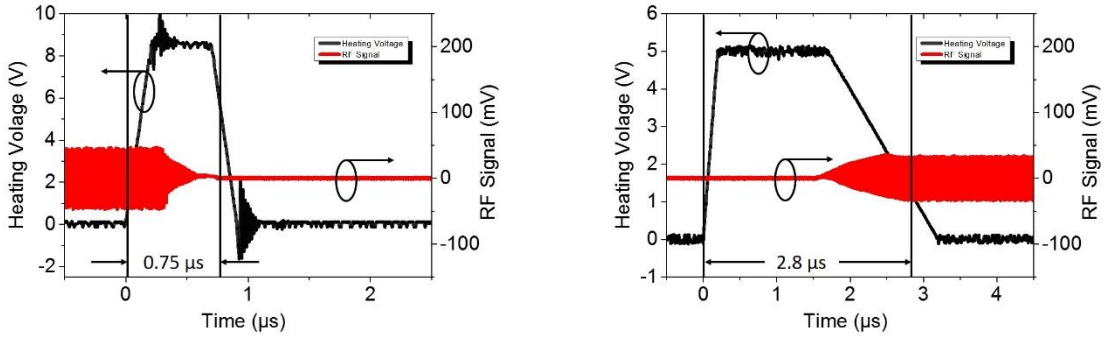

(a) (b)

Figure 3.19. Switching speed measurement of GeTe RF switch with direct heating scheme (a) from ON to OFF and (b) from OFF to ON.

3.2.2. Four-Terminal GeTe RF Switch with Indirect Heating Scheme

While the direct heating method is a novel and efficient way of delivering phase transition heat into the GeTe via of the RF switches, it has some limitations due to its structure. Even though it has been verified that the electrical isolation between the RF terminals and heater terminals can be maintained at a fairly high level, especially with the external RF choke, the direct electrical contact among all four terminals demand the use of a matching network, which adds to the overall size of the switch module. In order to

analyze and evaluate the advantage and disadvantage of the direct heating method, as well as to have an alternative heating scheme, we have also designed and developed four-terminal GeTe RF switches with the indirect heating method. In this type of GeTe RF switches, the heater is not directly connected through the GeTe via, but instead embedded underneath the main switch RF line and electrically isolated from the RF signal path. In phase change RF switch community, this has been the more popular method and had already been implemented and reported in several works with slightly different structures [69] [70]. This sub-section will discuss the structure, principle of operation, fabrication process, measurement and performance analysis of GeTe RF switches with indirect heating scheme and provide a brief comparison between the two heating methods.

3.2.2.1. Device Structure

Similar to the phase change RF switches with direct heating scheme, the switch with indirect heating one is also designed with two RF terminals laterally connected through a GeTe via, forming the RF signal transmission path. But instead of running the Joule heating current through the GeTe itself, a resistive heater is embedded underneath the GeTe via, and the RF path and the heater path are electrically isolated (but thermally coupled) with a dielectric layer.

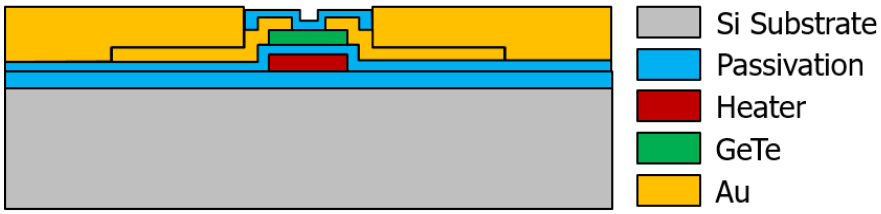

Figure 3.20. Cross-sectional schematic showing the structure of the four-terminal GeTe RF switch using the indirect heating method.

The cross-sectional schematic of the four-terminal GeTe RF switch with indirect heating scheme is shown in Figure 3.20. The resistive heater is first patterned and embedded by depositing an electrical isolation layer on top. After the heater layer embedding is complete, the RF signal path is built by patterning the single-layer GeTe via and then RF electrodes. Since there will not be a top heater layer like the previous design, the GeTe via area defined by the RF metal is exposed, so it is generally preferred to have a top passivation layer as a protection layer against oxidization and any other effects that may cause instability issues of the GeTe film. In order to evaluate the pros and cons of having a top passivation layer, devices without the top passivation dielectric have also been built for comparison. Details regarding design modifications and fabrication process are discussed later.

For thermal actuation, DC voltage pulses are applied through the heater terminals and current is drawn through the resistive heater underneath the GeTe via. The phase transition of GeTe relies on proper thermal coupling between the heater and the GeTe film. Therefore, choosing a proper electrical isolator and at the same time good thermal coupler material is critical to successful switching activities. The ideal material for the

isolation layer should have good thermal conductivity and low dielectric loss, and also should be compatible with the fabrication process. Based on thermal simulations with different materials, a few materials have been chosen as the isolation layer and have been tested.

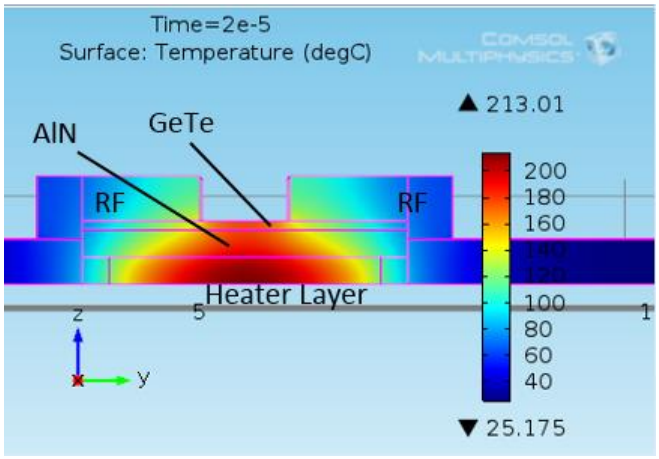

Figure 3.21. Thermal simulation using COMSOL FEA software showing the temperature distribution on the cross-section of the GeTe RF switch with indirect heating when a heating pulse is applied through the heater layer.

Thermal simulations have been performed using COMSOL to estimate the heat flow within the GeTe RF switch and the temperature distribution after a heating pulse is applied through the heater path. A temperature distribution plot is shown in Figure 3.21 as an example of how the heat generated by the resistive heater is delivered to the GeTe via. In this simulation, aluminum nitride (AlN) is used as the isolation layer between the heater and the GeTe film. From the plot, it can be seen that most of the thermal energy is generated closer to the center of the resistive heater, and is delivered outwards in all radial directions. In the GeTe layer, the GeTe via area between the two RF electrodes will

be the first volume of GeTe to be heated up, and the GeTe areas that overlap with the RF electrodes are heated up at a much slower rate. This heat distribution pattern has been noticed during the simulation and has been taken advantage of in the design. During the operation of the switch, the heating voltage pulses are controlled so that only the GeTe via area is going through the phase transitions. The GeTe areas overlapping with the RF electrodes will stay in the crystalline state at all times. This reduces the volume of GeTe going through phase transitions, and will help obtain a faster switching speed.

3.2.2.2. Fabrication Process

GeTe RF switches with indirect heating scheme are also fabricated on passivated silicon substrates. Since the indirect heating method needs to generate more thermal power than the direct heating method due to the different thermal coupling mechanism, a heat sink with a higher heat dissipation rate is preferred in order to maintain a high heating/cooling speed and avoid potential device cross-talk. In order to satisfy the heat dissipation speed requirements, the passivation layer needs to have a high thermal conductivity as well as a decent heat capacity. For the same reason, different isolation layer materials have also been tested. Details will be discussed in this sub-section.

The fabrication process of the GeTe RF switch with indirect heating has been modified over time to ensure good layer quality and performance. The modifications include both material choices and detailed fabrication parameters. A general process flow of the devices is shown in Figure 3.22.

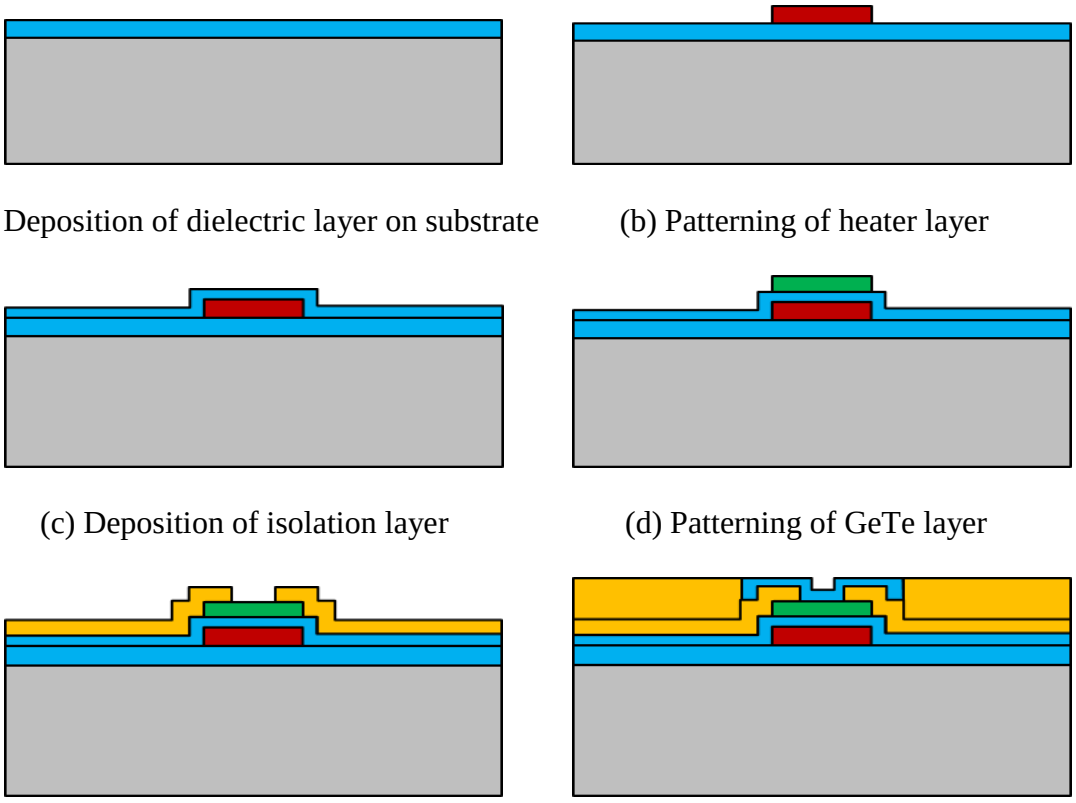

(a) Deposition of dielectric layer on substrate (b) Patterning of heater layer

(c) Deposition of isolation layer (d) Patterning of GeTe layer

(e) Patterning of RF electrodes layer (f) Deposition of top passivation and metals

Figure 3.22. Fabrication process flow of the GeTe RF switch with direct heating

The process starts with a dielectric layer deposition on the silicon substrate. This layer is used as passivation to prevent DC current leakage into the substrate, and also as a heat dissipation layer. The heater layer is patterned on top of the dielectric layer with a thickness between 100 nm and 200 nm. While TiN is often used as the heater layer, other materials including tungsten (W) and titanium-tungsten (TiW) have also been tested for this purpose. The patterned resistive heater needs to be embedded before the deposition of GeTe, and this is done by depositing another dielectric layer to ensure electrical insulation between the heater layer and the GeTe layer. Since the terminal pads of the

heater layers need to be in contact with the RF probes for device measurements, the dielectric layer is patterned through plasma etching to expose the pads of the heater layer. The GeTe film is patterned with a thickness of approximately 100 nm. Other thicknesses have also been used throughout the characterization as the thickness of GeTe film could affect the crystallization process. After the patterning of GeTe film is complete, the RF electrodes of gold with a thickness of 200 nm are patterned to establish contact with the GeTe film as well as to define the via area. Finally, the gold metal routing and top passivation layers are deposited and patterned.

During the GeTe deposition and patterning steps, it has been discovered that GeTe films are often prone to possible damage from later processing steps, such as the photoresist developer from the photolithography for the metal electrode contact layer, as well as the solvents used for GeTe pattern lift-off. Since the film quality of GeTe plays a vital role in the device performance, and it is important to ensure good GeTe-metal contact, an additional protection layer covering the GeTe film has been deposited in many fabricated sample. The deposition of the protection layer takes place immediately after the sputtering of GeTe, and a thin film of molybdenum (Mo) is usually used. After the metal electrode contact layer is patterned, the Mo protection layer on top of the GeTe film will be shorting the electrodes because of the low electrical resistivity of Mo. Therefore, an additional step to etch the exposed Mo layer is necessary to make sure that the metal electrodes are connected only through the GeTe via. Etching for Mo is performed using plasma SF_6 etching, and the etching process needs to be well controlled not to damage the GeTe layer underneath.

As discussed before, in GeTe RF switches with the direct heating scheme, the heater material needs to have a high resistivity to ensure proper isolation between RF and DC heating lines. In the indirect heating design, since the heater in not in direct contact with the GeTe via, other choices of heater materials can be considered. Since the localized peak temperature from the heater could be as high as 800°C, the heater material is required to be stable at high temperatures. While TiN has been proven to have high temperature durability, its high electrical resistivity results in high power consumption. Tungsten (W) has been tested as an alternative heater material since it has a much lower resistivity and decent high temperature stability. Other suitable materials tested include an alloy of titanium and tungsten (TiW). The reliability of the heater layer is very critical to the reliability of the switch. Therefore, further investigation into the heater robustness has been performed regarding both material choice and fabrication process that will be discussed later.

As previously mentioned, the bottom dielectric layer for substrate passivation and the isolation layer between the heater and GeTe also serve as heat conduction layers. In order to ensure fast and effective switching, the dielectric materials are preferred to have good thermal properties such has high thermal conductivity. Among the common choices of dielectric layers, aluminum nitride (AlN) has much higher thermal conductivity than silicon dioxide or silicon nitride [71], and is a good choice for both the bottom passivation layer and the isolation layer.

Table 3.1. Material properties of dielectric layers and parameters used in thermal analysis

Material	SiO_2	Si_3N_4	AlN
Relative Permittivity	3.9	7	~9
Thermal Expansion Coefficient (K^{-1})	0.5×10^{-6}	2.3×10^{-6}	4.5×10^{-6}
Specific Heat Capacity (J/kg·K)	730	700	740
Thermal Conductivity (W/m·K)	1.4	3 – 20	140 – 180

Thermal properties of a few dielectric materials are compared in Table 3.1. These values are believed to be close to the properties of materials deposited from our facility, and therefore, have been used in thermal simulations and analysis. It can be seen that among SiO_2, Si_3N_4 and AlN, the thermal expansion coefficients are at the same level with AlN being the highest and SiO_2 being the lowest, but they are all much lower compared to other materials such as metal, so the expansion caused by thermal stress can be ignored. Their heat capacities are also very close to one another. But in terms of thermal conductivity, they are very different, with AlN having much higher thermal conductivity than SiO_2 (over 100 times) and Si_3N_4 (~10 – 50 times), as mentioned before. Considering the function of the dielectric layer used for both substrate passivation and isolation between the resistive heater and GeTe via, it is preferred to have dielectric layers with high thermal conductivity for faster heat delivery to the via as well as rapid heat dissipation through the substrate and air. For this reason, AlN has been used in the GeTe switch fabrication process as both the substrate passivation layer and the electrical isolation layer. However, the only available deposition process for AlN from our facility is through high-temperature sputtering, which requires considerable optimization to reach

high-quality films. On the other hand, SiO_2 layers can be thermally grown using a mature process on silicon substrates, yielding very good film quality. And since compared to the silicon substrate, the passivation layer is much thinner, SiO_2 has also been considered as the passivation layer choice in some fabricated batches.

As for the isolation layer between the resistive heater and the GeTe film, while high thermal conductivity is preferred for fast heat delivery, another important factor to consider is the quality of the GeTe film deposited on the isolation layer. Experimental results show that the GeTe film deposited on top of an aluminum nitride layer tends to have degraded quality in terms of both adhesion and crystallinity after annealing. The reason may be low sputtered AlN quality in test samples or different crystalline structure of AlN and GeTe, making AlN a poor choice of seedlayer for GeTe. As an alternative, silicon nitride has been tested as the isolation layer, and GeTe films deposited on top of silicon nitride tend to have a better adhesion as well as better crystallization results. Even though the relatively low thermal conductivity of silicon nitride reduces the heating efficiency, but with a reduction in the layer's thickness as well as other fabrication detail modifications, the trade-off can be managed.

During the fabrication process, GeTe film quality issues aroused quite often. The most common issues include bad adhesion with GeTe peeling off after lift-off process, stress induced surface defects and cracking, and poor crystallization. Since the quality of GeTe films is critical to the functionality and performance of the switches, an alternative approach for GeTe layer patterning was developed. Instead of using lift-off as the patterning method, the GeTe film is patterned with plasma etching. According to the test

results, GeTe films can be patterned with a number of different gaseous etchants under RF bulk plasma such as Cl_2 and BCl_3. After characterization, a dry etching recipe with a combination of BCl_3 and Ar gas using RF generated plasma has been developed for GeTe etching that yielded both good etching rate and surface cleanness. The biggest advantage of dry etching over lift-off is that the GeTe patterns are much cleaner, since the lift-off process tends to leave GeTe residue on the substrate. However, the dry etching method also has process related issues. In the dry etching process, the patterns are usually defined with photoresist based masks, which become very difficult to remove after exposure under plasma. This directly affects the contact between GeTe and RF electrodes, and therefore a GeTe surface cleaning needs to be performed before further steps. The most effective way of removing photoresist residue is through O_2 plasma clean, but this step tends to easily oxidize the surface of GeTe film, and therefore, needs to be well characterized. To sum up, dry etching process serves well as an alternative patterning approach for the GeTe layer, which is tested to have better film quality, but the process is much more delicate and complicated to perform.

Another issue during the fabrication is the heater embedding process. Since the heater path has a thickness between 100 nm and 200 nm, the GeTe layer would need to be deposited and patterned on top of an uneven surface. While the sputtering process with GeTe is verified with good step coverage conformity, it is still preferred to have a flat surface for the deposition of the GeTe layer. This can be achieved by pre-etching the substrate passivation layer before the deposition of the heater layer. As long as the etched

thickness of the passivation layer is controlled to be the same as the heater layer, a flat surface can be achieved.

A schematic showing the difference between the substrate stack with and without the pre-etching process prior to the heater layer pattering is shown in Figure 3.23. With a well-controlled pre-etching process, the surface after deposition of isolation layer can be made flat for the GeTe layer deposition. In reality, however, the lift-off process of heater layers also tends to leave patterns with sharp edges, and the height of the wall-shaped edges is often several times more than the intended thickness of the layer. With this problem, even a pre-etching process of the passivation layer cannot ensure a good flat surface, and an additional polishing step is needed to address this issue. In this work, a meticulous heater embedding process flow has been developed and is shown in Figure 3.24. This procedure is performed after the deposition of the dielectric passivation layer on the silicon substrate. Before depositing the heater layer, a plasma etching is performed on the passivation layer. The heater layer is deposited and patterned using the same mask as the previous step, followed by a mechanical polishing process to remove any residue on the edges of the patterns. Then a dielectric layer is deposited on top as the isolation between the heater and GeTe. It is difficult to keep the surface perfectly flat at this point, because the pre-etching depth and the heater deposition thickness cannot be exactly matched. Therefore, a chemical-mechanical planarization (CMP) is used to polish the isolation layer. Since polishing could greatly reduce the thickness of the dielectric, an additional deposition is preferred afterwards. This heater embedding process can help

yield a better GeTe film quality as well as lower-resistance electrical contact between GeTe and RF electrodes.

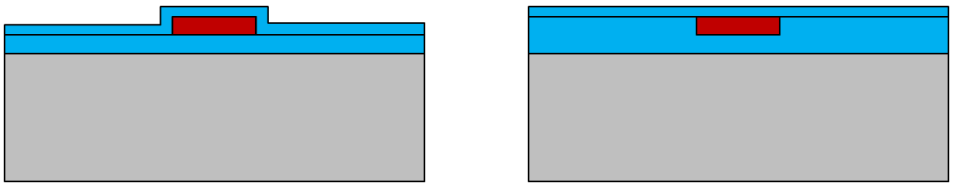

(a) (b)

Figure 3.23. Heater embedding process for GeTe RF switches with indirect heating. (a) Heater embedding without pre-etching of passivation layer, yielding an uneven surface. (b) Pre-etching process applied prior to heater layer patterning, resulting in a flat surface.

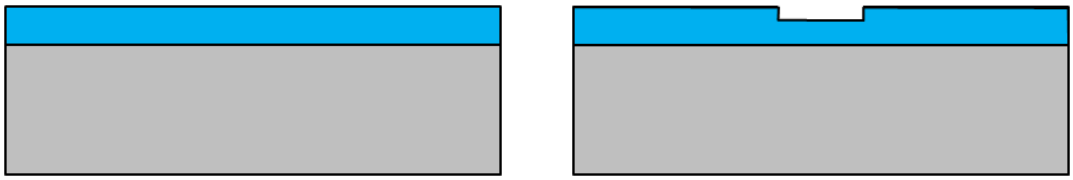

(a) Deposition of passivation layer on substrate (b) Pre-etching of passivation layer

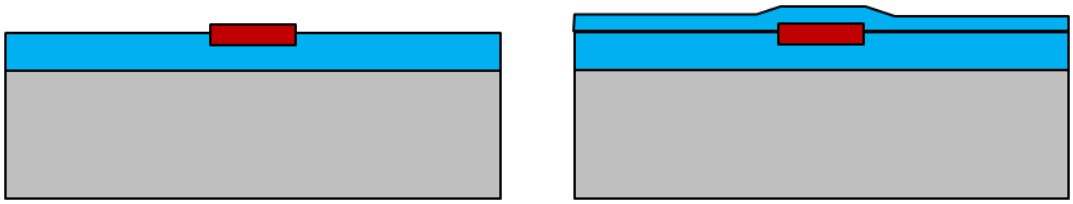

(c) Patterning and polishing of heater layer (d) Deposition of isolation layer

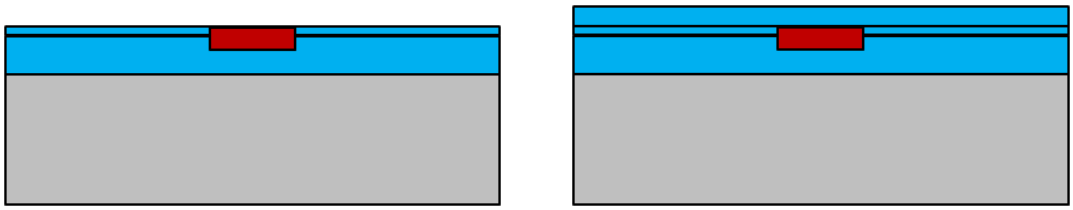

(e) CMP polishing of isolation layer (f) Additional deposition of isolation layer

Figure 3.24. Heater embedding process with multiple isolation layer deposition and polishing processes in order to obtain a flat surface before the deposition of GeTe layer.

After the fabrication process, SEM images have also been taken to visually evaluate the device quality. SEM images of a fabricated GeTe RF switch with direct heating

scheme are shown in Figure 3.25, with an entire device view (left) and a zoomed-in view of the GeTe via area (right).

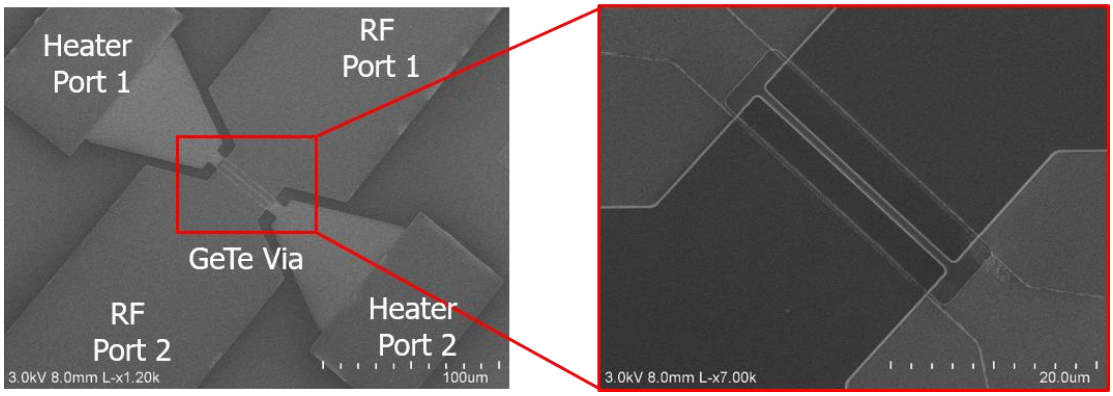

Figure 3.25. SEM images of the GeTe RF switch with indirect heating.

The RF and heater terminals as well as the ground ring in the device are similar to the device with the direct heating scheme. In the zoomed-in image on the right, the GeTe via area is the connection between the two RF ports, and the heater layer path is placed underneath through the GeTe via. The RF path and heater path are also perpendicular to each other in the same plane, but the two paths are not in direct electrical contact, instead, isolated by an isolation layer, as discussed before.

3.2.2.3. Measurement Results

The measurement process for this type of devices is similar to the process for the directly heated switches devices. RF measurements are performed using Cascade ACP probes landed on the RF terminal pads of the device, and the RF signal transmissions are evaluated with network analyzer. The on-wafer measurement results have also been de-

embedded based on the measurements from reference open and short devices from the same wafer in order to eliminate inaccuracy caused by probe contact and measurement setup. Electromagnetic simulation results acquired using ANSYS HFSS are also included as a comparison. The measured and simulated insertion loss and isolation of the GeTe RF switch with indirect heating are shown in Figure 3.26.

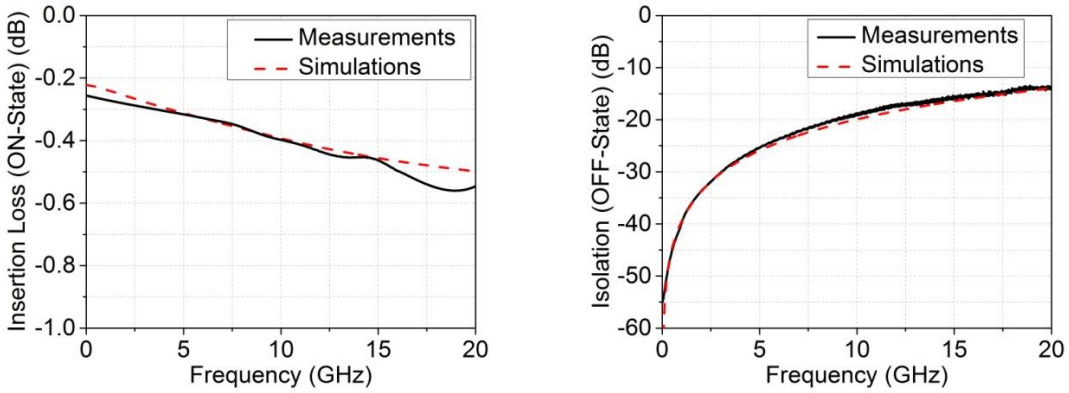

(a) (b)

Figure 3.26. Measured (de-embedded) and simulated RF response of the GeTe RF switch. (a) Insertion loss at the ON-state. (b) Isolation at the OFF-state.

As shown in the measured results, devices exhibit an insertion loss of less than 0.6 dB and an isolation over 11 dB from DC to 20 GHz. In order to compare the performance of the devices with the two different heating methods and structures, the device measured here also have an RF electrode width of 20 μm. In comparison to the previously shown results, the switch with the indirect heating method has a slightly worse insertion loss and isolation especially at higher frequencies. This is possibly because the embedded heater

underneath the GeTe via is creating a parallel-plate based capacitor with the RF metal and therefore introducing a large amount of parasitics. Regarding this issue, the structure has been modified to improve the performance, and results on performance improvement investigations are discussed in later sections of this thesis.

For the four-terminal indirectly heated GeTe switches, similar modeling methods are used for the GeTe material, but the equivalent circuit model is much simpler in comparison because the heater terminals are not connected to the GeTe via and the two electrical paths are separated. The equivalent circuit model is shown in Figure 3.27, which was first proposed in [72]. The GeTe via here uses the same model of a parallel connection of a resistor R_I, a capacitor C_I, and a series R-C connection. The parasitic capacitance formed between the heater path and the RF signal path is modeled by C_{P2}. Similarly, the parasitic components from the RF routing lines as well as the parallel-plate capacitance of the line to the substrate are model using R_S, L_S, and C_P.

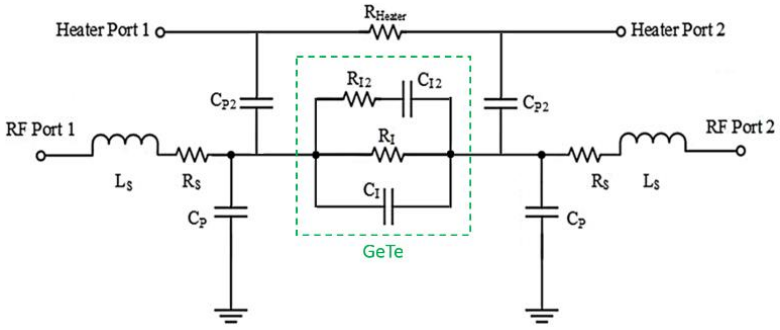

Figure 3.27. Equivalent circuit model of the four-terminal GeTe RF switch with indirect heating. The circuit elements shown in the model include resistive and reactive parts from the components of the GeTe switch and the external metal routing as well as the measurement setup.

When the switch is in the ON-state, the transmission between the two RF terminals is primarily enabled by the low resistance (R_I) of the crystalline state GeTe. When the

switch is in the OFF-state, the resistance between the RF terminals becomes much higher, and the capacitance becomes the dominant factor in determining the RF isolation. When the switch is turned ON, the resistance from the RF terminals is $R_{ON} \approx 3\ \Omega$, and when it is turned OFF, the capacitance from the RF terminals is $C_{OFF} \approx 12.5$ fF. Therefore, the switch is measured to have a cut-off frequency of 4.2 THz.

The key to improving the performance of the indirectly heated GeTe RF switch is to reduce the parasitic capacitance, which can be done by optimizing the structure and sizing of the GeTe via and the resistive heater. In the device measured above, the resistive heater path has a width of approximately 7 μm, which is decided according to the thermal simulation results. As discussed before, the resistive heater and the RF signal path form a parallel-plate based capacitor, which greatly increases the parasitics of the device. If the width of the heater path is reduced, the heater resistance is increased, which results in higher heating voltage for thermal actuation. On the other hand, the parasitic capacitance can be reduced so that the RF performance of the switch is improved. In order to explore this trade-off, devices with a heater width of 3 μm have been fabricated and tested. According to the test results, the required voltage of the heating pulses is 30% to 50% higher than the previous design, but the RF performance has shown great improvement, with the device having an insertion loss that is lower by ~0.3 dB.

With the width of the resistive heater path reduced, another significant change is the more localized heating on the GeTe film. The volume of GeTe film that is experiencing phase transitions is only limited to the via connecting the RF electrodes, rather than the entire GeTe pad as in the previous design.

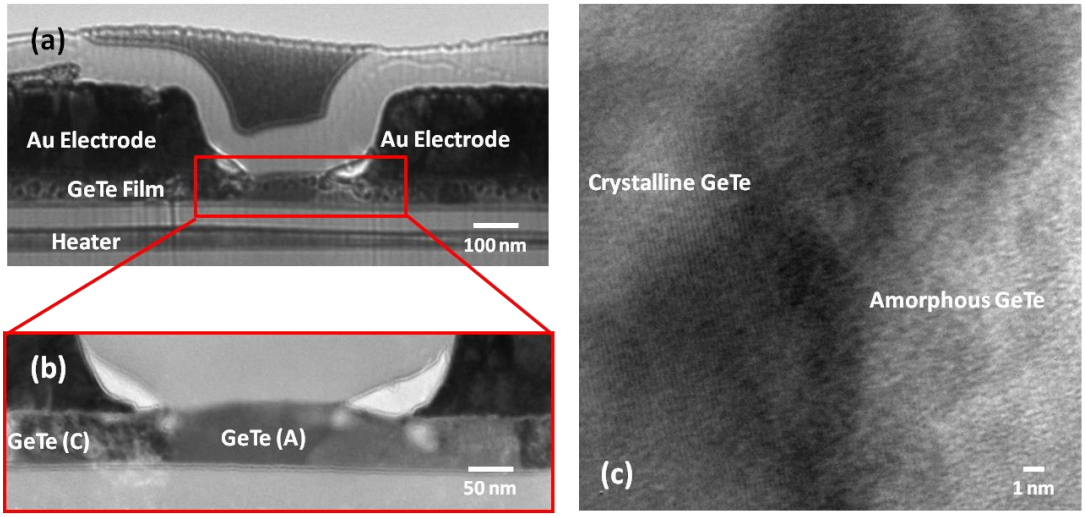

Figure 3.28. TEM images showing the GeTe RF switch (a) when in the OFF state, (b) the enhanced view of the GeTe film where only the GeTe volume at the via area is amorphous, and most GeTe volume remains crystalline. (c) High-resolution TEM image showing the crystalline-amorphous interface of the GeTe film.

As shown in Figure 3.28, with the width of the resistive heater path reduced in the modified design, when the GeTe switch is turned OFF, only the GeTe area between the RF electrodes is in amorphous phase, while the rest of the GeTe film stays in crystalline state at all times. Since the total volume of GeTe going through phase transitions during switching activities is reduced, the switching speed of the switch is improved. More importantly, since the amorphous state GeTe behaves like dielectric material with a high dielectric constant, this modified design reduces the parasitic capacitance formed between the RF electrodes and resistive heater path compared to the previous design. This is another significant contribution to the high-frequency performance of the GeTe switch.

Another design trade-off is between the thermal delivery efficiency and the parasitic capacitance. This is balanced by isolation layer thickness between the heater and the GeTe film. Although have a thin isolation layer ensures a fast and efficient heat delivery from the heater to the GeTe via, the reduced distance between the heater and the RF path results in a higher parasitic capacitance. The initial designs used an isolation layer with a thickness of approximately 50 nm, but modifications have been made to increase the thickness to 100~ 150 nm. This naturally results in degraded heating efficiency, but the parasitics can also be greatly reduced for better RF performance.

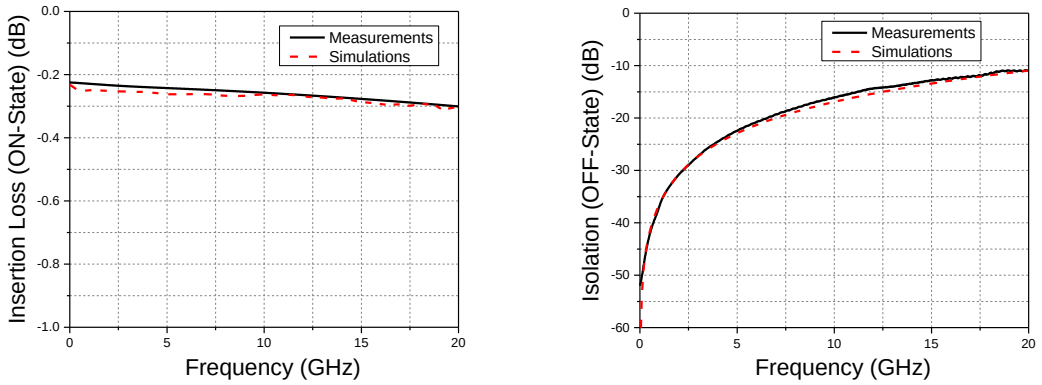

(a) (b)

Figure 3.29. Measured (de-embedded) and simulated RF response of the GeTe RF switch with modified design showing improved loss performance. (a) Insertion loss at the ON-state. (b) Isolation at the OFF-state.

With the design modifications to the GeTe RF switch with indirect heating scheme, the devices have been measured to evaluate the RF performance improvements. The de-embedded insertion loss and isolation are compared to the corresponding simulation

results (Figure 3.29). The ON-state insertion loss has been reduced to approximately 0.3 dB at 20 GHz. Other than the modifications discussed above, a more aggressive sizing has also helped reduce the insertion loss. The OFF-state isolation of the device is still above 11 dB from DC to 20 GHz. Even though the parasitics have been reduced, the isolation was traded off with the insertion loss. The figure-of-merit cut-off frequency for this improved design is approximately 5.6 THz, which is a performance improvement compared to the previous design.

The switching speed of the GeTe RF switch with indirect heating scheme is also evaluated using the same setup. Since the phase transition process is a property of the GeTe film, the switching speed of the switch with indirect heating is similar to that with direct heating. The difference in switching speed is due to the structural difference, which results in difference in heat delivery and dissipation rate. Figure 3.30 shows the measured switching speed for the device. The switching time is around 0.6 μs to turn the switch OFF and 2 μs to turn the switch ON.

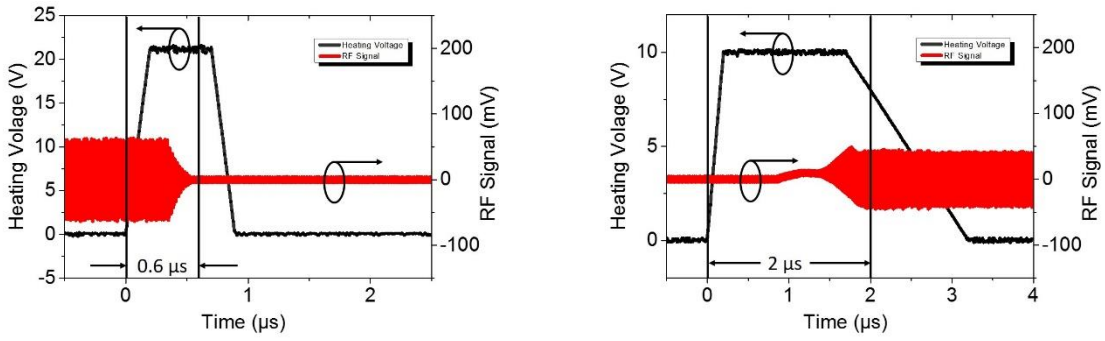

(a) (b)

Figure 3.30. Switching speed measurement of GeTe RF switch with indirect heating scheme (a) from ON to OFF and (b) from OFF to ON.

Table 3.2. Comparison of performance among different GeTe RF switch designs

Design	Insertion Loss	Isolation	R_{ON}	R_{OFF}	R_{OFF}/R_{ON}	C_{OFF}	f_{co}	Heating Power
Direct Heating	0.5 dB @ 20 GHz	18 dB	5 Ω	18 kΩ	4×10^3	8 fF	4 THz	85 mW/ cycle
Indirect Heating	0.6 dB @ 20 GHz	11 dB	3 Ω	20 kΩ	5×10^3	12.5 fF	4.2 THz	300 mW/ cycle
Indirect Heating (Modified)	0.3 dB @ 20 GHz	11 dB	2.7 Ω	22 kΩ	8×10^3	10.5 fF	5.6 THz	500 mW/ cycle

In order to better compare the RF performance among the different types of switches, some of the RF measurement data are shown in Table 3.2. With similar dimensions, the first two designs of switches show similar RF responses, and the differences mainly result from the structure induced parasitics, which are different for the two switch types. The modified GeTe switch with indirect heating scheme uses more aggressive sizing for improved RF performance, but the heating power is increased as a trade-off. In terms of integration compatibility and ease of fabrication, the indirectly heated switch design is advantageous.

3.3. Power Handling Analysis and Thermoelectric Modeling

Due to the fact that the GeTe phase change switches rely on thermal actuation to achieve switching, the transmitted RF signals could interfere with the phase transitions of GeTe if the RF power level gets sufficiently high, and the switch linearity and power handling capability could therefore be affected. This kind of self-actuation needs to be

avoided. In order to better analyze the thermal properties of the GeTe switches, a modeling method linking the thermal and electrical properties of the GeTe via and the switch was proposed. This method can be used to model the switch operation at different RF power levels, and explore how high RF power interferes with the stability of the GeTe film and the linearity of the RF response. The earliest reported effect to model the non-linearity response of the GeTe based RF switch can be found in [73], which relates the physical properties of GeTe such as the electrical resistivity and thermal conductivity to the heating effect from the RF signals. An improved modeling method based on this was later proposed with more accurate results on predicting the input third-order intercept point (IIP_3) and 1-dB compression point (P_{1dB}) for the switch [72]. This new method, the thermoelectric modeling method, relates the thermal activity caused by the RF signals through the switch to the property change of the GeTe film. The diagram for the thermoelectric model is shown in Figure 3.31.

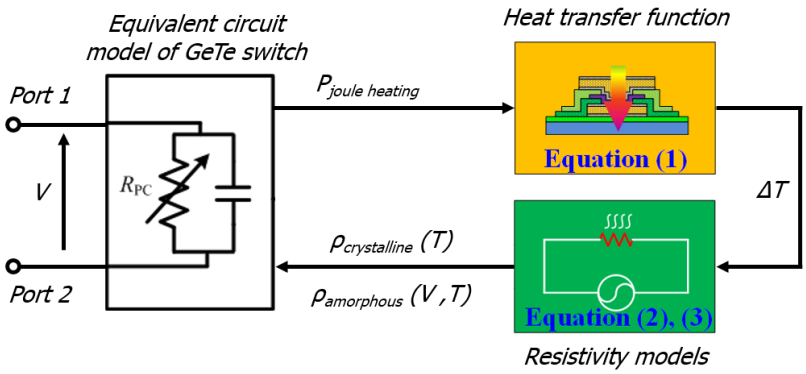

Figure 3.31. The thermoelectric model of the GeTe based RF switches. This model consists of a simplified equivalent circuit model of the phase change switch, and the heat transfer function as well as the modeling of the changing electrical resistivity of GeTe with changing temperature and voltage across the phase change layer.

In this model, the equivalent circuit for the GeTe switch is simplified to a parallel connection of a resistor with a changing resistance and a capacitor, with different element values for each type of the switch. The heat transfer function is modeled based on Equation (3.1). The electrical resistivity of the GeTe at the crystalline and amorphous states are modeled based on Equations (3.2) and (3.3), where k, q, τ_0, E_F, V, Δz and u_a indicate the Boltzmann constant, elementary charge, time constant for trapped electrons, Fermi level, applied voltage, short trap distance, and effective thickness of the GeTe layer, respectively.

$$H(\omega) = \frac{\Delta T}{P} = \frac{1}{V_m} \cdot \frac{d_m[(d_f/k_f)\cdot(\tanh\beta_f/\beta_f)+R_B]}{1+j\omega C_m d_m[(d_f/k_f)\cdot(\tanh\beta_f/\beta_f+R_B)]}, \beta_f = d\_f\sqrt{j2\pi f_h \frac{C_f}{k_f}} \cdot \text{(3.1)}$$

$$\rho_{crystalline} = \rho_0[1 + \alpha(T - T_{ref})] \text{ .....(3.2)}$$

$$\rho_{amorphous} = \frac{kT\tau_0}{(q\Delta z)^2 N_T} e^{-\frac{(E_C - E_F)}{kT}} \cosh^{-1}\left(\frac{qV_A}{kT}\frac{\Delta z}{2u_a}\right) \text{ .....(3.3)}$$

The temperature rise (ΔT) of the GeTe layer from the heating power (P) can be estimated using the heat transfer function (Equation (3.1)) [74]. At the crystalline state, the resistivity exhibits metal-like temperature dependence (Equation (3.2)) [55]. We measured the TCR (α) of GeTe to be 2.3×10^{-3}/K in this state, which is close to the value reported in [55]. The Poole-Frenkel (PF) model is used in the amorphous state to model the change of the resistivity of GeTe (Equation (3.3)) [47]. The two main parameters in Equation (3.3) are E_C-E_F (energy distance between the Fermi level and the conduction

band) and N_T (trap concentration). Reducing E_C-E_F and increasing N_T make the amorphous resistivity vary less with temperature rise and high voltage swings, respectively, which results in improved P_{1dB} and IIP_3.

The simulated frequency of the heat transfer function based on Equation (3.1) show a low-pass characteristic for both types of switches [74]. The low frequency transfer function gain is much dependent on the dimensions of the GeTe patch connecting the RF pads and the thermal properties of the material surrounding the GeTe [72]. The two switch types that were measured have similar thermal transfer functions since they have similar dimensions of the GeTe pad, and similar thermal properties of the two structures, except that the directly heated switch has both a top and bottom heater layer in contact with GeTe, whereas the indirectly heated switch only has a bottom isolation layer underneath with a smaller thickness. Therefore, the directly heated switch has a better heat capacitance compared to the indirectly heated one, resulting in a slightly better linearity.

The measured response of the switch and predicted response using the thermoelectric model are compared in Figure 3.32. As can be seen, the input third-order intercept points (IIP_3s) are both measured to be around 30 dBm, which vary at different center frequencies and different frequency offsets. For both types of switches, the IIP_3 response at the ON state shows an increasing trend as the frequency offset increases. This is because with a higher frequency offset, the mixed term in the IIP_3 measurement is suppressed, so the third-order inter-modulation signal is lower, and thus the linearity is better. The changing center frequency, however, barely affects the linearity since the

frequency response of the switches at the ON state shows a relatively flat transmission (Figure 3.13(a), Figure 3.26(a) and Figure 3.29(a)). On the other hand, The IIP_3 response at the OFF state is independent of the frequency offset, since the high switch impedance at the OFF state results in a much lower heat generated from RF signals, but the IIP_3 increases with an increased center frequency, because at the OFF state the linearity depends on the voltage across the switch, which is a function of the switch impedance [72]. The discrepancy between the measurement and simulation, especially in the modeling of IIP_3 with changing frequency offset, indicates that other possible factors, such as current crowding, crystalline orientation, and phase change nucleation mechanisms, should be taken into account.

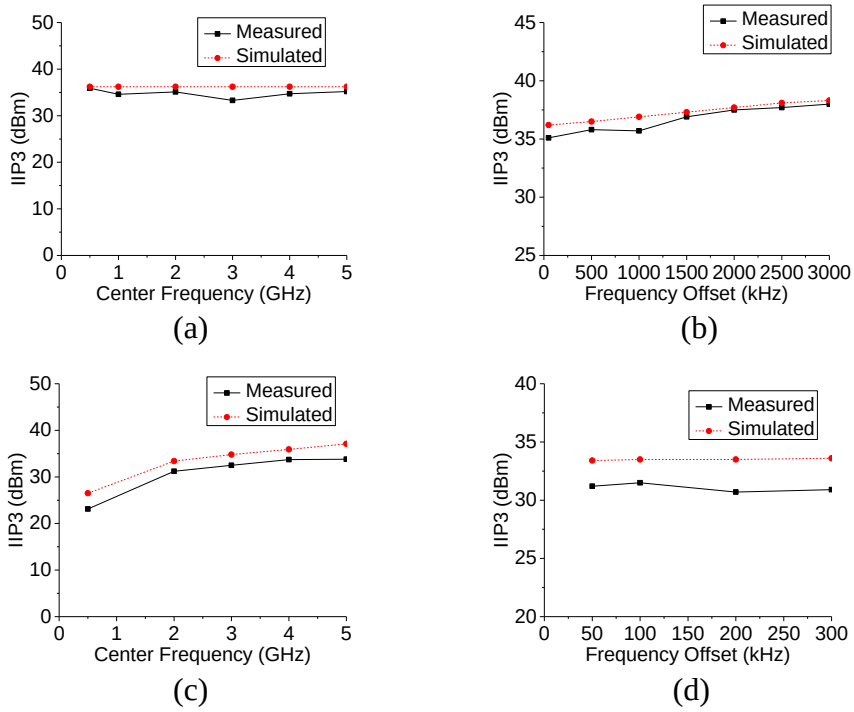

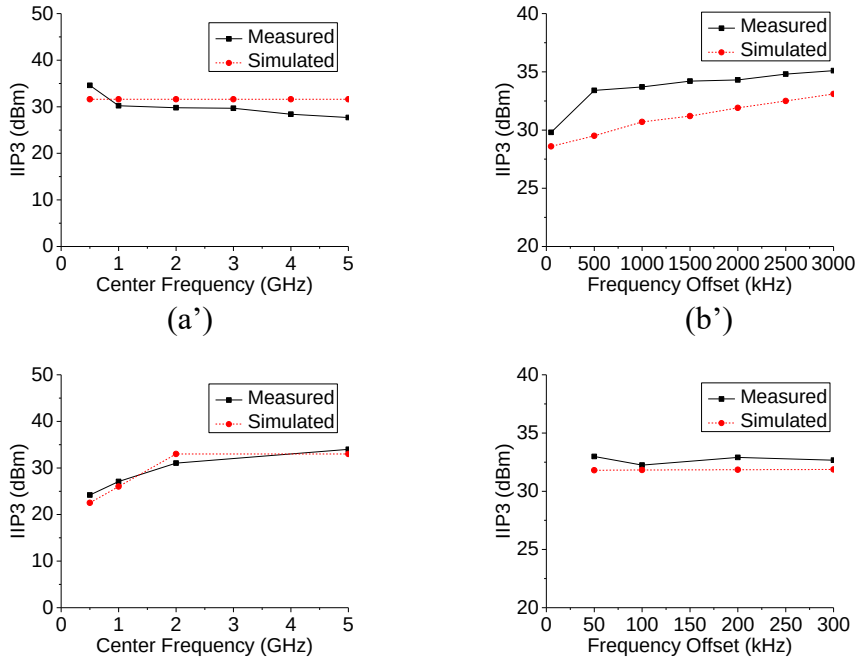

Figure 3.32. Simulated and measured IIP_3 of a directly heated switch at (a), (b) crystalline state and (c), (d) amorphous state with (a), (c) changing center frequency and a constant 50 kHz frequency offset, and (b), (d) changing frequency offset and a constant 2 GHz center frequency. (a') – (d') show the corresponding plots for an indirectly heated switch.

The power handling capability of the GeTe RF switches are also evaluated by measuring the 1-dB compression point (P_{1dB}) of the devices. The measurement results are shown in Figure 3.33. Due to setup limitations, the RF signal power did not go higher than 20 dBm during this measurement, but the output power compression has not reached 1 dB at the input power of 20 dBm for either type of devices, indicating that P_{1dB} is higher than 20 dBm.

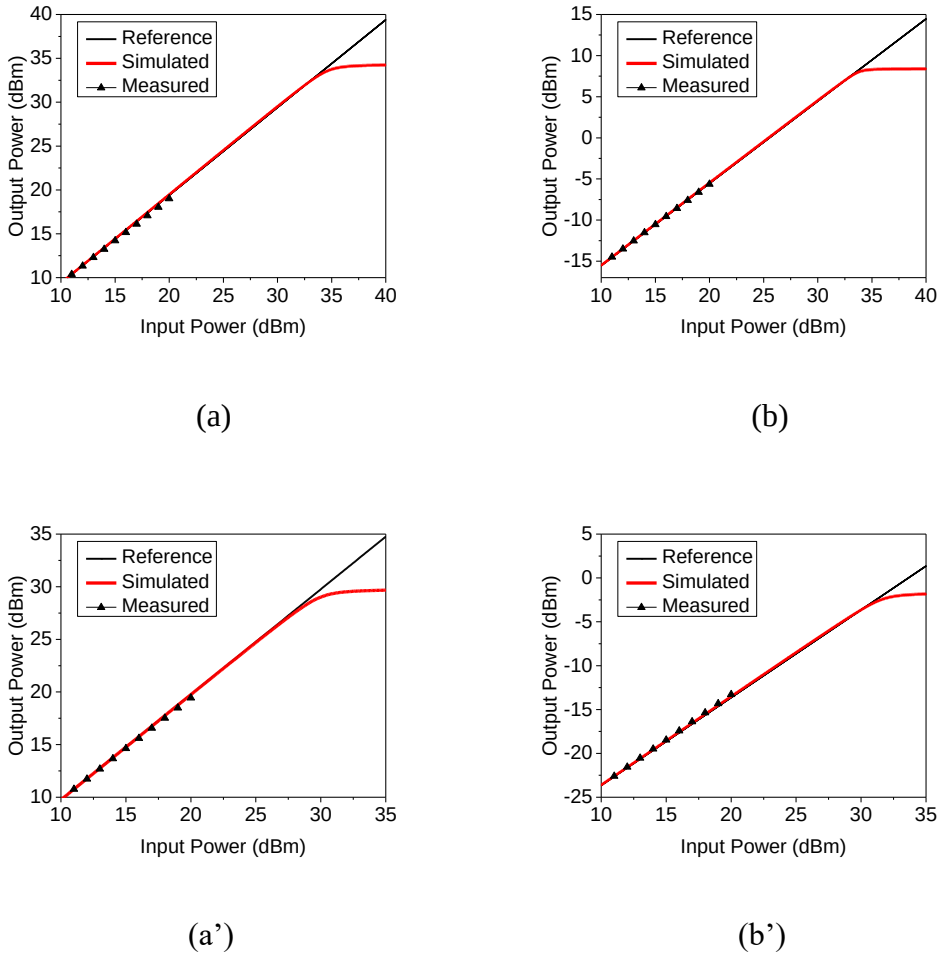

Figure 3.33. P_{1dB} measurement and simulation results for GeTe RF switches (a), (b) with direct heating scheme and (a'), (b') indirect scheme and (a), (a') in ON state and (b), (b') in OFF state. The measured results show that both types of devices have P_{1dB} higher than 20 dBm at both states, and the simulated results indicate P_{1dB} is generally around 30 dBm.

3.4. Reliability Analysis and Improvement

Switching reliability is a significant aspect of RF switches, since all switching applications require a fair amount of switching activity during which the switches need to survive and function consistently. In the case of GeTe RF switches, the switch reliability

is largely dependent on the reliable phase transitions of the GeTe and the stability of the heater. In order to make sure the GeTe switches function reliably, we need to look into both the material properties of GeTe to explore methods for better phase transitions, and explore design optimization to build reliable heaters that endure repeated heating pulses.

3.4.1. Switch Breakdown Analysis

The GeTe RF switches that we have built, even though showing good RF performance, are often observed to fail during the measurement process, especially after a certain amount of switching cycling. Failure generally occurs when the switches are no longer able to be turned on or off using heating current pulses as designed. The most common reasons for a GeTe switch to stop working include heater breakdown and GeTe material fatigue resulting in transition failure.

The joule heating method relies on the heat generated by drawing a short-duration and high-amplitude current from the resistive heater layer. The heat generated by this joule heating scheme is much localized, and thus causes a high temperature gradient among different layers around the GeTe pad area. In practice, the required voltage for the heating pulse can be as high as 20 V, or even higher depending on the sizing of the heater and the GeTe pad. As a result, the stress generated by the heating pulse can cause the heater path to break down. The image in Figure 3.34 shows a heater layer breakdown after several cycles of phase transitions at a certain spot along the heater path because of this reason. In more common cases, even though no obvious heater breakdown like this

takes place, the stress generated by the heating pulses could result in gradual increase of the heater resistance, which eventually causes the heater to fail.

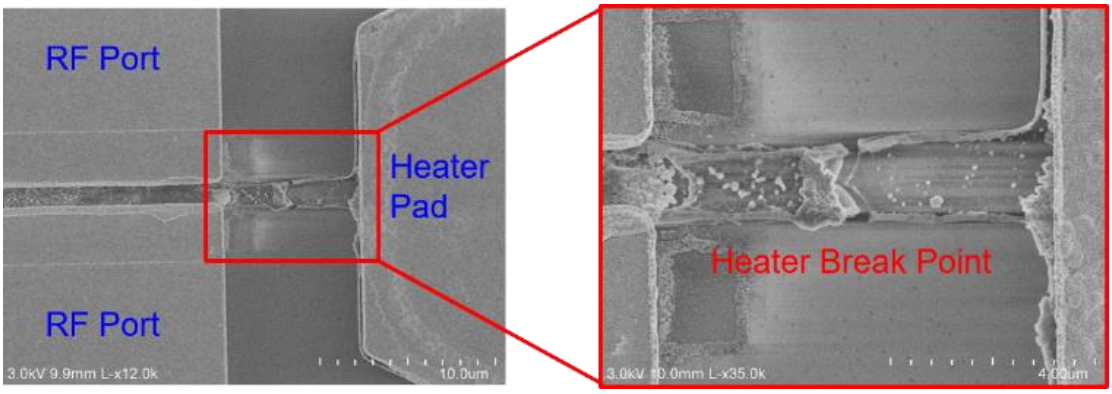

Figure 3.34. SEM images of a GeTe phase change switch with a breaking point along the heater path. This breakdown is cause by the high stress generated due to the high voltage of the heating pulses during phase transitions.

Among reported works on GeTe based phase change switches, the thin-film resistive materials that have been used for heater include SiCr, NiSiCr, TiN as well as a few types of metals such as Ti or W. The bottom passivation layer underneath the heater path is most typically SiN, AlN, or SiO_2, and the passivation layer on top of the heater path that serves as the isolation/thermal coupling layer is usually Si_3N_4. Based on the thermal and dielectric properties of these materials, a simulation recreating the heat distribution condition during phase transition is performed to analyze how much stress is generated. The simulated result of the heater in the SiO_2-W-Si_3N_4 configuration is shown in Figure 3.35(a). As comparison, a layer configuration with aluminum nitride (AlN) as the substitute material for SiO_2 and Si_3N_4 for both the passivation layer and isolation layer is simulated and included in Figure 3.35(b), considering the good thermal conductivity of

AlN for faster heat dissipation in order to reduce the stress generated during the heating process. The simulations show that a rather high stress is generated at the heater patterns, especially where the heater path is anchored, so the heater breakdown situation described in Figure 3.34 is possible to happen under a high voltage. But from the simulation results, it can be seen that the second configuration with AlN shows a lower stress level with the same amount of heat generated by the heating currents. Therefore, using a high-quality AlN film, the stress issue and the heater breakdown issue could very well be addressed.

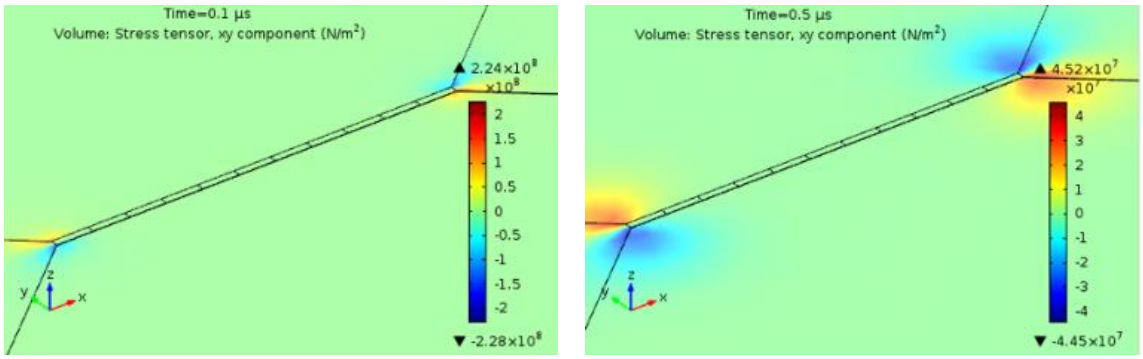

(a) (b)

Figure 3.35. Thermal simulations using COMSOL on the heater structure with the (a) SiO_2-W-Si_3N_4 and the (b) AlN-W-AlN material configuration. For both simulations, the structures and dimensions are kept the same, and the electrical heating pulses are tuned separately for each simulation to ensure the same temperature profile (with a peak temperature of approximately 750 °C) is achieved. In the thermal simulations, the thermal boundaries are defined such that the back side of the Si substrate and the top of the air box (with a thickness of 100 µm above the device) are at room temperature, and thermal conduction models are used among the material domains in contact with each other. The peak stress generated is approximately 228 MPa in (a) and 45.2 MPa in (b).

Another common cause for failure in phase transition comes from the GeTe layer. Ideally, the GeTe pad that is connecting the RF ports is treated as a conductor in the ON (crystalline) state, and a dielectric insulator in the OFF (amorphous) state. As previously

discussed, in the OFF-state, the switch has been optimized so that only the GeTe via area is in the amorphous state, and GeTe areas that are overlapping with the RF electrodes stay in the crystalline area at all times during switch operation, as shown in Figure 3.28. This operation reduces the volume of GeTe going through phase transitions during switching, which helps with fast and reliable switching activities. An example TEM image of the crystalline-amorphous interface within the GeTe layer in the device is also captured and shown in Figure 3.36.

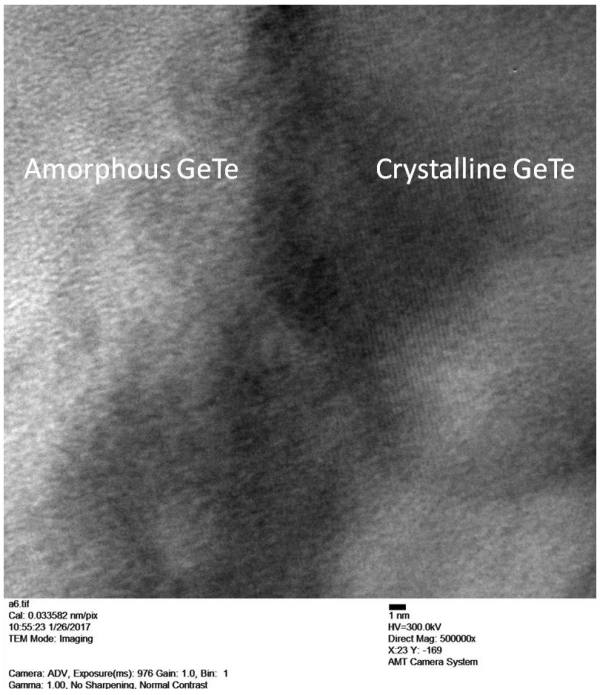

Figure 3.36. TEM image of the GeTe layer showing the amorphous-crystalline interface in the RF switch. In the crystalline GeTe area a lattice orientation can be clearly seen, and in the amorphous (bright) GeTe area the lattice can hardly be seen.

In reality, however, with improper heating pulse configurations, the GeTe pad can be switched into an intermediate state, where conductivity of the GeTe is degraded compared to the crystalline state GeTe, but it is much more conductive than the amorphous state GeTe. In this situation, it is much more difficult to achieve successful phase transitions through thermal actuation, as the GeTe pad has developed into a mixture of crystalline and amorphous states at different portions of the volume. Figure 3.37 shows a TEM image of the atomic structure of the GeTe layer from a phase change switch device that has failed the phase transition process.

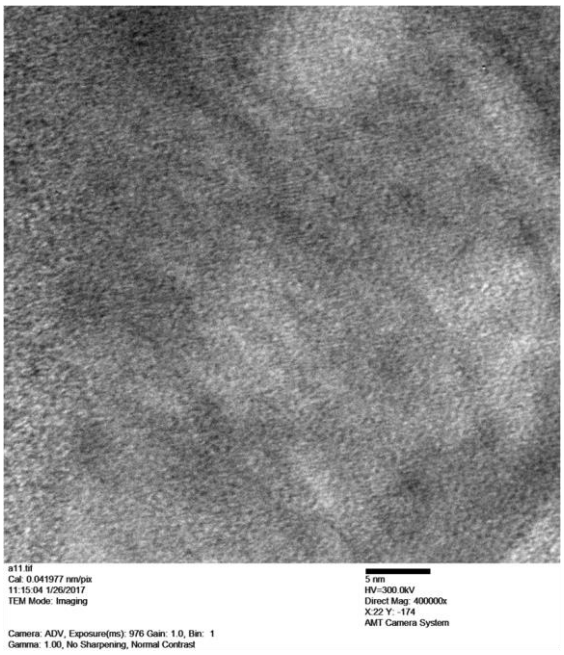

Figure 3.37. TEM image of amorphous GeTe with material fatigue failing further phase transitions. In the image, small scattered crystalline areas can be seen, but the GeTe is mostly amorphous.

Other than the improper heating pulses applied, the phase transition failure in the GeTe film also has another potential cause related to the oxidization and other forms of

impurity introduced to the film. In order to further explore the GeTe film quality and determine the impurity level change in the GeTe film before and after switching activities in the device, energy-dispersive X-ray spectroscopy (EDXS) measurements are taken Figure 3.38(a) and Figure 3.38(b). The element percentages for Si, O, Te and Ge are 33.42%, 40.78%, 9.80% and 8.73% before switching, and 37.42%, 54.44%, 3.76% and 3.01% after switching failure. Considering the errors during the EDXS measurements, the O/Si ratio instead of O percentage alone is used to estimate the amount of oxygen element in the GeTe film. The increased O/Si ratio indicates possible GeTe film oxidization. Other reactions may also have caused the increased impurity and thus switching failure. The measurement shown in Figure 3.38 was performed on a GeTe switch where the GeTe film does not have top passivation, and is exposed in air during both the switching activities and the EDXS measurements, which could have possibly encouraged the reaction between oxygen in air and the GeTe film. Measurements have also been done on devices where GeTe films are passivated with a thin Si_3N_4 layer on top. Even though the issue with film reaction and oxidization is mitigated with the presence of a top passivation layer, the increased amount of impurity can still be observed in the measurements.

In order to avoid quality degradation of GeTe film, it is important to ensure an even heat distribution across the entire GeTe pad, and well-designed passivation for GeTe protection. To achieve even heat distribution, the heater needs to provide evenly generated heat along the path and the thermal coupling layers needs to have good thermal conduction at the GeTe pad area. In order to prevent or mitigate the GeTe film impurity

issue, better GeTe layer starting quality and proper protection are also needed in future designs to achieve better switch reliability.

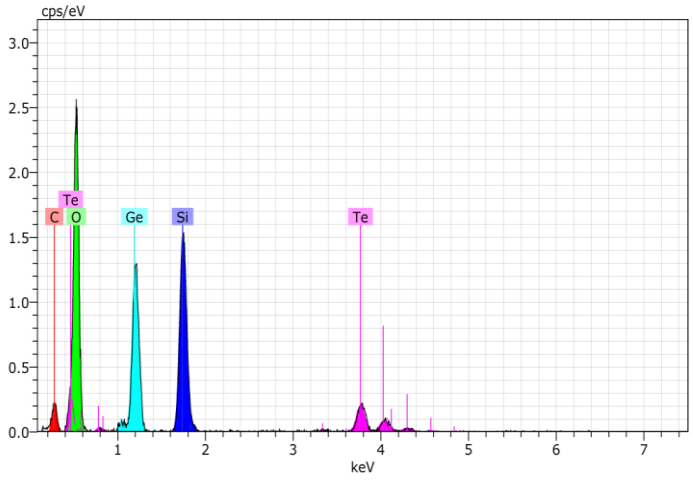

(a)

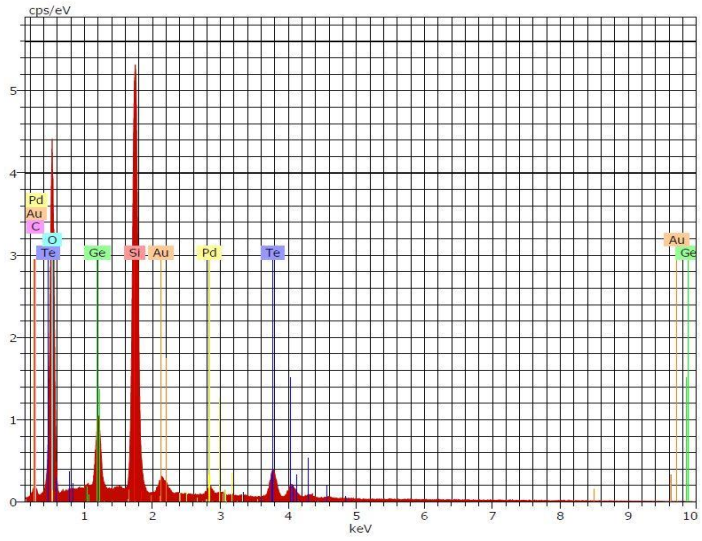

(b)

Figure 3.38. Energy-dispersive X-ray spectroscopy (EDXS) measurements of the GeTe film in the RF switch (a) before any switching activities have been applied and (b) after the device has failed switching after a certain amount of switching activity.

3.4.2. Switch Reliability Evaluation

In order to evaluate the reliability of the GeTe RF switch under frequent switching activities, a repeated switch measurement has been performed. This process includes turning the switch ON and OFF repeatedly by applying heating voltage pulses, and record the resistance of the switch after each switching activity. If the switch becomes very difficult or impossible to turn ON or OFF in the process, the measurement is stopped. In this measurement the GeTe switch with indirect heating method is used.

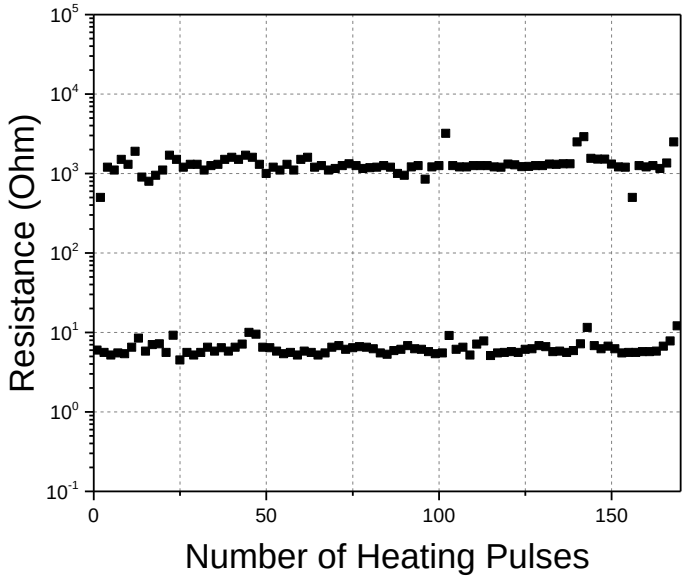

Figure 3.39. Resistance response of the indirectly heated switch measured with repeated switching activities using thermal actuations.

The reliability measurements have been performed on different batches of fabricated devices as well as different devices within the same batches. The results show a great

variation among devices in terms of reliability. While some devices survived only a few cycles of switching activities, many devices are able to be switched for over a hundred cycles without experience any issue. A typical resistance measurement during the switching activities is shown in Figure 3.39.

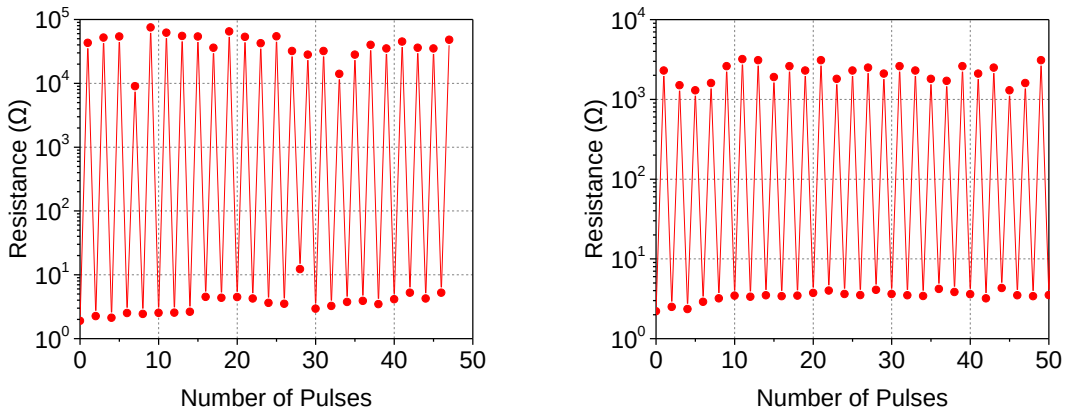

(a) (b)

Figure 3.40. : ON and OFF state resistance of GeTe switches using indirect heating, after each time a successful phase transition through a heating pulse is observed. (a) a resistance value above 10 kΩ is treated as a successful transition to the OFF state, and the resistance values at both states are generally stable with occasional fluctuations; (b) a resistance value above 1 kΩ is treated as a successful transition to the OFF state, and the ON state resistance values are more stable in comparison to (a).

Generally, phase transition of GeTe from the crystalline to amorphous state is called successful when an OFF resistance of over 10 kΩ is achieved. However, due to the imperfection in the thermal actuation process and partial phase transitions of GeTe, in some cycles the ON state resistance is higher, and the OFF state resistance is lower than others, which indicates certain instability. An alternative approach used to reduce the

heater power consumption and increase switching cycles is to apply enough power to get an OFF state resistance of above 1 kΩ. Since the isolation in the OFF state is mostly dependent on the capacitance between the RF terminals, a relatively lower resistance of 1 kΩ will not greatly affect the isolation of the switch, but this makes the phase transitions much easier for an extended number of switching cycles. The resistance responses of these two types of measurements are shown in Figure 3.40.

3.5. Summary

In this chapter, chalcogenide phase change materials, especially GeTe, in RF switching applications have been discussed. The two types of four-terminal GeTe RF switches are presented in detail, including the design and fabrication process as well as the performance evaluation and reliability analysis. Overall, GeTe has shown its promising potential in the application of reconfigurable RF modules and systems. A brief performance comparison among different RF switching technologies is provided in Table 3.3.

In Table 3.3, measured results of two types of GeTe RF switch designs from this work and another reported GeTe based phase change switch design are included, along with other technologies such as RF MEMS, SOI/SOS and pHEMT. It is shown that GeTe RF switches have competitive performance overall compared to existing technologies, with a wider operating frequency range and high RF performance at high frequencies compared to most solid-state based switches. Compared to RF MEMS switches, although GeTe switches are generally showing a lower cut-off frequency, they offer the advantage

of smaller size, lower operating DC voltage, good scalability and integration compatibility, as well as easier fabrication and lower cost. While GeTe switches are showing higher power consumption for switching activities than other designs, the switching power is pulse based and therefore the total energy budget can be well managed.

Table 3.3. Comparison of RF switch designs using different technologies.

Technology	GeTe (Direct Heating Scheme)	GeTe (Indirect Heating Scheme)	GeTe (Indirect Heating Scheme)	RF MEMS	0.18 μm SOI	0.25 μm SOS	0.15μm GaAs pHEMT
Example(s)	This work [64] [65]	This work [72] [75]	[63] [76]	[20]	[12] [77]	[11]	[78]
Operating Frequency Tested	Up to 20 GHz	Up to 20 GHz	Up to 40 GHz	Up to 50 GHz	Up to 10 GHz	Up to 2.5 GHz	Up to 0.9 GHz
Insertion Loss	0.5 dB @ 20 GHz	0.3 dB @ 20 GHz	0.2 dB @ 20 GHz	0.2 dB @ 50 GHz	<1.5 dB @ 10 GHz	<1 dB @ 2.5 GHz	0.25 dB @ 9 GHz
Isolation	18 dB @ 20 GHz	11 dB @ 20 GHz	15 dB @ 20 GHz	25 dB @ 50 GHz	17 dB @ 10 GHz	-	-
f_{co}	>4 THz	>5.6 THz	>12.5 THz	>20 THz	0.637 THz	0.355 THz	0.366 THz
Switching Speed (Typically)	<3 μs	<2 μs	-	~1 μs	0.1-1 μs	0.1-1 μs	~1 μs
Switching Power (Typically)	<100 mW (Pulse)	<2 W (Pulse)	<2 W (Pulse)	0 static power	μW – mW (static)	~μW – mW (static)	~mW (static)
Control Voltage	<10 V	<20 V	-	<100 V	~2.5 V	~4 V	~5 V
Power Handling (Typically)	>>20 dBm	>>20 dBm	>35 dBm	<30 dBm	30 – 50 dBm	30 – 50 dBm	20 – 0 dBm
Size (Typically)	<500 μm^2	<500 μm^2	<500 μm^2	>10 mm^2	0.1 – 10 mm^2	0.1 – 10 mm^2	~10 mm^2
Cost	Low	Low	Low	Medium-high	Very low	Low	Low-Medium

CHAPTER 4 Reconfigurable Bandpass Filter Using GeTe RF Switches

A reconfigurable bandpass filter for X-band applications has been implemented using our GeTe-based phase change switches. The design methods and performance measurements have been reported in [79]. This filter has been implemented as a proof of concept to demonstrate applicability of GeTe switches in frequency agile RF modules, showing promising performance compared to existing reconfigurable bandpass filter designs at a similar frequency range.

4.1. Motivation and Background

There is a high demand for compact and low-loss reconfigurable filters for various advanced wireless applications. A number of common applications of reconfigurable filters can be named including cognitive radios, modern transceivers, anti-jamming communication systems, *etc*. [80]. With reconfigurable filters, wireless communication systems that require multiple operating frequency bands can be implemented with smaller size and reduced cost compared to conventional systems using multiple single-frequency filters. Compared to low-pass or high-pass filters, bandpass filters provide an improved signal-to-noise ratio (SNR) and better rejection of out-of-band signals [81].

There have been various designs reported for implementing tunable or reconfigurable filters. The frequency tuning for such devices is achieved electronically by technologies such as solid-state varactors or switches [82], RF MEMS switches or capacitors [83],

magnetic or ferroelectric components [84, 85, 86], *etc*. Solid state tuning elements such as varactors and switches are the commercialized type of devices used in tunable or reconfigurable filters. While they are commonly used in wireless systems with good reliability and compatibility for integration, they tend to have relatively high losses (high electrical resistance), especially at high frequencies (>10 GHz) and linearity issues limiting their application areas. MEMS tuning elements, such as electrostatic switches, are proven to have much better insertion loss and isolation performance across a wide frequency range [20]. They typically use suspended or other types of mechanical structures to switch between states, and provide very low contact resistance when switched on because of the direct metal contact, and extremely high resistance when switched off. However, a high DC voltage (usually more than 20 V) is typically required for pull-in and a constant voltage need to be applied to maintain the ON state. In addition, due to their suspended mechanical structures, the fabrication process of such devices is usually complicated and has yield and reliability issues.

The X band, which is defined as the frequency range from 7.0 to 11.2 GHz (or 8.0 to 12.0 GHz according to IEEE standards), is commonly used by civil, military and government radar applications such as weather monitoring, air traffic control, defense tracking, law enforcement, *etc*. There are several reported designs of X band and near X band planar tunable filters that provide good performance using MEMS switches [83], yttrium iron garnet/gadolinium gallium garnet (YIG/GGG) [85], ferroelectric barium-strontium-titanate (BST) capacitors [86], and vanadium oxide (VO_x) switches [87] as the tuning elements. The tunable bandpass filter design reported in [83] is based on a 2-bit

tuning structure using ohmic contact MEMS switches that provide frequency tuning ranges of 20% and 44% at the frequencies between 12 GHz and 15 GHz with two different device sets. The fabricated devices are measured to have a fractional bandwidth of 5.7% and an insertion loss lower than 3.2 dB at all states, with an unloaded quality factor of better than 75. The work reported in [85] utilizes YIG/GGG layers on a RT/Duroid substrate to achieve frequency tuning in the X-band. This filter operates at different center frequencies from 8 GHz to 12 GHz, with 3-dB fractional bandwidths of approximately 10% to 14%, and an insertion loss of 2.5 dB. The design reported in [86] is a two-pole microstrip line based tunable filter using ferroelectric BST capacitors as the tuning elements with a center frequency around 10 GHz and a constant fractional bandwidth of 8.5% within the tuning range of approximately 8.3%. This reported design provides an insertion loss lower than 2.7 dB. The work reported in [87] presents a reconfigurable bandpass filter that integrates VO_x microwave switches into a spilt ring resonator based design. The VO_x is a relatively new type of material for RF applications that provides fast and reversible semiconductor-to-metal transition, and is used in microwave switches to achieve reconfigurability. This work shows a filter insertion loss within 5 dB and a 3-dB bandwidth of 12-13%. The challenge with VO_x switches is that they have a low power handling capability and comparably poor linearity. They also require a constant bias to stay in one state. In [79], we presented a reconfigurable bandpass filter for X-band applications using a new tuning technique. Here, the design and fabrication process are discussed, and the performance of filters is analyzed and compared to the designs mentioned above.

As previously discussed, RF switches using phase change materials have gained a lot of attention as they offer fast switching speed (< 10 μs), large cut-off frequency (> 4 THz), high OFF/ON resistance change ratio (amorphous/crystalline resistivity ratio of > 10^4), small size (in few μm^2 range), zero in-state power consumption, high power handling capability (P_{1dB} > 25 dBm), and high linearity (IIP_3 > 50 dBm) [61, 62, 72]. The phase change material based switches show great potential in reconfigurable RF applications. However, the focus so far has been on implementing the switching element and only a handful of reports exist on exploiting phase change switches in functional RF modules [88, 89]. The idea of employing phase change material based RF switches in the design of tunable/reconfigurable filters has been realized in [79]. With the development and maturing of phase change material based RF switches, the reconfigurable filter that we proposed is showing competitive performance results and further analysis and evaluation have also been performed [90].

4.2. Design Procedure

The two main types of GeTe based RF switches that we have designed use direct heating and indirect heating. Although the design with direct heating provides advantages such as high switching power efficiency, the design with indirect heating has a simpler fabrication process, better electrical isolation between the RF signal transmission path and the heater terminals, and is therefore preferable to use in the proof-of-concept design of the reconfigurable bandpass filter.

This filter prototype is designed to target the X-band frequencies for military communication applications with an uplink band frequency of 8.15 GHz and a downlink band frequency of 7.5 GHz. For both bands, the 3-dB bandwidth is targeted at 500 MHz, and the target insertion loss for both bands is 4 dB or lower. The main structure of the filter is implemented with microstrip lines, and the reconfigurability of the filter is realized using the GeTe RF switches with indirect heating that are integrated on chip.

The filter is based on coupled microstrip line resonators, which uses an open-loop λ/2 microstrip line configuration. The frequency band selection is realized through shifting the center frequency of the resonators with switchable capacitors (open-circuited microstrip line stubs). The capacitor switching is achieved using the GeTe based RF switches. The external coupling of the filter is achieved by coupled feed lines at the terminals. The detailed schematic of the filter structure is shown in Figure 4.1.

In order to obtain the targeted constant absolute bandwidth (CABW) of 500 MHz from the specifications, calculations and simulations are done to tune the element parameters of the filter. The design procedure starts based on a low-pass Butterworth filter prototype, with elements g_0, g_1, g_2 and g_3. According to the target center frequencies (f_1 and f_2) and the 3-dB fractional bandwidth (Δ), one can calculate the corresponding required external quality factor (Q_{ext}) and the coupling coefficients (k_{12}) of the microstrip line resonators. The calculations can be done with Equations (4.1)-(4.3). In Equations (4.1a)-(4.1d), the admittance parameters $[Y]$ correspond to the impedance parameters $[Z]$, and the constant parameters used are listed in Table 4.1.

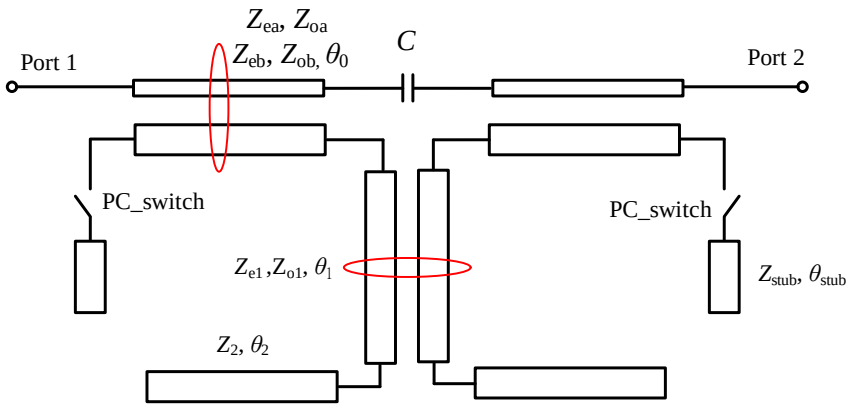

(a)

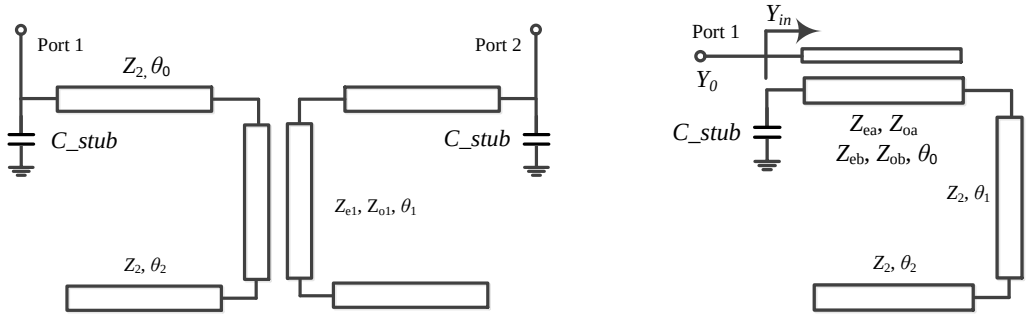

(b) (c)

Figure 4.1. The schematics of the X-band reconfigurable bandpass filter using GeTe based RF switches showing (a) the entire circuit model, (b) the section with the coupled resonators, and (c) the circuit model of the resonator with the external coupling circuit.

$$Y_{11} = j\omega C_{stub} + \frac{Y_{ine}+Y_{ino}}{2} \quad \text{(4.1a)}$$

$$Y_{12} = \frac{Y_{ine}-Y_{ino}}{2} \quad \text{(4.1b)}$$

$$Y_{ine,o} = Y_2 \frac{Y'_{ine,o}+jY_2\tan\theta_0}{Y_2+jY'_{ine,o}\tan\theta_0} \quad \text{(4.1c)}$$

$$Y'_{ine,o} = Y_{e1,o1} \frac{jY_2\tan\theta_2+jY_{e1,o1}\tan\theta_1}{Y_{e1,o1}-Y_2\tan\theta_1\tan\theta_2} \quad \text{(4.1d)}$$

$$Im[Y_{11}(\omega_0)] = 0 \quad \text{.....(4.2a)}$$

$$\frac{Im[Y_{12}(\omega_0)]}{b} = \frac{\Delta}{\sqrt{g_1 g_2}} = k_{12}, b = \frac{\frac{\omega_0}{2}\partial Im[Y_{11}(\omega_0)]}{\partial \omega} \quad \text{.....(4.2b)}$$

$$Q_{ext} = \frac{b}{Y_0} = \frac{\frac{\omega_0}{2Y_0}\partial Im[Y_{in}(\omega_0)]}{\partial \omega} = \frac{g_1 g_2}{\Delta} \quad \text{.....(4.3)}$$

Table 4.1. Constant parameters used in the design calculations.

Parameter	Value
Z_{e1}	37 Ω
Z_{o1}	23.3 Ω
Z_2	33Ω
θ_0	55°
θ_1	23°
θ_2	95°

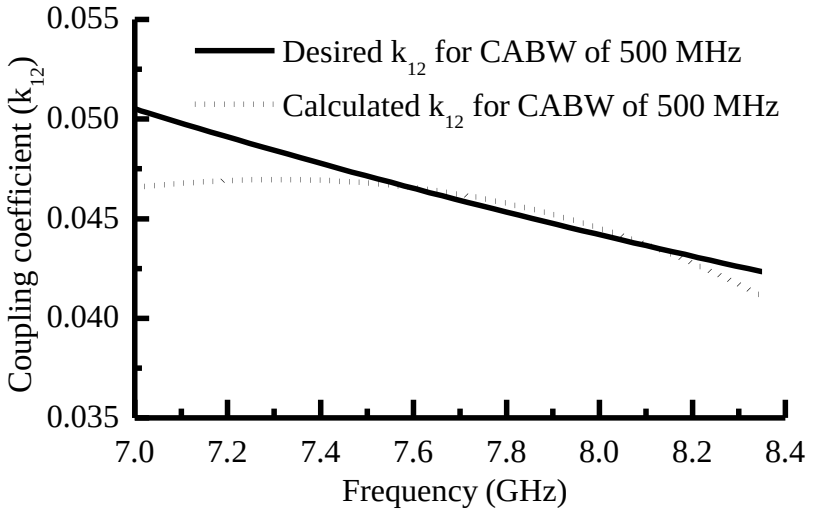

Figure 4.2. Desired and achieved coupling coefficients of the coupled resonators in the filter as a function of frequency.

The admittance parameters Y_{11} and Y_{12} are first calculated based on Equations (4.1a) - (4.1d). In order to achieve constant absolute bandwidth (CABW), the coupling coefficient conditions are required to satisfy Equation (4.2b) across the entire tuning range and the external Q should satisfy Equations (4.3) [91]. The required and calculated coupling coefficient k_{12} for a constant bandwidth of 500 MHz at the two target center frequencies are plotted in Figure 4.2.

In summary, the design procedure of the phase change reconfigurable filter is as following: 1) Given the filter specifications, including the center frequencies (f_1 = 7.5 GHz, f_2 = 8.15 GHz) and the absolute bandwidth (BW_{3dB}), we obtain the desired values of external quality factors and the coupling coefficients by using Equations (4.1)- (4.3). 2) Then, we design the half-wavelength resonators to operate at f_1. The frequency f_2 is mainly determined by the length of resonators, *i.e.*, (l_1+l_2+l_3). The lower passband frequency f_1 is mainly determined by the dimensions of stub, *i.e.*, (w_3, l_4). The mixed coupling between resonators is realized using coupling lines (l_2). Once the line width w_1 and the length l_2 are fixed, the coupling coefficients depend on the gap s. By changing impedances of the coupled lines (Z_{e1}, Z_{o1} and θ_1), k_{12} can be synthesized with different slopes for low-band (f_1) and high-band (f_2) modes. Then, the initial values of w_1, l_1, l_2, l_3 and s can be obtained. 3) Once the line width w_1 and the line length l_1 are fixed, the external quality factor Q_{ext} is controlled by the gap g_0 and the width w_2. 4) The GeTe switch design follows the procedure outlined in [72]. 5) Finally, using the initial parameters from the above-mentioned steps, we perform full-wave simulations using *ANSYS HFSS* to take all parasitic effects into account and we optimize and finalize the

design. In addition, the simulated performance of the GeTe RF switches showing the insertion loss and isolation is shown in Figure 4.3, which is used in the overall system simulation in case of any parameter shift from the GeTe switches when fabricated alone. A top-view schematic of the filter design layout along with a zoomed-in view of the GeTe RF switch is shown in Figure 4.4.

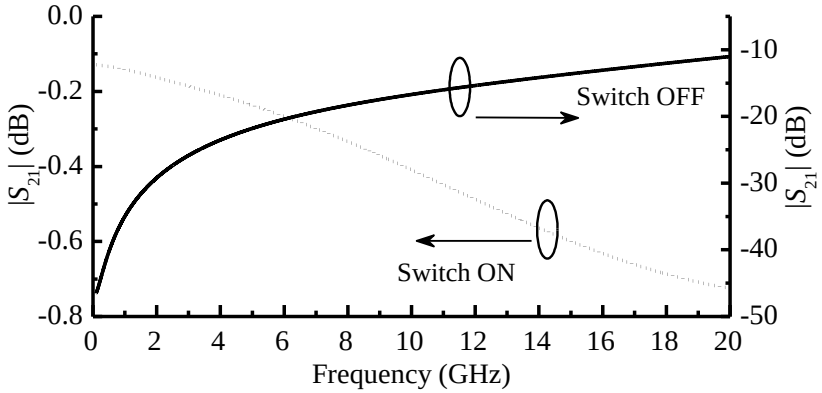

Figure 4.3. Simulated S-parameters of the GeTe RF switch showing the insertion loss and isolation used as a reference for the simulation of the filter design.

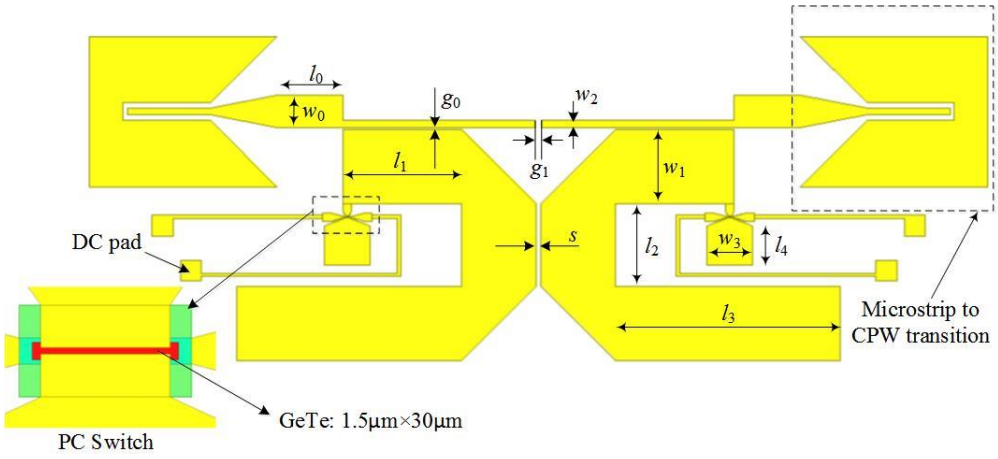

Figure 4.4. Top-view layout of the reconfigurable bandpass filter using GeTe based RF switches. A zoomed-in view of a GeTe RF phase change switch is also included.

4.3. Fabrication Process

The fabrication process of the GeTe RF phase change switches using indirect heating has been discussed in the previous chapter. Since the reconfigurable bandpass filter consists of both microstrip line coupled resonators and GeTe RF switches, a fabrication process is designed to integrate the GeTe switches on chip with the microstrip line structures. The cross-sectional schematic of the device is shown in Figure 4.5.

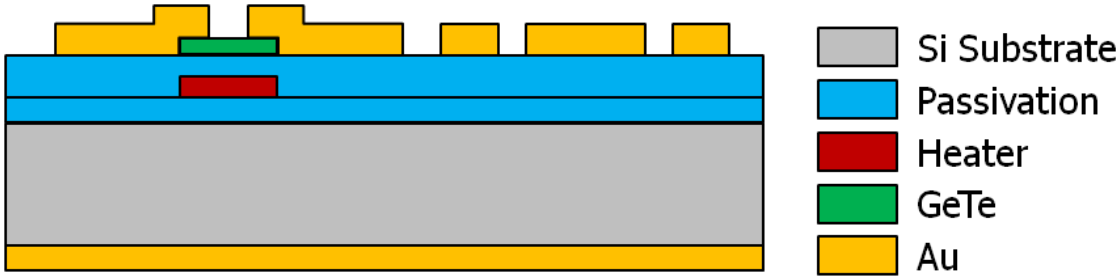

Figure 4.5. Cross-sectional schematic showing structure of the filter design. The microstrip lines share the gold layer from the GeTe switches. This diagram is intended to show the layer configuration, and does not reflect the actual device layout. The device layout is shown in Figure 4.4.

The fabrication of the GeTe RF switch based reconfigurable bandpass filter is performed on a double-side polished high-resistivity Si substrate for its high dielectric constant, high thermal conductivity, low substrate loss and compatibility with the GeTe RF switch fabrication processes. The detailed fabrication process flow is shown in Figure 4.6. The process starts with a back side coating of Au layer with a thickness of 500 nm to form the back plate. The front side process is similar to the GeTe RF switch process when fabricated standing alone. A SiO_2 passivation layer with a thickness of 2 μm is

deposited as the passivation layer, followed by the patterning of the thin film resistive tungsten (W) heater layer with a thickness of 200 nm. The heater layer is then covered by a 50 nm Si_3N_4 isolation layer for the heating embedding process, and the GeTe layer is then patterned on top, with a thickness of approximately 100 nm. The RF contact electrodes for the GeTe switches are patterned on top, with a thickness of 200 nm. Finally, the patterning of the RF metal routing for both the GeTe switch and the microstrip line structures are performed on top of the wafer. Additional passivation layers for device protection are also deposited. A microscope image of the fabricated device is shown in Figure 4.7. The device size is approximately 11 mm by 5 mm.

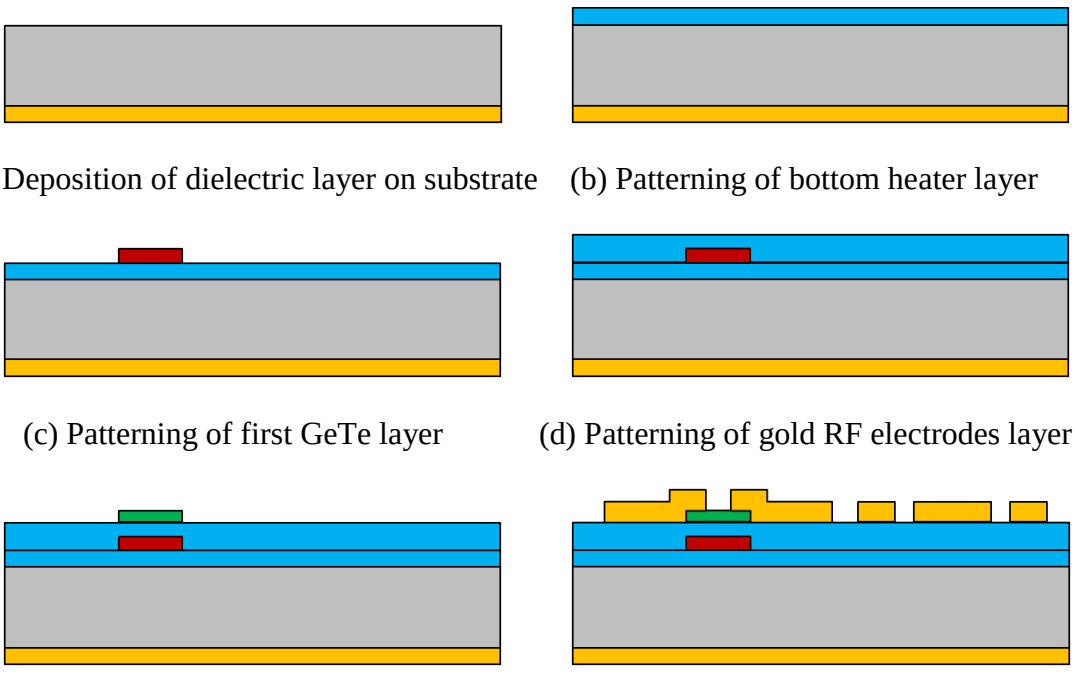

(a) Deposition of dielectric layer on substrate (b) Patterning of bottom heater layer

(c) Patterning of first GeTe layer (d) Patterning of gold RF electrodes layer

(e) Patterning of second GeTe layer (f) Patterning of top heater layer

Figure 4.6. Fabrication process flow of reconfigurable bandpass filters using GeTe phase change switches.

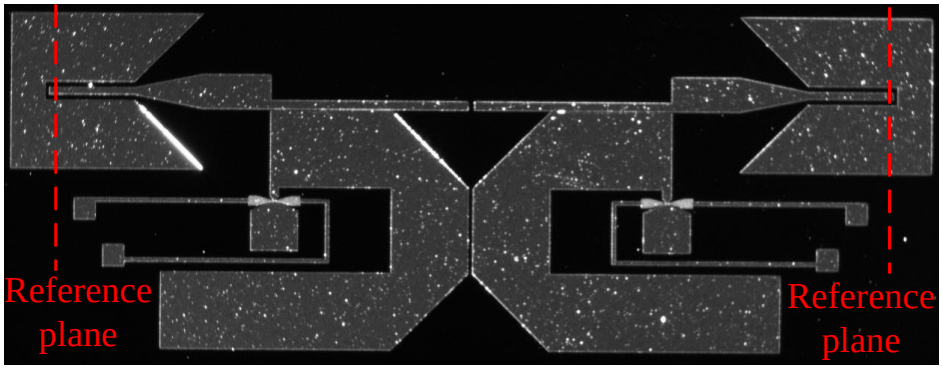

Figure 4.7. Microscope image of the fabricated reconfigurable bandpass filter.

4.4. Measurement Results

The fabricated reconfigurable filter is measured to evaluate its RF performance. When the GeTe switches are ON, a lower frequency pass band of 7.45 GHz (7.5 GHz from simulations) is achieved with an insertion loss of 3.2 dB, 3-dB bandwidth of 482 MHz, and return loss > 30 dB. When the GeTe switches are OFF, the filter is switched to the higher frequency band of 8.07 GHz (8.15 GHz from simulations) with insertion loss of 2.6 dB, bandwidth of 520 MHz, and return loss >18 dB. The unloaded quality factor Q_u of the microstrip resonators with GeTe RF switches estimated using Equation (4.4) [92] is 59/73 in the downlink/uplink bands, respectively. The measured and simulated S-parameters are shown in Figure 4.8.

$$I.L.(dB) = 4.343 \sum_{i=1}^{n} \frac{g_i}{FBW\ Q_{ui}} \quad \text{.....(4.4)}$$

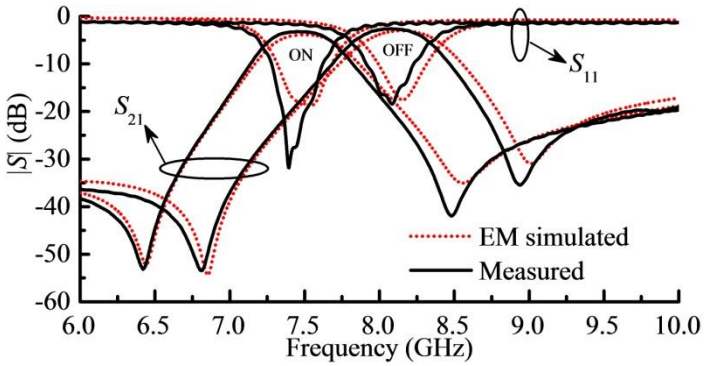

Figure 4.8. Measured and simulated S-parameters of the reconfigurable bandpass filter using GeTe switches.

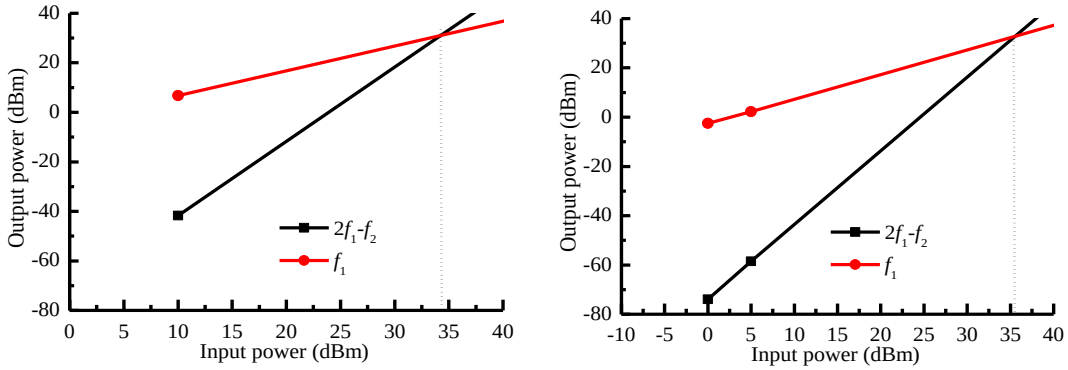

(a) (b)

Figure 4.9. Measured IIP_3 at the (a) downlink band (7.45 GHz) (b) uplink band (8.07 GHz) of the reconfigurable bandpass filter.

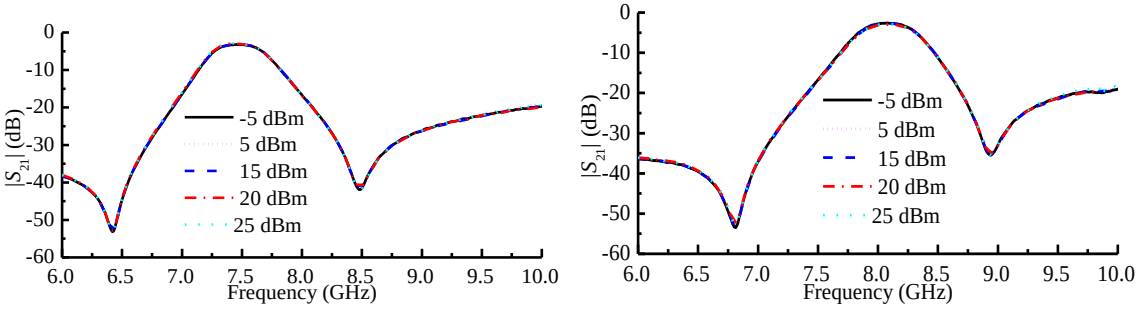

(a) (b)

Figure 4.10. Measured S21 of the filter at varying input power levels at the (a) downlink band (7.45 GHz) (b) uplink band (8.07 GHz).

The linearity and power handling capability of the device are also evaluated by measuring its IIP_3 and P_{1dB}, respectively. The IIP_3 is measured at the center frequencies of the pass band. The extracted IIP_3 at 1 kHz offset is better than 30 dBm for both states (Figure 4.9). Measured results also show that the tunable filter can handle more than 25 dBm of input power at both states of the switch before 1-dB compression occurs (Figure 4.10).

Table 4.2. Performance comparison of the GeTe RF switch based reconfigurable bandpass filter to other reported designs targeting the similar frequency range.

Ref.	**Tuning elements**	**BW_{3dB} (%)**	**IL (dB)**	**Range (GHz)**	**Estimated Q_u**	**Bias voltage (V)**	**Size (mm^2)**	**Tuning Speed**	**Power Consumption**
[83]	MEMS switch	5.8	2.6-2.9	12-15	77-81	60	~5×4	~10 µs	Near 0
[84]	YIG	8-14	2.5	8-12	< 25	N/A	40×15	N/A	N/A
[86]	BST capacitor	8.5	2.0-2.7	10-10.56	< 40	30	3.1×6.9	N/A	N/A
[87]	VO_x switches	12-13	5	8.6-9.2	< 20	60	9×7	<10µs	1.8 W (pulse)
This work	GeTe switches	6.4-6.5	2.6-3.2	7.45-8.07	59-73	15 to 20	3.9×10.8	< 6 µs	0.5~1.5W (pulse)

Table 4.2 compares the performance specifications of this filter with reported filters in the X band. As shown, the proposed filter offers competitive performance. Compared to MEMS tunable filters, our reported filter shows a faster response time and requires lower amplitude voltage pulses for actuation. Compared to ferroelectric and YIG-type filters, it shows a comparable IL for a much higher filter *Q* and finally, compared to VO_x type filters, it offers better linearity and does not consume static power to stay in the ON or OFF state.

CHAPTER 5 Conclusions and Future Directions

5.1. Thesis Contributions

The research work discussed in this thesis provides the following key contributions:

1. Investigation into properties of GeTe phase change material and its thermally actuated phase transition activities.
    - This work combines the investigation of phase change materials in a semiconductor physics perspective and exploration of phase change material behaviors in RF applications based on testing and measurement results. A literature summary of phase change material studies in the early stages has been provided in the thesis, showing the progress from early discovery of disordered semiconducting material consisting of Te, As, Si and Ge, to generalized chalcogenide phase change material property study. Specifically, the study of GeTe has been performed to explore the phase transition properties.
    - The comparison of electrical and optical properties between amorphous and crystalline GeTe films have been performed, assisted by SEM and TEM imaging, XRD measurement, EDS material study, as well as optical ellipsometry measurements. The crystallization and amorphization processes of GeTe films have also been explored with varying parameters and conditions to determine the optimal process to achieve most complete phase transitions. This study

contributed to a step towards optimization of GeTe-based RF phase change ohmic switches in terms of RF performance and switching reliability.

2. Development of GeTe-based RF phase change ohmic switches with the four-terminal structures.
    - Based on the previously proposed GeTe-based RF phase change ohmic switch with the two-terminal structure, a new four-terminal structure has been devised and developed. While inheriting the direct heating method from the two-terminal structure, the four-terminal switch is able to separate the thermal actuation pulses from the RF signals. With this structure, the RF signal transmission path and the heating path can be separately optimized for their functionality, while maintaining decent switching power efficiency. The device has been implemented and optimized with good RF performance, with an insertion loss less than 0.5 dB and an isolation above 18 dB from DC to 20 GHz, showing a figure-of-merit cut-off frequency over 4 THz. This indicates competitive performance compared to existing RF switch designs with solid-state or MEMS technology. The switch has also been verified to have good linearity and power handling capability.
    - A four-terminal structure with indirect heating scheme for the GeTe-based RF phase change ohmic switch has also been developed. Compared to the direct heating scheme, this indirect heating scheme results in a simplified device structure and fabrication process. The heater embedding process for this device structure ensures electrical isolation between the RF and heater terminals, which minimizes RF signal leakage into the heater terminals, and therefore provides

better integration compatibility with other modules within certain RF systems. Since the resistive heater path in this structure is relatively independent from the GeTe connection of the switch, it is possible to build switch stacks where the GeTe switches can be connected in series or parallel sharing a single resistive heater for better voltage or current handling capability. The GeTe RF switch with indirect heating method has also been fabricated and tested, showing good performance. The optimized design shows an insertion loss within 0.3 dB and an isolation above 11 dB from DC to 20 GHz, indicating a figure-of-merit cut-off frequency over 5.6 THz.

- A series of nano/micro-fabrication processes have been developed for GeTe-based RF switches. A plasma induced sputtering process has been characterized for GeTe thin-film deposition with a single GeTe target. The detailed parameters for the sputtering process has been optimized for best film quality of GeTe, which is essential for successful crystallization and reliable phase transitions of GeTe vias in RF switches. Two different patterning methods for GeTe films using lift-off and plasma etching, respectively, have been developed and compared in terms of film and pattern quality. Depending on the device structure, fabrication process and applications, both patterning methods have been used and a process has been characterized for both methods. Other fabrication process steps, including the GeTe-metal contact characterization, the heater embedding process, and surface polishing and cleaning process have also been characterized to yield an optimized switch performance.

- A thermoelectric modeling method that was previously developed has been used for the GeTe RF switches with both direct heating and indirect heating to relate the thermal and electrical properties of the devices. The model analyzes the impact of RF signals to the switches when operated at high RF power levels in order to predict potential issues including self-actuation, non-linearity, and limited power handling capability. Corresponding measurements have been taken to verify good accuracy of the modeling method.
- Reliability and breakdown analysis of the GeTe switches have been performed. Repeated switching activities have been applied to the devices under test to evaluate the stability and reliability of the GeTe RF switches. Upon switching failure, the device is investigated to determine the cause for breakdown. Common reasons for device switching failure have been identified such as the heater breakdown, GeTe material fatigue and oxidation, *etc*. High-resolution imaging techniques including SEM and TEM have been used to facilitate the analysis.

3. GeTe Switches in Reconfigurable RF Applications
    - A reconfigurable bandpass filter for the X-band communication applications has been implemented using GeTe-based RF switches as the reconfigurable elements. An integrated fabrication process has been developed for the GeTe switches to be fabricated on chip with the microstrip line coupled-resonator based filter. The RF measurement results of the filter shows promising performance, and a comparison among novel designs of reconfigurable/tunable filters using technologies such as

MEMS, ferroelectric, and VO_2 is also provided to evaluate the potential and advantage of GeTe-based switches in reconfigurable RF applications.

5.2. Future Research Directions

The research work in this thesis has contributed to better understanding of material of GeTe phase change material property at radio frequencies, the development of high-performance RF switches using GeTe, and their applications in reconfigurable RF systems. Based on the results achieved and issues discovered during the course of this research, possible directions for future research are suggested below.

5.2.1. GeTe Atomistic Structure Modeling and Analysis

Although a number of different possible atomistic structures of crystalline GeTe has been proposed facilitated by high-resolution TEM imaging and X-ray diffraction measurements [54, 59], it is still not completely clear how the crystalline structures within thin-film GeTe is formed, and what exact structures they possess given different crystallization conditions. According to our findings, the properties of GeTe films (and also phase change materials in general) can be significantly process dependent, and because of that, different reported material study results can been found when the film preparation and annealing processes are performed in different works under different conditions. Even though the GeTe film study and phase transition analysis in this work has resulted in findings that agree with other reported works in terms of general material behavior and trends, the exact numbers such as electrical and optical parameters,

crystallization temperature, phase transition speed, *etc*. are not always the same. It can be reasonably assumed that the formation of the crystalline structure within the GeTe films during the crystallization process is not entirely the same when performed under different setups, and the differences in the crystallization and amorphization process have resulted in differences in electrical and optical properties of the GeTe films.

For the reasons mentioned above, it is very useful to further investigate the exact atomistic structure of the crystalline GeTe films and the formation process of the GeTe crystal. From our TEM imaging results, it has been noted that the GeTe films deposited and crystallized following our process steps exhibit a poly-crystalline structure, with different crystalline volumes showing different lattice orientations. But it is not known if the different crystalline volumes also have a structural difference other than an orientation difference. A better understanding of the crystalline structure can help with the optimization of the annealing process, obtaining GeTe films with better crystallinity, which will help improve the performance of GeTe-based RF switches.

5.2.2. Performance Improvement of GeTe RF Switches

Further performance and reliability improvement of the GeTe based RF switches is essential to their applications in reconfigurable RF modules. Some existing designs of GeTe-based RF switches reported in the recent years have been modified for performance improvements through both structural modifications and fabrication process refinement [93, 94, 95, 96, 76]. Future research regarding further performance improvement of GeTe

RF switches continuing from this thesis can be focused on the exploration of structural variations of the devices and further fabrication process enhancement.

5.2.2.1. Structural Variations

The two main structures of the four-terminal GeTe-based RF phase change switches discussed in this thesis use the direct heating and indirect heating schemes. The structure of both types of devices can be varied in terms of layer configuration and terminal placement. Such variations of the devices can help compare the performance in terms of RF operation and switching activities.

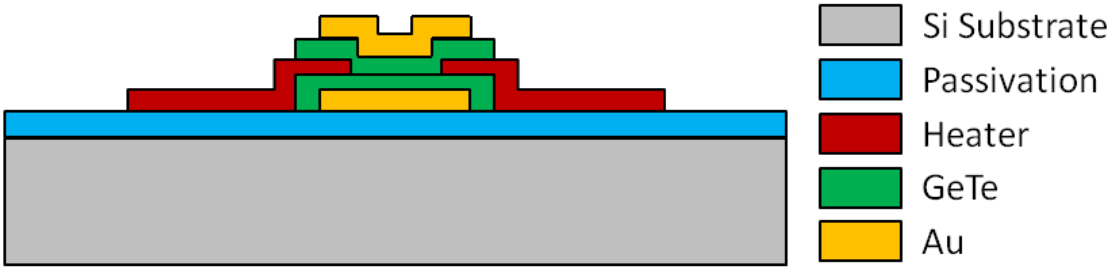

Figure 5.1. An alternative structure of the four-terminal GeTe based RF ohmic switch using direct heating with two heater terminals laterally connected and two RF terminals vertically connected by the GeTe via.

For the direct heating scheme, the previously discussed structure of the GeTe switches consists of a laterally connected RF signal transmission path and a vertically connected heater path. This in-line structure is designed for low-resistance RF metal contact out of fabrication process considerations, since the two RF electrodes in this structure is symmetrical and RF contact metals stepping over a thick layer are avoided.

The heater terminals are connected vertically since the heater path impedance needs to be matched for efficient heat delivery and low resistance is not critical for the heater terminals. However, there is a possible alternative to switch position between the RF and heater terminals, with the RF electrodes vertically connected by the GeTe via, and the heater terminals connected laterally, instead, as shown in Figure 5.1. This structure provides the advantage of an even lower resistance between the RF terminals, since the thickness of the GeTe film is much smaller than its length or width. The potential issue with this structure is the low isolation between the RF terminals because of the significantly increased capacitance between the RF electrodes due to the spacing. Sizing of the RF metal is important to balance the trade-off between the switch insertion loss and isolation. The heater terminals are instead connected laterally, and due to the increased resistance of the GeTe via in the lateral direction, the heater design could possibly be simplified.

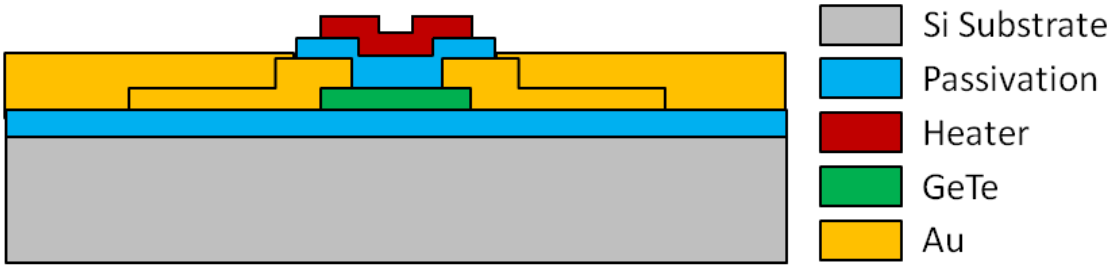

Figure 5.2. An alternative structure of the four-terminal GeTe based RF ohmic switch using indirect heating with a top heater configuration.

For the indirect heating scheme, there is also an alternative structure that can further simplify the fabrication process as well as the GeTe-metal contact quality. Instead of embedding a resistive heater underneath the GeTe via, a top heater layer is patterned after the patterning of the RF electrodes and a top passivation layer to isolate the heater from GeTe and RF electrodes. A simplified schematic of the cross-sectional diagram for this structure is shown in Figure 5.2. Without the heater embedding, the fabrication process is significantly simplified. In this structure, the GeTe via is patterned first, which ensures a flat substrate for GeTe layer growth. This is also beneficial to the GeTe-metal contact quality. The potential issue with this structure is the slow heat dissipation rate into the substrate, since the heater is placed on the top, and slow heat dissipation could increase the temperature overtime resulting in slower possible duty cycle for the device.

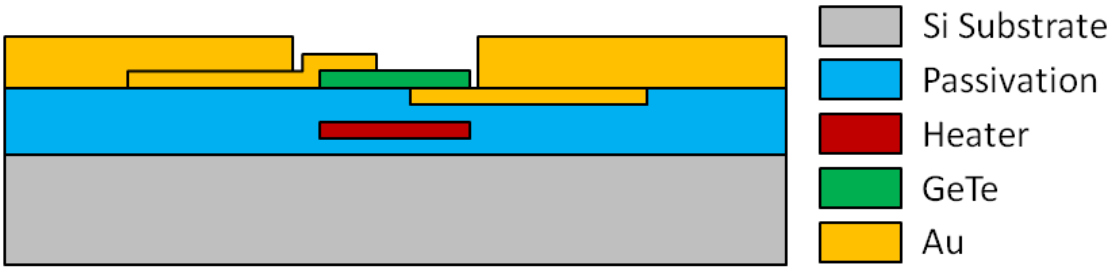

Figure 5.3. An alternative structure of the four-terminal GeTe based RF ohmic switch using indirect heating with an embedded heater and a vertically connected RF signal path.

Other possible alternative structures can also be designed to explore and compare the functionality and performance of the switch. With the differences in each possible structure, they will each provide performance-related advantages and disadvantages, ease

of fabrication process, *etc*. Another example of a structural variation is shown in Figure 5.3, where a resistive heater is embedded underneath the GeTe via for indirect heating, but the RF terminals are connected through the GeTe via vertically, which provides more degrees of freedom when optimizing the switch performance. But the GeTe-metal contact configuration and layer stack requires more accurate photo-lithography in the fabrication process. Other than the ohmic switch configuration, a capacitive shunt switch configuration can also be built with GeTe phase change material. A proposed structure of a GeTe RF shunt switch has been reported, where the GeTe via is used to connect the shunt path between the transmission lines [97]. In this design the switch is turned ON when the GeTe is in the amorphous state, and the RF terminals are connected through the conductive transmission line, providing very low insertion loss. When the GeTe is crystallized, the switch is turned OFF at high frequencies due to the shunt element. A good isolation has also been verified at the OFF state of the switch.

5.2.2.2. Fabrication Process Improvements

While the exploration of structural variations can help with improvement of the functionality and performance of GeTe RF switches, efforts can also be made to improve the effectiveness of phase transitions of the GeTe via. A lot of fabrication process related characterizations can be done to obtain GeTe films with higher quality, better phase transition reliability and better GeTe-metal contact stability.

In this work, the development process of GeTe RF switches has been using $Ge_{50}Te_{50}$, due to its low crystalline state electrical resistivity and high amorphous-crystalline

resistivity ratio. The low crystallization temperature of $Ge_{50}Te_{50}$ compared to GeTe films with other stoichiometric ratios as suggested in Figure 2.8 also provides the advantage of low phase transition power. However, it is possible to explore GeTe films with composite ratios close to 50:50 and observe the trend of resistivity and phase transition temperature change, in order to optimize the phase transition characteristics of GeTe films [35]. This can be realized by co-sputtering from a Ge and a Te target, or multiple GeTe targets with different ratios.

In the film preparation process of GeTe or chalcogenide phase change materials, works have been reported to manipulate the phase transition temperature, phase transition speed, reliability, *etc*., through the introduction of doping elements, or impurity and defects into the phase change material films [98, 99, 100]. In [99], Co has been used as dopant to identify vacancies in crystalline GeTe, and the Co-doped GeTe films with different Co concentrations are showing different response in the X-ray diffraction and photoelectron spectroscopy measurements, indicating different crystalline structures. This is primarily because the Ge vacancies in the rock-salt structure GeTe are replaced with Co where Co-Te bonds are formed. The work in [100] has reported an ultralow-power switching mechanism of GeTe phase change material through defect engineering. By properly introducing defects in the crystalline GeTe, the carrier-lattice coupling can be enhanced and therefore the required work to introduce bond distortions necessary for amorphization is significantly reduced. This has eventually allowed reduction of required current density of at least 80 times in order to amorphize the GeTe film compared to sample without the introduction of defects. Similar approaches to the reported works

above can be explored to manually modify the phase transition characteristics in order to obtain GeTe phase change material films with better phase transition power efficiency, better crystalline films with higher grain size and other properties that will better suit reconfigurable RF applications.

The GeTe-metal contact is also important to the performance of the GeTe RF switches. Ideally, the electrical contact between the GeTe film and RF metal is required to have minimal contact resistance, in order to achieve low insertion loss when the GeTe is in crystalline state. Since Au is the RF electrode material used in this work and many other similar works [93] [95], it is important to ensure good contact by implementing the proper contact layer stack between the GeTe-Au interface. In theory, the preferred contact material depends on the carrier type of GeTe. In our case the GeTe film is measured to be high carrier density p-type, and therefore a metal layer with high work function is better in order to form an ohmic contact. However, a lot of fabrication related detail including chemical selection, surface treatment condition, contact layer structure, *etc*. can affect the contact quality and phase transition process of GeTe [101]. Further exploration can be performed to optimize the GeTe-metal contact in order to achieve lower contact loss and more reliable switching activities.

BIBLIOGRAPHY

[1] A. Gopinath and J. B. Rankin, "GaAs FET RF Switches," *IEEE Transactions on Electron Devices,* vol. 32, no. 7, pp. 1272-1278, 1985.

[2] R. H. Caverly, "Distortion in Off-State Arsenide MESFET Switches," *IEEE Transactions on Microwave Theory and Techniques,* vol. 41, no. 8, pp. 1323-1328, 1993.

[3] K. W. Kobayashi, A. K. Oki, D. K. Umemoto, S. K. Z. Claxton and D. C. Streit, "Monolithic GaAs HBT p-i-n Diode Variable Gain Amplifiers, Attenuators, and Switches," *IEEE Transactions on Microwave Theory and Techniques,* vol. 41, no. 12, pp. 2295-2302, 1993.

[4] W. Arden, M. Brillouet, P. Cogez, M. Graef, B. Huizing and R. Mahnkopf, "More-than-Moore White Paper," 2010. [Online]. Available: http://www.itrs2.net/uploads/4/9/7/7/49775221/irc-itrs-mtm-v2_3.pdf. [Accessed 9 3 2017].

[5] B. Razavi, "Challenges in Portable RF Transciver Design," *IEEE Circuits and Devices Magazine,* vol. 12, no. 5, pp. 12-25, 1995.

[6] C. A. Liechti, "Microwave Field-Effect Transistors," *IEEE Transactions on Microwave Theory and Techniques,* vol. 24, no. 6, pp. 279-300, 1976.

[7] J. Goel and H. J. Wolkstein, "A 4-8 GHz Dual Gate M.E.S.F.E.T. Amplifier," *Electronic Letters* , vol. 14, no. 6, pp. 167-168, 1978.

[8] R. V. Garver, "Microwave Semiconductor Control Devices," *IEEE Transactions on microwave Theory and Techniques,* vol. 27, no. 5, pp. 523-529, 1979.

[9] K. Miyatsuji and D. Ueda, "A GaAs High Power RF Single Pole Dual Throw Switch IC for Digital Mobile Communication System," *IEEE Journal of Solid-State Circuits,* vol. 30, no. 9, pp. 979-983, 1995.

[10] K. W. Kobayashi, L. Tran, A. K. Oki and D. C. Streit, "A 50 MHz-30 GHz Broadband CO-Planar Waveguide SPDT PIN Diode Switch with 45-dB Isolation," *IEEE Microwave and Guided Wave Letters,* vol. 5, no. 2, pp. 56-58, 1995.

[11] D. Kelly, C. Brindle, C. Kemerling and M. Stuber, "The State-of-the-Art of Silicon-on-Sapphire CMOS RF Switches," in *IEEE Compound Semiconductor Integrated Circuit Symposium*, 2005.

[12] A. Botula, A. Joseph, J. Slinkman, R. Wolf, Z. X. He, D. Ioannou, L. Wagner, M. Gordon, M. Abou-Khalil, R. Phelps, M. Gautsch, W. Abadeer, D. Harmon, M. Levy, J. Benoit and J. Dunn, "A Thin-film SOI 180nm CMOS RF Switch Technology," in *IEEE Topical Meeting on Silicon Monolithic Integrated Circuits in RF Systems*, 2009.

[13] A. Tombak, "Silicon-on-Insulator (SOI) Switches for Cellular and WLAN Front-End Applications," IEEE Radio Frequency Integrated Circuit Symposium Workshop, 2012.

[14] T. Y. Lee and S. Lee, "Modeling of SOI FET for RF Switch Applications," in *IEEE Radio Frequency Integrated Circuits Symposium*, 2010.

[15] K. E. Petersen, "Micromechanical Membrane Switches on Silicon," *IBM Journal of Research and Development,* vol. 23, no. 4, pp. 376-385, 1979.

[16] J. J. Yao and M. F. Chang, "A surface micromachined miniature switch for telecommunications applications with signal frequencies from DC up to 4 GHz," in *International Conference on Solid-State Sensors and Actuators*, 1995.

[17] C. Goldsmith, T. H. Lin, B. Powers, W. R. Wu and B. Norvell, "Micromechanical Membrane Switches for Microwave Applications," in *IEEE MTT-S International Microwave Symposium*, 1995.

[18] S. P. Pacheco, L. P. B. Katehi and C. T. C. Nguyen, "Design of Low Actuation Voltage RF MEMS Switch," in *IEEE MTT-S International Microwave Symposium Digest*, 2000.

[19] C. L. Goldsmith, Z. Yao, S. Eshelman and D. Denniston, "Performance of Low-Loss RF MEMS Capacitive Switches," *IEEE Microwave and Guided Wave Letters,* vol. 8, no. 8, pp. 269-271, 1998.

[20] G. M. Rebeiz and J. B. Muldavin, "RF MEMS switches and switch circuits," *IEEE Microwave Magazine,* vol. 2, no. 4, pp. 59-71, 2001.

[21] S. Raoux, C. T. Rettner, Y.-C. Chen, J. Jordan-Sweet, Y. Zhang, M. Caldwell, H. -S. P. Wong, D. Milliron and J. Cha, "Scaling Properties of Phase Change Materials," in *Non-Volatile Memory Technology Symposium*, Albuquerque, NM, 2007.

[22] S. Raoux, H.-Y. Cheng, B. Munoz and J. Jordan-Sweet, "Crystallization characteristics of Ge-Sb and Ge-Te phase change materials," in *Eur Phase Change*

Ovonic Science Symposium, 2009.

[23] S. R. Ovshinsky, "Reversible electrical switching phenomena in disordered structures," *Physical Review Letters,* vol. 21, no. 20, pp. 1450-1453, 1968.

[24] N. Yamada, E. Ohno, K. Nishiuchi and N. Akahira, "Rapid-phase transitions of GeTe-Sb2Te3 pseudobinary amorphous thin films for an optical disk memory," *Journal of Applied Physics,* vol. 69, no. 5, pp. 2849-2856, 1991.

[25] A. Pirovano, A. L. Lacaita, A. Benvenuti, F. Pellizzer and R. Bez, "Electronic Switching in Phase-Change Memories," *IEEE Transactions on Electron Devices,* vol. 51, no. 3, pp. 452-459, 2004.

[26] J. Feinleib, J. deNeufville, S. C. Moss and S. R. Ovshinsky, "Rapid reversible light-induced crystallization of amorphous semiconductors," *Applied Physics Letters,* vol. 18, no. 6, pp. 254-257, 1971.

[27] T. Takamori, R. Roy and G. J. McCarthy, "Observations of Surface-Nucleated Crystallization in Memory-Switching Glasses," *Journal of Applied Physics,* vol. 42, no. 6, pp. 2577-2578, 1971.

[28] J. H. Coombs, A. P. J. M. Jongenelis, W. VanEs-Spiekman and B. A. J. Jacobs, "Laser-induced crystallization phenomena in GeTe-based alloys. I. Characterization of nucleation and growth," *Journal of Applied Physics,* vol. 78, no. 8, pp. 4906-4917, 1995.

[29] J. H. Coombs, A. P. J. M. Jongenelis, W. VanEs-Spiekman and B. A. J. Jacobs, "Laser-induced crystallization phenomena in GeTe-based alloys. II. Composition dependence of nucleation and growth," *Journal of Applied Physics,* vol. 78, no. 8, pp. 4918-4928, 1995.

[30] A. P. J. M. Jongenelis, J. H. Commbs, W. VanEs-Spiekman and B. A. J. Jacobs, "Laser-induced crystallization phenomena in GeTe-based alloys. III. GeTeSe alloys for a CD compatible erasable disk," *Journal of Applied Physics,* vol. 79, no. 11, pp. 8349-8356, 1996.

[31] B. Hyot, X. Biquard and L. Poupinet, "Local structures of morphous and crystalline GeTe and GeSbTe," *Proceedings of EPCOS,* 2003.

[32] S. Raoux, B. Munoz, H.-Y. Cheng and J. L. Jordan-Sweet, "Phase transitions in Ge–Te phase change materials studied by time-resolved x-ray diffraction," *Applied Physics Letters,* 2009.

[33] A. H. Edwards, A. C. Pineda, P. A. Schultz, M. G. Martin, A. P. Thompson, H. P. Hjalmarson and C. J. Umrigar, "Electronic structure of intrinsic defects in crystalline germanium telluride," *Physical Review B,* vol. 73, no. 4, p. 045210, 2006.

[34] S. Raoux, H. -Y. Cheng, M. A. Caldwell and H.-S. P. Wong, "Crystallization times of Ge–Te phase change materials as a function of composition," *Applied Physics Letters,* 2009.

[35] M. Chen, K. A. Rubin and R. W. Barton, "Compound materials for reversible, phase-change optical data storage," *Applied Physics Letters,* vol. 49, no. 9, pp. 502-504, 1986.

[36] K. N. Chen, L. Krusin-Elbaum, D. M. Newns, B. G. Elmegreen, R. Cheek, N. Rana, A. M. Young, S. J. Koester and C. Lam, "Programmable via Using Indirectly Heated Phase-Change Switch for Reconfigurable Logic Applications," *IEEE Electron Device Letters,* vol. 21, no. 1, pp. 131-133, 2008.

[37] M. Takenaga, N. Yamada, S. Ohara, K. Nishiuchi, M. Nagashima, T. Kashihara, S. Nakamura and T. Yamashita, "New optical erasable medium using tellurium suboxide thin film," *Proceedings of SPIE,* vol. 420, pp. 173-177, 1983.

[38] N. Yamada, M. Takao and M. Takenaga, "Te-Ge-Sn-Au Phase change recording film for optical disk," *Proceedings of SPIE,* vol. 695, pp. 79-85, 1986.

[39] M. Terao, T. Nishida, Y. Miyauchi, S. Horigome, T. Kaku and N. Ohta, "In-Se Based Phase Change Reversible Optical Recording Film," *Proceedings of SPIE,* vol. 695, pp. 105-109, 1986.

[40] J. C. Rhee, M. Okuda and T. Matsushita, "Write-Erase Characteristics of Phase Change Optical Recording in Ga–Se–Te Systems," *Japanese Journal of Applied Physics,* vol. 26, no. 1, pp. 102-105, 1987.

[41] N. Yamada, E. Ohno, N. Akahira, K. Nishiuchi, K. Nagata and M. Takao, "High Speed Overwritable Phase Change Optical Disk Material," *Japanese Journal of Applied Physics,* vol. 26, no. S4, pp. 61-66, 1987.

[42] K. Nishimura, M. Suzuki, I. Morimoto and K. Mori, "Ge–Te–Sb Based Overwritable Phase Change Optical Disk," *Japanese Journal of Applied Physics,* vol. 28, no. S3, pp. 135-139, 1989.

[43] H. Iwasaki, Y. Ide, M. Harigaya, Y. Kageyama and I. Fujimura, "Completely Erasable Phase Change Optical Disk," *Japanese Journal of Applied Physics,* vol.

31, no. S2, pp. 461-465, 1992.

[44] K. A. Rubin and M. Chen, "Progress and issues of phase-change erasable optical recording media," *Thin Solid Films,* vol. 1, no. 2, pp. 129-139, 1989.

[45] G. Wicker, "Nonvolatile, High Density, High Performance Phase Change Memory," in *Asia Pacific Symposium on Microelectronics and MEMS*, 1999.

[46] J. Hegedus and S. R. Elliott, "Microscopic origin of the fast crystallization ability of Ge–Sb–Te phase-change memory materials," *Nature Materials,* vol. 7, no. 5, pp. 399-405, 2008.

[47] D. Ielmini and Y. Zhang, "Analytical model for subthreshold conduction and threshold switching in chalcogenide-based memory devices," *Journal of Applied Physics,* vol. 102, no. 5, p. 054517, 2007.

[48] S. Lai, "Current status of the phase change memory and its future," in *IEEE International Electron Devices Meeting*, 2003.

[49] B. Yu, X. Sun, S. Ju, D. B. Janes and M. Meyyappan, "Chalcogenide-Nanowire-Based Phase Change Memory," *IEEE Transactions on Nanotechnology,* vol. 7, no. 4, pp. 496-502, 2008.

[50] M. K. Qureshi, V. Srinivasan and J. A. Rivers, "Scalable High Performance Main Memory System Using Phase-Change Memory Technology," *ACM SIGARCH Computer Architecture News,* vol. 37, no. 3, pp. 24-33, 2009.

[51] H.-S. P. Wong, S. Raoux, S. Kim, J. Liang, J. P. Reifenberg, B. Rajendran, M. Asheghi and K. E. Goodson, "Phase Change Memory," *Proceedings of the IEEE,* vol. 98, no. 12, pp. 2201-2227, 2010.

[52] H. Lo, E. Chua, J. C. Huang, C. C. Tan, C.-Y. Wen, R. Zhao, L. Shi, C. T. Chong, J. Paramesh, T. E. Schlesinger and J. A. Bain, "Three-Terminal Probe Reconfigurable Phase-Change Material Switches," *IEEE Transactions on Electron Devices,* vol. 57, no. 1, pp. 312-320, 2010.

[53] E. K. Chua, L. P. Shi, R. Zhao, K. G. Lim, T. C. Chong, T. E. Schlesinger and J. A. Bain, "Low resistance, high dynamic range reconfigurable phase change switch for radio frequency applications," *Applied Physics Letters,* vol. 97, no. 18, p. 183506, 2010.

[54] K. L. Chopra and S. K. Bahl, "Amorphous versus Crystalline GeTe Films. I. Growth and Structural Behavior," *Journal of Applied Physics,* vol. 40, no. 10, pp.

4171-4178, 1969.

[55] S. K. Bahl and K. L. Chopra, "Amorphous versus Crystalline GeTe Films. III. Electrical Properties and Band Structure," *Journal of Applied Physics,* vol. 41, no. 5, pp. 2196-2212, 1970.

[56] S. K. Bahl and K. L. Chopra, "Amorphous Versus Crystalline GeTe Films. II. Optical Properties," *Journal of Applied Physics,* vol. 40, no. 12, pp. 4940-4947, 1969.

[57] M. Jafari and M. Rais-Zadeh, "Zero-static-power phase-change optical modulator," *Optics Letters,* vol. 41, no. 6, pp. 1177-1180, 2016.

[58] M. Jafari and M. Rais-Zadeh, "A 1550 nm Phase Change Electro-Optical Shutter," in *IEEE 29th International Conference on Micro Electro Mechanical Systems*, 2016.

[59] T. Okabe and M. Nakagawa, "Crystallization Behavior and Local Order of Amorphous GexTe1− x Films," *Journal of Non-Crystalline Solids,* vol. 88, no. 2-3, pp. 182-195, 1986.

[60] M. R. King, B. P. Wagner, E. B. Jones, N. El-Hinnawy, P. Boroduiln, S. R. McLaughlin, J. S. Mason, R. S. Howell, M. J. Lee and R. M. Young, "Development of cap-free sputtered GeTe films for inline phase change switch based RF circuits," *Journal of Vacuum Science & Technology B,* vol. 32, no. 4, p. 041204, 2014.

[61] Y. Shim, G. Hummel and M. Rais-Zadeh, "RF switches using phase change materials," in *IEEE 26th International Conference on Micro Electro Mechanical Systems (MEMS),* Taipei, 2013.

[62] N. El-Hinnawy, P. Borodulin, B. Wagner, M. R. King, J. S. Mason, E. B. Jones, S. McLaughlin, V. Veliadis, M. Snook, M. E. Sherwin, R. S. Howell, R. M. Young and M. J. Lee, "A Four-Terminal, Inline, Chalcogenide Phase-Change RF Switch Using an Independent Resistive Heater for Thermal Actuation," *IEEE Electron Device Letters,* vol. 34, no. 10, pp. 13131-1315, 2013.

[63] N. El-Hinnawy, P. Borodulin, B. P. Wagner, M. R. King, J. S. Mason, E. B. Jones, V. Veliadis, R. S. Howell, R. M. Young and M. J. Lee, "A 7.3 THz Cut-Off Frequency, Inline, Chalcogenide Phase-Change RF Switch Using an Independent Resistive Heater for Thermal Actuation," in *IEEE Compound Semiconductor Integrated Circuit Symposium*, 2013.

[64] M. Wang, Y. Shim and M. Rais-Zadeh, "A Low-Loss Directly Heated Two-Port RF Phase Change Switch," *IEEE Electron Device Letters,* vol. 35, no. 4, pp. 491-493, 2014.

[65] M. Wang and M. Rais-Zadeh, "Directly Heated Four-Terminal Phase Change Switches," in *IEEE MTT-S International Microwave Symposium*, Tampa, FL, 2014.

[66] M. Rais-Zadeh, Y. Shim and M. Wang, "Directly heated RF phase change switch". US Patent US9419213 B2, 5 June 2014.

[67] R. F. Bunshah, Deposition Technologies for Films and Coatings: Developments and Applications, Park Ridge, NJ: Noyes Publications, 1982.

[68] K. Nakamura, K. Inagawa, K. Tsuruoka and S. Komiya, "Applications of Wear-Resistant Thick Films Formed by Physical Vapor Deposition Processes," *Thin Solid Films,* vol. 40, pp. 155-167, 1977.

[69] J. Moon, H. Seo and D. Le, "Development toward High-power Sub-1-ohm DC-67 GHz RF Switches using Phase Change Materials for Reconfigurable RF Front-end," in *IEEE MTT-S International Microwave Symposium*, 2014.

[70] N. El-Hinnawy, P. Borodulin, E. B. Jones, B. P. Wagner, M. R. King, J. S. Mason, J. Hartman, R. S. Howell, M. J. Lee and R. M. Young, "Improvements in GeTe-Based Inline Phase-Change Switch Technology for RF Switching Applications," in *CS MANTECH Conference*, 2014.

[71] T. B. Jackson, A. V. Virkar, K. L. More, R. B. Dinwiddie and R. A. Cutler, "High-Thermal-Conductivity Aluminum Nitride Ceramics: The Effect of Thermodynamic, Kinetic, and Microstructural Factors," *Journal of the American Ceramic Society*, vol. 80, no. 6, pp. 1421-1435, 1997.

[72] M. Wang, F. Lin and M. Rais-Zadeh, "Performance Measurements and Non-Linearity Modeling of GeTe Phase Change RF Switches with Direct and Indirect Heating Schemes," in *2015 IEEE MTT-S International Microwave Symposium*, Phoenix, AZ, 2015.

[73] Y. Shim, G. Hummel and M. Rais-Zadeh, "Non-Linearity Analysis of RF Ohmic Switches Based on Phase Change Materials," *IEEE Electron Device Letters,* vol. 35, no. 3, pp. 405-407, 2014.

[74] Y. S. Ju, K. Kurabayashi and K. E. Goodson, "Thermal Characterization of IC Passivation Layers Using Joule Heating and Optical Thermometry," *Microscale*

Thermophysical Engineering, vol. 2, no. 2, pp. 101-110, 1998.

[75] M. Wang and M. Rais-Zadeh, "Development and evaluation of germanium telluride phase change material based ohmic switches for RF applications," *Journal of Micromechanics and Microengineering,* vol. 27, no. 1, p. 013001, 2016.

[76] N. El-Hinnawy, P. Borodulin, M. Torpey, F. Kuss, A. Ezis, J. Paramesh, J. Bain, T. E. Schlesinger, R. S. Howell, M. J. Lee, D. Nichols and R. M. Young, "Reconfigurable Inline Phase-Change Switches for Broadband Applications," in *IEEE MTT-S International Microwave Symposium*, 2015.

[77] R. Wolf, A. Joseph, A. Botula and J. Slinkman, "A Thin-film SOI 180nm CMOS RF Switch," in *IEEE Topical Meeting on Silicon Monolithic Integrated Circuits in RF Systems*, 2009.

[78] S. Makioka, Y. Anda, K. Miyatsuji and D. Ueda, "Super Self-Aligned GaAs RF Switch IC with 0.25 dB Extremely Low Insertion Loss for Mobile Communication Systems," *IEEE Transactions on Electron Devices,* vol. 48, no. 8, pp. 1510-1514, 2001.

[79] M. Wang, F. Lin and M. Rais-Zadeh, "An X-Band Reconfigurable Bandpass Filter Using Phase Change RF Switches," in *IEEE 16th Topical Meeting on Silicon Monolithic Integrated Circuits in RF Systems*, Austin, TX, 2016.

[80] Y. Shim, Z. Wu and M. Rais-Zadeh, "A High-Performance Continuously Tunable MEMS Bandpass Filter at 1 GHz," *IEEE Transactions on Microwave Theory and Techniques,* vol. 60, no. 8, pp. 2439-2447, 2012.

[81] S. Lucyszyn, "Review of radio frequency microelectromechanical systems technology," *IEE Proceedings-Science, Measurement and Technology,* vol. 151, no. 2, pp. 93-103, 2004.

[82] A. R. Brown and G. M. Rebeiz, "A Varactor-Tuned RF Filter," *IEEE Transactions on Microwave Theory and Techniques*, vol. 48, no. 7, pp. 1157-1160, 2000.

[83] A. Pothier, J. -C. Orlianges, G. Zheng, C. Champeaux, A. Catherinot, D. Cros, P. Blondy and J. Papapolymerou, "Low-loss 2-bit tunable bandpass filters using MEMS DC contact switches," *IEEE Transactions on Microwave Theory and Techniques,* vol. 53, no. 1, pp. 354-360, 2005.

[84] P. S. Carter, "Magnetically-Tunable Microwave Filters Using Single-Crystal Yttrium-Iron-Garnet Resonators," *IRE Transactions on Microwave Theory and*

Techniques, vol. 9, no. 3, pp. 252-260, 1961.

[85] Y. Zhu, G. Qiu, K. H. Chi, B. B. T. Wang and C. S. Tsai, "A Tunable X-Band Band-Pass Filter Module Using YIG/GGG Layer on RT/Duroid Substrate," *IEEE Transactions on Magnetics,* vol. 45, no. 10, pp. 4195-4198, 2009.

[86] S. Courreges, Y. Li, Z. Zhao, K. Choi, A. Hunt and J. Papapolymerou, "Two-Pole X -Band-Tunable Ferroelectric Filters With Tunable Center Frequency, Fractional Bandwidth, and Return Loss," *IEEE Transactions on Microwave Theory and Techniques,* vol. 57, no. 12, pp. 2872-2881, 2009.

[87] D. Bouyge, A. Crunteanu, J. -C. Orlianges, D. Passerieux, C. Champeaux, A. Catherinot, A. Velez, J. Bonache, F. Martin and P. Blondy, "Reconfigurable Bandpass Filter Based on Split Ring Resonators and Vanadium Dioxide (VO2) Microwave Switches," in *2009 Asia Pacific Microwave Conference*, Singapore, 2009.

[88] R. Singh, G. Slovin, M. Xu, A. Khairi, S. Kundu, T. E. Schlesinger, J. A. Bain and J. Paramesh, "A 3/5 GHz Reconfigurable CMOS Low-Noise Amplifier Integrated with a Four-Terminal Phase-Change RF Switch," in *IEEE International Electron Devices Meeting*, 2015.

[89] G. Hummel, Y. Hui and M. Rinaldi, "Reconfigurable Mode of Vibration in AlN MEMS Resonators Using Phase Change Materials," in *IEEE International Ultrasonics Symposium,* 2014.

[90] M. Wang, L. Feng and M. Rais-Zadeh, "Need a Change? Try GeTe: A Reconfigurable Filter Using Germanium Telluride Phase Change RF Switches," *IEEE Microwave Magazine,* vol. 17, no. 12, pp. 70-79, 2016.

[91] S. Park and G. M. Rebeiz, "Low-Loss Two-Pole Tunable Filters With Three Different Predefined Bandwidth Characteristics," *IEEE Transactions on Microwave Theory and Techniques,* vol. 56, no. 5, pp. 1137-1148, 2008.

[92] G. L. Matthaei, L. Young and E. M. T. Jones, Microwave Filters, Impedance Matching Networks and Coupling Structures, Norwood, MA: Artech House, 1980.

[93] N. El-Hinnawy, P. Borodulin, B. P. Wagner, M. R. King, E. B. Jones, R. S. Howell, M. J. Lee and R. M. Young, "Low-loss latching microwave switch using thermally pulsed non-volatile chalcogenide phase change materials," *Applied Physics Letters,* vol. 105, no. 1, p. 013501, 2014.

[94] E. K. Chua, "Development of Phase Change Switches with Low Resistance in the “ON state”," Diss. Carnegie Mellon University, Pittsburgh, PA, 2011.

[95] J. S. Moon, H. C. Seo, D. Le, H. Fung, A. Schmitz, T. Oh, S. Kim, K. A. Son, D. Zehnder and B. Yang, "11 THz Figure-of-Merit Phase-change RF Switches for Reconfigurable Wireless Front-ends," in *IEEE MTT-S International Microwave Symposium*, 2015.

[96] N. El-Hinnawy, P. Borodulin, E. B. Jones, B. P. Wagner, M. R. King, J. S. Mason, J. Bain, J. Paramesh, T. E. Schlesinger, R. S. Howell, M. J. Lee and R. M. Young, "12.5 THz Fco GeTe Inline Phase-Change Switch Technology for Reconfigurable RF and Switching Applications," in *IEEE Compound Semiconductor Integrated Circuit Symposium*, 2014.

[97] J. S. Moon, H. C. Seo and D. Le, "Development toward High-power Sub-1-ohm DC-67 GHz RF Switches using Phase Change Materials for Reconfigurable RF Front-end," in *IEEE MTT-S International Microwave Symposium*, 2014.

[98] A. Fantini, V. Sousa, L. Perniola, E. Gourvest, J. C. Bastien, S. Maitrejean, S. Braga, N. Pashkov, A. Bastard, B. Hyot, A. Roule, A. Persico, H. Feldis, C. Jahan, J. F. Nodin, D. Blachier, A. Toffoli, G. Reimbold, F. Fillot, F. Pierre, R. Annunziata, D. Benshael, P. Mazoyer, C. Vallee, T. Billon, J. Hazart, B. De Salvo and F. Boulanger, "N-doped GeTe as Performance Booster for Embedded Phase-Change Memories," in *IEEE International Electron Devices Meeting*, 2010.

[99] F. Tong, X. S. Miao, Y. Wu, Z. P. Chen, H. Tong and X. M. Cheng, "Effective method to identify the vacancies in crystalline GeTe," *Applied Physics Letters,* vol. 97, no. 26, p. 261904, 2010.

[100] P. Nukala, C.-C. Lin, R. Composto and R. Agarwal, "Ultralow-power switching via defect engineering in germanium telluride phase-change memory devices," *Nature Communications,* vol. 7, 2016.

[101] H. M. Aldosari, H. Simchi, Z. Ding, K. A. Cooley, S. Y. Yu and S. E. Mohney, "Impact of Premetallization Surface Preparation on Nickel-based Ohmic Contacts to Germanium Telluride: An X-ray Photoelectron Spectroscopic Study," *ACS Applied Materials & Interfaces,* vol. 8, no. 50, pp. 34802-34809, 2016.